PEOPLE'S DEMOCRATIC REPUBLIC OF ALGERIA

MINISTRY OF HIGH EDUCATION AND SCIENTIFIC

RESEARCH

UNIVERSITY YAHIA FARES OF MEDEA



Faculty of Technology

Department of Electrical Engineering

MASTER THESIS

Branch: Electrotechnics

Specialty: Renewable Energies in Electrotechnics

Theme:

Inverter Control of The PV-Wind Hybrid System Grid-Connected by SRF Algorithm

Presented by:

- Muntaser Mohammed Nasser Ali AL-SHARFI
- Ahmad khalid Abd Al-khalik YAHYA

Proposed and Directed by:

- Dr. Abdelkader MORSLI
- Mr. Fayçal HADJ MIHOUB SIDI MOUSSA

Academic Year 2022 / 2023

DEDICATION

I dedicate this humble work:

To my dear parents *who sacrificed their lives for my success and for my success Encourage them throughout my studies.*

To my dear brothers ***Ali*** *and* ***Bashir***

To my dear sisters ***Saud, Hayat, Asma*** *and* ***Amira****.*

To my aunts, uncles, and cousins

To all of my family ***AL-SHARAFI***

Without forgetting all of my teachers who contributed to my work and participated in my education, especially to mention:

Dr. Abdelkader MORSLI

Mr. Fayçal HADJ MIHOUB SIDI MOUSSA

To all my foreign colleagues and friends.

To all the students in my class and especially the RE students in electrical engineering.

To all those I love, who love me, and to all who knew me.

To everyone who helped me complete this Memor.

Muntaser AL-SHARFI.

DEDICATION

I dedicate this humble work:

To my dear parents *who sacrificed their lives for my success and*

for my successEncourage them throughout my studies.

To my dear brothers

(Abdul_ Khaleq, Diaa Ghassan, Wael, and Yahya)

To my dear sister (Heba)

To my aunts, uncles, and cousins

To all of my family ***AL-YAHYA***

Without forgetting all of my teachers

who contributed to my work and participated

in my education, especially to mention:

Dr. Abdelkader MORSLI

Mr. Fayçal HADJ MIHOUB SIDI MOUSSA

To all my foreign colleagues and friends.

To all the students in my class and especially

the RE students in electrical engineering.

To all those I love, who love me, and to all who knew me.

To everyone who helped me complete this Memoir.

Ahmad YAHYA

ACKNOWLEDGMENTS

My biggest thanks to God *who single-handedly guided me in the right direction during my life and helped me to accomplish this humble work.*

I would like to thank my supervisor, ***Dr. Abdelkader MORSLI****, for suggesting this topic and for the continuous follow-up throughout the realization of this work.*

*I do not forget to thank my promotion partner who has been in constant follow-up throughout the realization of this work "****Mr. Fayçal HADJ MIHOUB SIDI MOUSSA****"*

I express my deepest gratitude to ***my parents*** *for their encouragement, support, and sacrifices.*

I also express my thanks and gratitude to ***my brothers, sisters,*** *and all* ***the families*** *for their endless support and encouragement.*

My sincere thanks to ***the members of the jury*** *for the honor they have done us by participating in the judgment of this work.*

I also thank ***all the teachers*** *in the Department of Electrical Engineering at Dr. University Yahya Fares of Medea, who participated in our training throughout the university session.*

Finally, I would like to express my gratitude to all ***my friends and colleagues*** *for all the moral and material support.*

Muntaser & Ahmad

ملخص :يناقش هذا العمل دمج مصادر الطاقة المتجددة الهجينة (HRES)، والكهروضوئية الشمسية (PV)، و طاقة الرياح القائم على PMSG، في شبكة الطاقة باستخدام عاكس ثلاثي الطور يتم التحكم فيه عبر نهج الإطار المرجعي المتزامن (SRF). أصبح استخدام مصادر الطاقة المتجددة ذا أهمية متزايدة للحد من انبعاثات الكربون والتخفيف من تغير المناخ. ومع ذلك، فإن الطبيعة المتقطعة لمصادر الطاقة الشمسية وطاقة الرياح تشكل تحديات لاستقرار الشبكة وموثوقيتها. لمواجهة هذه التحديات، يستخدم النظام المقترح استراتيجية تحكم تنسق إنتاج الطاقة لمصادر الطاقة الشمسية وطاقة الرياح وتزامنها مع الإطار المرجعي للشبكة. ينتج عن ذلك خرج طاقة مستقر يتطابق مع تردد الشبكة ومتطلبات الجهد. يتم تنفيذ استراتيجية التحكم باستخدام استراتيجية متزامنة للتحكم في الإطار المرجعي تضمن انتقالًا سلسًا بين تشغيل الوضع المتصل بالشبكة. يتم تقييم النظام المقترح من خلال اختبارات المحاكاة باستخدام MATLAB/SIMULINK. تُظهر النتائج فعالية وموثوقية استراتيجية الإطار المرجعي المتزامن وتثبت قدرتها على دمج نظام الطاقة المتجددة الهجين بنجاح في الشبكة الكهربائية

كلمات مفتاحية : مصادر الطاقة المتجددة الهجينة ، الطاقة الشمسية الكهروضوئية ، طاقة الرياح القائمة على PMSG ، شبكة الطاقة ، العاكس ثلاثي الطور ، الإطار المرجعي المتزامن.

Abstract: This work discusses the integration of hybrid renewable energy sources(HRES), solar photovoltaic (PV), and wind energy-based PMSG, into the power grid using a three-phase inverter controlled via the synchronous reference frame (SRF) approach. The use of renewable energy sources is becoming increasingly important to reduce carbon emissions and mitigate climate change. However, the intermittent nature of solar and wind energy sources poses challenges to grid stability and reliability. To address these challenges, the proposed system utilizes a control strategy that coordinates the energy output of the solar and wind sources and synchronizes it with the grid reference frame. This results in a stable power output that matches the grid frequency and voltage requirements. The control strategy is implemented using a synchronous reference frame control strategy that ensures a smooth transition between the grid-connected mode operation. The proposed system is evaluated through simulation tests using MATLAB/SIMULINK. The results demonstrate the effectiveness and reliability of the synchronous reference frame strategy and prove its ability to integrate successfully the hybrid renewable energy system into the electrical grid.

Keywords: Hybrid Renewable Energy Sources, Solar Photovoltaic, Wind Energy-Based PMSG, Power Grid, Three-Phase Inverter, Synchronous Reference Frame.

Résumé : Ce travail traite de l'intégration des sources d'énergie renouvelables hybrides (HRES), du photovoltaïque solaire (PV) et du PMSG basé sur l'énergie éolienne, dans le réseau électrique à l'aide d'un onduleur triphasé contrôlé par l'approche du cadre de référence synchrone (SRF). L'utilisation de sources d'énergie renouvelables est de plus en plus importante pour réduire les émissions de carbone et atténuer les changements climatiques. Cependant, la nature intermittente des sources d'énergie solaire et éolienne pose des défis pour la stabilité et la fiabilité du réseau. Pour relever ces défis, le système proposé utilise une stratégie de contrôle qui coordonne la production d'énergie des sources solaire et éolienne et la synchronise avec le cadre de référence du réseau. Il en résulte une puissance de sortie stable qui correspond aux exigences de fréquence et de tension du réseau. La stratégie de contrôle est mise en œuvre à l'aide d'une stratégie de contrôle du cadre de référence synchrone qui assure une transition en douceur entre le mode connecté au réseau. Le système proposé est évalué au moyen d'essais de simulation au moyen de MATLAB/SIMULINK. Les résultats démontrent l'efficacité et la fiabilité de la stratégie de cadre de référence synchrone et prouvent sa capacité à intégrer avec succès le système d'énergie renouvelable hybride dans le réseau électrique.

Mots-clés : Énergies Renouvelables Hybrides, Photovoltaïque Solaire, PMSG Eolien, Réseau Electrique, Onduleur Triphasé, Cadre De Référence Synchrone.

Contents

Contents I

List of Figure V

List of Tables VII

Abbreviations VIII

symbols and units of measurement x

Constants xii

General Introduction 1

Chapter I:

Overview of the Solar and Wind Energy System Connected to the Electrical Grid

I.1. Introduction 4

I.2. Definition of solar energy 4

I.2.1. History of Photovoltaics 4

I.2.2. Photovoltaic solar energy 5

I.3. Solar electricity by the photovoltaic effect 5

I.3.1. Principle of operation 5

I.3.2. Different types of photovoltaic cells 6

I.3.3. PV SYSTEM TYPES 7

I.3.3.1 Stand-alone systems 8

I.3.3.2. Grid-connected systems 9

I.3.4. Advantages and disadvantages of the photovoltaic system 11

I.3.4.1. Advantages of the photovoltaic system (VPS) 11

I.3.4.2. Disadvantages of the photovoltaic system 11

I.4. wind turbine generation 12

I.4.1. Definition of wind turbine 12

I.4.2. History of Wind Uses 12

I.4.3. Types of wind turbines 13

I.4.3.1. Horizontal axis wind turbines 13

I.4.3.2 Vertical axis wind turbines 14

I.4.4. Main parts of a wind turbine 14

I.4.5. Advantages and disadvantages of wind turbines 15

I.4.5.1. Advantages 15

I.4.5.2. Disadvantages 15

I.5. Topologies and development of wind turbine generators 16
I.5.1. Synchronous machine (SM) 17
I.5.1.1. Wound rotor machine (WRSG): 17
I.5.1.2. The permanent magnet synchronous generator: 18
I.5.2. Induction Generator 18
I.5.2.1.Squirrel Cage Induction Generator (SCIG) 19
I.5.2.2. Doubly Fed Induction Generator (DFIG): 19
I.6. Fixed and Variable Speed Wind Turbine 19
I.6.1. Fixed-speed wind turbine directly connected to the offshore station 19
I.6.2. Variable speed wind turbine 20
I.7. Standards for the interconnection of electrical energy sources on the Grid 20
I.7.1 Interconnection Standards 21
I.7.2. UL standards (Underwriters Laboratories) 21
I.7.3. Standards related to power quality in terms of harmonic content 21
I.8. Conclusion 22

Chapter II:

Modeling and control of photovoltaic systems

II.1. Introduction 24
II.2. PV SYSTEM MODELING 24
II.2.1. PV Generator (GPV) 24
II.2.2. Design the PV array solar 27
II.2.3. characteristics of the PV module 28
II.2.4. Influence of irradiation and temperature on the I(V) and P(V) characteristics of (PVG) 29
II.2.4.1. The effect of irradiation 29
II.2.4.2 The effect of temperature 30
II.3. "Boost Converter" step-up chopper 31
II.3.1. Operation Boost converter: 31
II.3.2. Equivalent mathematical model: 32
II.3.3. Calculation of Boost Converter: 33
II.3.3.1. Selection of inductor (L): 33
II.3.3.2. Selection of capacitor (C): 34
II.4. Maximum Power Point Tracking (MPPT) 34
II.4.1. Principle of MPPT 34
II.4.2. Classification of commonly used MPPT Technique 36

II.4.2.1. Perturb & Observe (P&O) algorithm 37
Ii.5. Simulation Results 40
II.6. Conclusion 42

Chapter III:

Modeling and Control of Wind Turbine System

III.1. Introduction 45
III.2. Wind turbine modeling 45
III.2.1. Modeling of a horizontal axis wind turbine 45
III.2.1.1. Modeling of the Wind Turbine 45
III.2.1.2. Analytical model of the power coefficient 46
III.2.1.3. Speed Multiplier Model 48
III.2.1.4. Mechanical shaft model 49
III.3. PMSG Modeling 51
III.4. Three-phase PWM rectifier 53
III.4.1. Three-Phase PWM rectifier Principle 53
III.5. Direct power control (DPC) 54
III.5.1. Definition 54
III.5.2. Principle of direct power control 54
III.5.3. The voltage estimator 55
III.5.4. Estimated instantaneous power 56
III.5.5. Switching table 57
III.5.6. Sector determination 57
III.5.7. DC bus voltage control using the conventional PI regulator: 58
III.5.8. Hysteresis controller: 59
III.6. Simulation Results 60
III.7. Discussion Results 62
III.8. Conclusion 63

Chapter IV:

Hybrid System Solar and Wind Energies Connected to the Grid Via Inverter Controlled by SRF Strategy

IV.1 Introduction 65
IV.2. hybrid PV-PMSG wind turbine system connected to the grid 65
IV.3. Invertre control on the electrical grid side 66
IV.3 .1. SRF algorithm 66

IV.3 .2. Unity power factor 67
IV.3 .3. AC voltage regulation 68
IV.3 .4. DC voltage control by PI anti-windup 68
IV.4. Simulation Results 71
IV.5. Discussion results 75
IV.6. Conclusion 75
General Conclusion 76
LIST OF BIBLIOGRAPHIC REFERENCES 78
ANNEX 83

List of Figure

Figure I.1.Architecture of a photovoltaic system [11]. 5
Figure I.2. The Photovoltaic Effect in a Solar Cell 6
Figure I.3.Types of Solar Panels 7
Figure I.4.Types of PV systems 8
Figure I.5.Schematic representation of (a) a simple DC PV system to power a water pump with no energy storage and (b) a complex PV system including batteries, power conditioners, and both DC and AC loads [14] 9
Figure 1.6: Grid-Connected PV System Topologies: (a): Centralized inverter topology. (b): String inverter topology. (c): Multistring inverter topology. (d): AC module inverter topology 11
Figure 1.7: Modular topology for connecting PV systems to the grid 11
Figure 1.8. (a) Upwind HAWT (b) Downwind HAWT 13
Figures I.9. Darrius-type VAWTs and H-type VAWTs 14
Figure.I.10: Main parts of a wind turbine 15
Figure.I.11. DFIG wind turbine connected to the grid 16
Figure.I.12. Different offshore wind turbine machines 17
Figure.I.13. Wind turbine diagram and system structure power conversion WRSG 18
Figure.I.14: Diagram of wind turbine and power conversion system structure of PMSG 18
Figure I.15: diagram representation of the squirrel cage induction generator (SCIG)-based wind energy conversion (WEC) system. 19
Figurer.I.16: Principle diagram of wind turbine connected to the offshore station 19
Figure II.1 Synoptic structure of a photovoltaic energy production system. 24
Figure II.2 Equivalent model of the PV cell. 25
Figure II.3. I_V and P_V characteristics of the PV module offered at 25°C and 1000W/m2 28
Figure II.4.I-V and P-V characteristics of PV panel at 25°C and 1000W/m2 29
Figure II.5. Influence of irradiation variation on the I-V characteristic at a constant temperature 29
Figure II.6. Influence of irradiance variation on the P-V characteristic at a constant temperature. 30
Figure II.7. Influence of temperature on I_V characteristic 30
Figure II.8. Influence of temperature on P_V characteristic 31
Figure (II.10): Current and voltage timing diagrams of a boost chopper. 32
Figure II.11. Circuit diagram of a closed Boost chopper 32
Figure II.12. Circuit diagram of an open Boost chopper 33
Figure II.13. Boost chopper simulation scheme 34
Figure II.14 Solar energy conversion chain including MPPT control 35
Figure II.15 Principe de la commande MPPT 36
Figure II.16. Classification of commonly used MPPT 36
Figure II.17. P&O Algorithm 38
Figure II.18. P-V characteristics of the P&O algorithm 38
Figure II.19. Simulink Model of P&O MPPT 39
Figure II.20. Simulink Model of PWM signal generator 39
figure II.21. the block diagram in MATLAB SIMULINK PV system 40
figure II.22. The photovoltaic output voltage 40
Figure II.23. The photovoltaic output current 41

Figure II.24. The photovoltaic output power 41
Figure. II.25. The photovoltaic output voltage with the variation of irradiation 41
Figure II.26. The photovoltaic current with the variation of irradiation 42
Figure II.27. The photovoltaic power with the variation of irradiation 42
Figure. III.1. Simplified mechanical model of the turbine 45
Figure.III.2. Power coefficient curves of and Cp tip speed ratio λ for different pitch blade angles β .. 48
Figure III.3. Schematic diagram of the turbine model 50
Figure III.4. Equivalent circuit, (a) in q axis and (b) in d axis. 53
Figure III.5. structure of a three-phase rectifier 54
Figure III.6: General configuration of the DPC command. 55
Figure.III.7. Sectors in (α, β) plan 58
Figure.III.8. DC-link control system structure 59
Figure.III.11. PSMG output voltages 61
Figure.III. 12. PSMG output currents 61
Figure.III.13. Active power PMSG. 61
Figure.III.14. Reactive power PMSG. 62
Figure.III.15. DC bus voltage. 62
Figure IV.1. Grid Connected Hybrid (Photovoltaic-PMSG) System Diagram 66
Figure IV.2. Structure of a PI anti-windup controller [32] 70
Figure IV.3. Structure SRF-controlled inverter of a hybrid system 70
Figure IV.4: General model simulink of the Matlab hybrid system. 71
Figure IV.5. DC bus voltage and reference 71
Figure. IV.6. The output current of the inverter 72
Figure. IV.7. The current of the Nonlinear Load 72
Figure. IV.8. The current of the grid 72
Figure IV.9. The output voltage of the inverter 73
Figure IV.10. The voltage of the Nonlinear Load 73
Figure IV.11. The voltage of the grid 73
Figure. IV.12. The current of the load 73
Figure. IV.13. THD output Current of the inverter 74
Figure. IV.14. THD Current of the nonlinear load R1 74
Figure. IV.15. THD Current of the nonlinear load R2 74
Figure. IV. 16. THD Current of the grid 75

List of Tables

Table I. 1 characteristics Types of Solar Panels 7
Table II. 2 PV Module Parameters 27
Table III. 3 Switching table twelve Sector of the DPC command 57
Table 4: PV Module Parameters 83
Table 5: Parameters of the boost converter 83
Table 6: parameters of the wind turbine 84
Table 7: Parameters of the PMSG 84
Table 8: Parameters of the load 84
Table 9: Parameters of the inverter 85
Table 10 Parameters of the Grid 85

Abbreviations

AC: Alternating Current

CP: Power Coefficient

CPV: Concentrated Photovoltaics

CSC: Current Source Converter

DC: Direct Current

DFIG: Doubly Fed Induction Generator

DPC: Direct Power Control

DTC: Direct Torque Control

EWEA: European Wind Energy Association

ESCR: Extended Short Circuit Ratio

FFT: Fast Fourier Transform

f: System Frequency

HAWT: Horizontal Axis Wind Turbine

HVAC: High Voltage Alternating Current

HVDC: High Voltage Direct Current

IEEE: Institute of Electrical and Electronics Engineers

IEC: International Electrotechnical Commission

IGBT: Insulated Gate Bipolar Transistor

IM: Induction Machine

IMAG: Induction Machine Asynchronous Generator

I-V: Current-Voltage

LCC: Line Commutated Converters

MPPT: Maximum PowerPoint Tracking

NL: Non-Linear

P&O: Perturb and Observe

P-Q: Active and Reactive Power

PCC: Point of Common Coupling

Pmax: Maximum Power

PI: Proportional Integral Regulator

PLL: Phase-Locked Loop

PMSG: Permanent Magnet Synchronous Generator

PV: Photovoltaic

PWM: Pulse Width Modulation

RES: Renewable Energy Source

SCC: Current Source Converter

SCIG: Squirrel Cage Induction Generator

SM: Synchronous Machine

SMSG: Synchronous Squirrel Cage Induction Generator

SRF: Synchronous Reference Frame

THD: Harmonic Distortion Rate

UPF: Unity Power Factor

VAWT: Vertical Axis Wind Turbine

VSC: Voltage Source Converter

WECS: Wind Energy Conversion System

Symbols and Units of Measurement

- A: Ampere (A)
- β: Blade pitch angle in degrees
- C: Capacitance of the DC bus (farad, F)
- Cf: Filter capacitance
- Cp(λ): Power coefficient
- Eg: Energy gap of the semiconductor (electronvolt, eV)
- F: Friction (newton per radian per second, N/rad/s)
- Hz: Hertz (Hz)
- Id: Junction current (A)
- I0: Reverse saturation current of the diode (A)
- Ick: Current of the rectifier in the dq plane (A)
- Idq: Line current in the dq reference frame (A)
- I*dq: Reference current (A)
- Im: Current amplitude (A)
- Iph: Photocurrent (A)
- Ipv: Photovoltaic current (A)
- Isc: Short-circuit current (A)
- J: Moment of inertia (kilogram-meter squared, $kg.m^2$)
- Ki: Integral gain
- kg: Kilogram (kg)
- Kp: Proportional gain
- L: Line inductance (Henry, H)
- λ: Specific speed
- m: Meter (unit of length)
- m^2: Square meter
- m^3: Cubic meter
- mF: Millifarad (mF)
- mH: Millihenry (mH)
- PW: Active power of the wind turbine (watt, W)

- p: Number of pole pairs
- q: Electron charge (coulomb, C)
- ρ: Air-specific density (kilogram per cubic meter, kg/m^3)
- r: Radius of the wind turbine blades (meter, m)
- R: Line resistance
- R: Radius of the wind turbine (meter, m)
- s: Second (s)
- S: Swept area by the turbine blades (square meter, m^2)
- Sn: Subscribed power (kilovolt-ampere, kVA)
- Tc: Cell temperature (°C)
- T: Wind turbine torque (newton-meter, N.m)
- V: Volt (V)
- V0: Open-circuit voltage (V)
- Vabc: alternating voltage (V)
- Vdc: DC bus voltage (V)
- Vdc_ref: Reference voltage of the DC bus (V)
- Vm: Voltage amplitude (V)
- Vpv: Photovoltaic output voltage (V)
- Vrms: Root mean square voltage (V)
- Vw: Wind speed (meter per second, m/s)
- vcdq: Converter voltage in the dq plane (volt, V)

Constants

Symbol	Description	Unit	Value
e	Electron charge	Coulomb [C]	$1.602 \cdot 10^{-19}$
K	Boltzmann constant	J/K	$1.381 \cdot 10^{-23}$
ρ_{air}	Density of air	kg/m^3	1.225 at STC

General Introduction

Algeria's need for electricity is rising quickly as a consequence of economic expansion and demographic changes, and in the next ten years, the country's electrical producing capacity may need to double. The Algerian government has understood the significance of renewable energy to protect fossil fuel reserves and develop sustainable solutions to lessen the effects of global climate change, particularly greenhouse gas emissions, as a result of the fast depletion of fossil fuels and the rise in the electricity demand. Algeria has started an ambitious initiative to promote energy efficiency and the development of renewable energies, which has helped to produce a green wave. This program relies on a strategy that is centered on growing and extending the use of non-depletable resources, such as solar and wind energy, to diversify the sources of power [1].

Renewable power usage increased by more than 7% year on year in 2020, with renewables boosting their proportion of worldwide electricity consumption from 26.3 percent in 2019 to 28.2 percent in 2020. This is the most yearly advancement made in the last three decades. Because of increased dependence on renewable energy and the stability of global power demand in 2020, nonrenewable electricity usage fell 2.8 percent year on year. Hydropower is by far the most important source of renewable energy worldwide, followed by wind and solar photovoltaic (PV). Nonetheless, wind and solar PV deployment are rising; they had the highest absolute yearly growth in 2020 and account for two-thirds of the worldwide rise in renewable power consumption seen since 2015 [2].

Solar and wind energy system is one of the most prominent sources of energy. The utilization of solar and wind energy systems has become increasingly popular due to their modular and environment-friendly nature. Solar and wind energy system works normally in standalone or grid-connected mode, but the efficiency of these sources is less due to the stochastic nature of solar and wind resources. The significant characteristics of HRES are to combine two or more renewable power generation technologies to make proper use of their operating characteristics and to obtain efficiencies higher than that could be obtained from a single power source [3]. This memoir presents a review of solar–wind hybrid renewable energy system covering issues such as pre-feasibility study, modeling, controlling, optimization technique, reliability, and power quality of the system

The PV array produces the dc power, and hence power electronics and control equipment points are required to convert dc to ac power. The control system consists of a current control strategy and a voltage control strategy. The current control strategy is used to achieve the dc voltage regulation at the

dc link and unity power factor at the grid and the voltage control strategy is applied to achieve maximum power point tracking. Maximum power point tracking (MPPT) can effectively improve the solar energy conversion efficiency of PV systems. In this work, Perturb-and-observe (P&O) method is used to achieve this function.

Among the electric generators, the PMSG is preferred due to its high efficiency, reliability, power density, gearless construction, and light weight and self-excitation characteristics. Among various types of gear train coupling, the gearless or directly allied permanent magnet type wind generators are more popular nowadays in the wind energy market in on-shore applications. The control of the PMSG to achieve the maximum power point can be done by varying its load using an electronic power interface circuit [4].

Grid-connected PV-WIND hybrid system inverter control by SRF algorithm is a simple and robust control strategy to improve the quality of grid-connected renewable energy. This strategy is based on the maximum power delivered to the grid from wind and solar PV sources. The considered system is composed of a photovoltaic array and a wind energy conversion system (WECS) based on a permanent magnet synchronous generator (PMSG) [5].

The SRF control based on PI Anti-windup based on the estimation of AC reference currents by controlling the VSC is considered one of the most attractive techniques based on current regulation.

The objective is to simulate this control strategy (SRF) based on the anti-windup proportional-integral (PI) controller. To improve the power quality at the PCC point in the presence of linear and non-linear loads. In addition, the MPPT of wind and photovoltaic systems should be obtained to improve the overall system efficiency

This memoir includes four chapters, in the 1st chapter an overview of hybrid renewable energy sources (Solar PV /Wind energy), in 2nd and 3rd modeling and simulation of photovoltaic and wind turbines, respectively. Finally, in chapter 4th application of the SRF technique for PV/Wind turbine grid-connected.

Chapter I:

Overview of the Solar and Wind Energy System Connected to the Electrical Grid

I.1. Introduction

Solar energy and wind energy are two forms of renewable energy that are increasingly being connected to the electrical grid as a way to reduce reliance on fossil fuels and combat climate change.

Solar energy is generated by capturing the energy from the sun using solar panels, which convert sunlight into direct current (DC) electricity. This DC electricity is then converted into alternating current (AC) electricity using an inverter, which is then fed into the electrical grid. Solar energy can be generated on a small scale, such as for individual homes, or on a large scale, such as for solar farms [6].

Wind energy, on the other hand, is generated by capturing the kinetic energy of the wind using wind turbines. The wind causes the blades of the turbine to rotate, which in turn generates electricity. Like solar energy, this electricity is converted from DC to AC using an inverter and then fed into the electrical grid. Wind energy can be generated onshore or offshore and on a small or large scale [8].

Both solar energy and wind energy are intermittent sources of energy, meaning that they are dependent on weather conditions and only generate electricity when the sun is shining or the wind is blowing. As a result, these sources of energy are often paired with energy storage systems, such as batteries, to ensure that electricity can be supplied even when there is no sunlight or wind. Additionally, they can be integrated into a larger grid system to balance the intermittency of the sources and to ensure that electricity demand is met [9].

Overall, solar energy and wind energy are two key renewable energy sources that are helping to transition the world toward a more sustainable and carbon-free future.

I.2. Definition of solar energy

Solar energy is the radiant energy that is emitted by the sun and harnessed by various technologies to produce electricity or heat. The energy is collected through the use of solar panels, which convert sunlight into electrical energy or thermal energy [6].

I.2.1. History of Photovoltaics

The solar energy falling on Earth in a year is ten thousand times more than the existing fuel sources available on Earth. The elements such as silicon, germanium, etc. used in making the PV cell are also copiously available on Earth. The PV cells can be classified as pollution-free as they do not produce any by-products that may contribute towards air/water pollution and also do not contain any

moving parts that may cause noise pollution. The first PV cell introduced to the world was described in a paper dated back in 1877 [7].

In 1883, Charles [5] constructed a selenium solar cell, which was as popular as the silicon PV cell used today. During the early days, the efficiency of a solar cell, which is defined as the percentage of the solar energy falling on the surface of the PV cell, which was converted into electricity, was almost 1%. During the first half of the twentieth century, the Chaplin-Fuller-Pearson team developed a new PV cell made up of semiconductors. In the early 1950s, they utilized silicon slices in producing the PV cells and they succeeded in getting the efficiency up to 6%. After further research, the efficiency of the current PV cells available in the market went up to 17% [10].

I.2.2. Photovoltaic solar energy

Photovoltaic solar energy is an electrical energy produced from solar radiation. The photovoltaic cell is an electronic component that is the base of the installations producing this energy. It works on the principle of the photoelectric effect. Several cells based on silicon are interconnected on a photovoltaic solar module or panel, and several panels are grouped to form a solar installation [6].

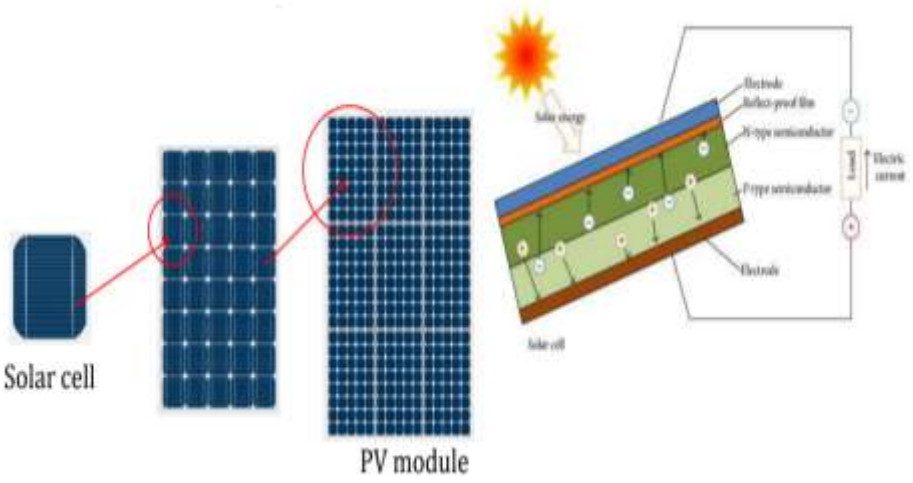


Figure I.1.Architecture of a photovoltaic system [11].

I.3. Solar electricity by the photovoltaic effect

I.3.1. Principle of operation

The photovoltaic effect was discovered by the French physicist BECQUEREL in 1839, the photovoltaic effect makes it possible to directly convert the light energy of the sun's rays (photon) into electricity (Volt), through the production and transport in a semiconductor material of positive and

negative electric charges under the effect of light. This material has two parts, one with an excess of electrons and the other with a deficit of electrons, called n-type doped and p-type doped respectively. When the first is brought into contact with the second, the excess electrons in the n material diffuse into the p material.

The initially n-doped area becomes positively charged, and the initially p-doped area becomes negatively charged. An electric field is therefore created between them which tends to push back the electrons in the n zone and the holes towards the p zone [12].

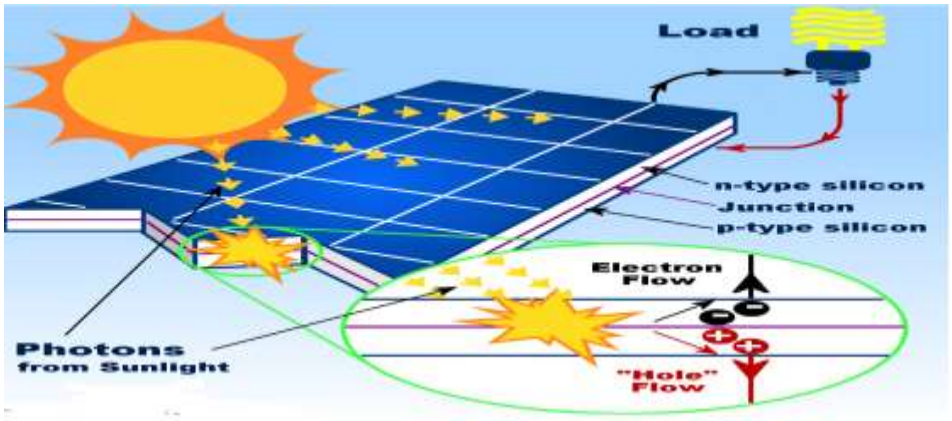


Figure I.2. The Photovoltaic Effect in a Solar Cell

I.3.2. Different types of photovoltaic cells

a) **Monocrystalline solar modules**: They have the best efficiency per m² and are mainly used when space is limited. However, their higher cost compared with other installations of the same power thwarts the development of this technique.

b) **Polycrystalline solar module:** Currently they have the best ratio (quality/price), which is why they are the most used. They have a good yield and a good lifetime (over 35 years).

c) **The amorphous solar modules:** will certainly have a good future because of their flexibility and good yield (better production in low light). However, the amorphous silicon has a yield divided by two compared to that of the lens, so this solution requires a larger area for the same installed power. In addition, the price per m² installed is lower than for solar panels composed of crystalline cells [13].



Monocrystalline Polycrystalline Thin-film

Figure I.3.Types of Solar Panels

Table I. 1 characteristics Types of Solar Panels

Monocrystalline	**Polycrystalline**	**Thin-film**
– Pure silicon. – 24.4 % efficiency – Moderate cost – Longest lifespan	– Melted silicon crystals – 19.9 % efficiency – – Least expensive – Moderate lifespan	– Variety of materials. – 18.9 % efficiency – Most expensive – Shortest lifespan

I.3.3. PV SYSTEM TYPES

PV systems can be divided into two categories: Grid-connected PV Systems and Stand-alone PV Systems. Grid-connected PV Systems can further be separated into two categories: those that are Directly Connected to the utility and those that are classified as Bimodal PV Systems.

Systems that are Directly Connected to the Utility are without a storage system, and systems that are classified as Bimodal PV Systems do have storage systems.

Stand-alone PV Systems can be divided into three categories: Without Battery, With Battery, and Hybrid PV Systems. Without Battery systems are Direct-Coupled systems, and Battery systems may include Self-Regulating DC Systems or AC Systems with a charge controller for the battery and load. Hybrid PV Systems may include systems with wind turbines, hydro turbines, diesel generators, or with fuel cells, or other sources.

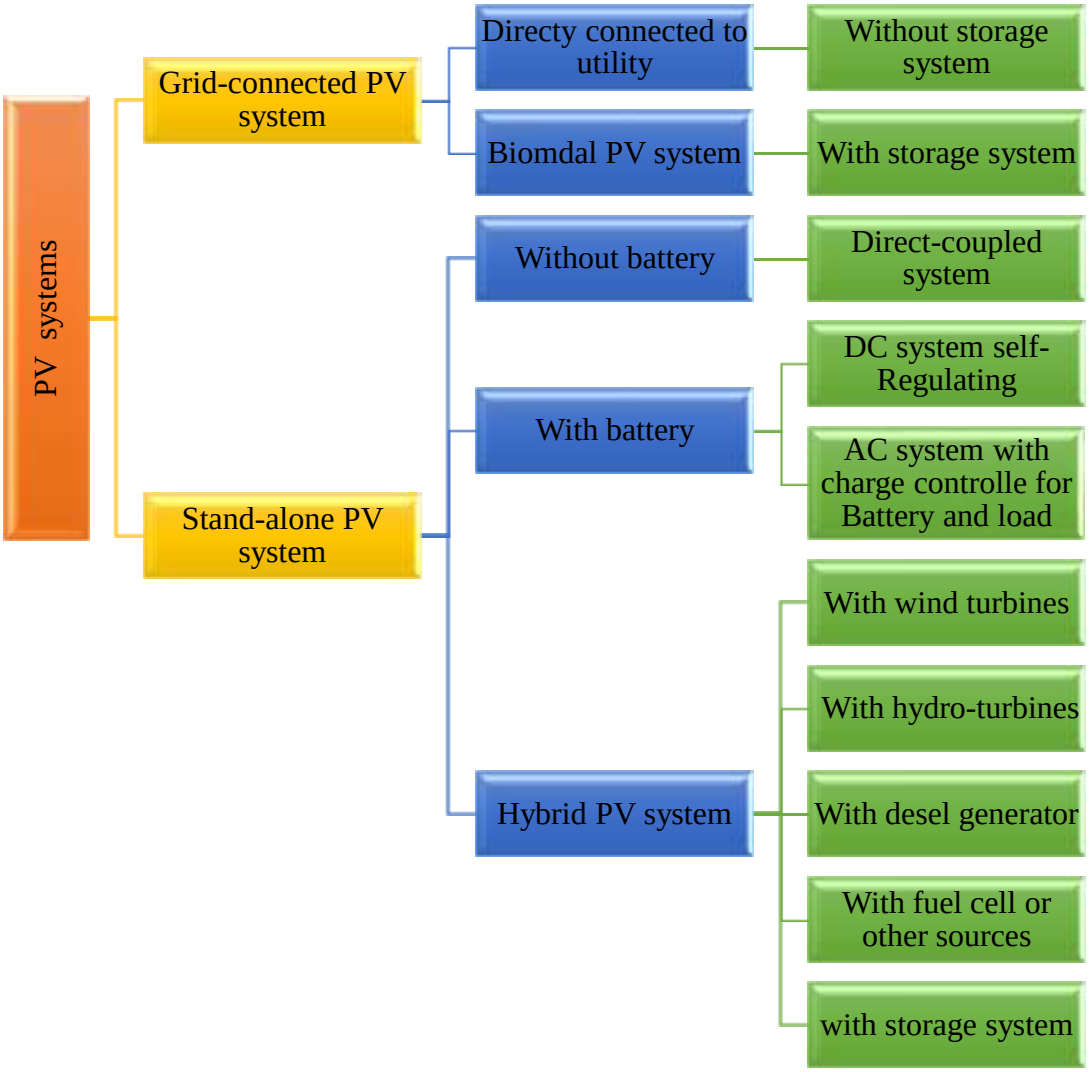


Figure I.4.Types of PV systems

I.3.3.1 Stand-alone systems

Stand-alone systems rely on solar power only. These systems can consist of PV modules and a load only or they can include batteries for energy storage. When using batteries charge regulators are included, which switch off the PV modules when batteries are fully charged and may switch off the load to prevent the batteries from being discharged below a certain limit. The batteries must have enough capacity to store the energy produced during the day to be used at night and during periods of poor weather [14].

Figure 1.5. shows schematically examples of stand-alone systems; (a) a simple DC PV system without a battery and (b) a large PV system with both DC and AC loads.

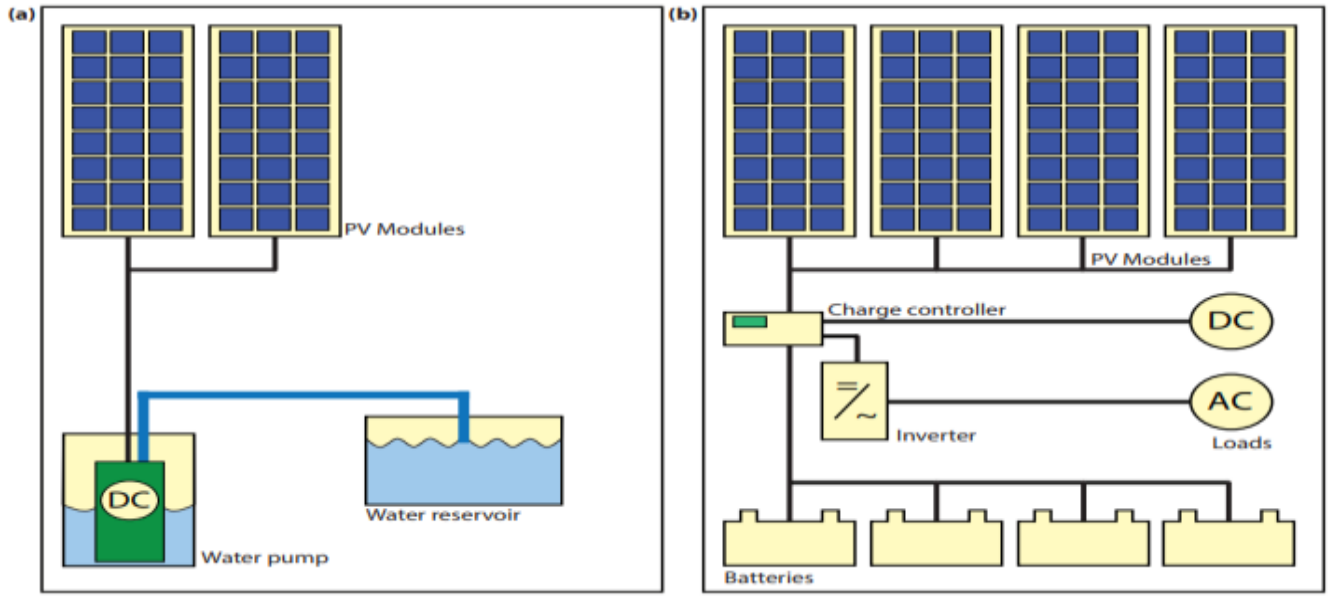


Figure I.5.Schematic representation of (a) a simple DC PV system to power a water pump with no energy storage and (b) a complex PV system including batteries, power conditioners, and both DC and AC loads [14]**.**

I.3.3.2. Grid-connected systems

Photovoltaic cells deliver direct current (DC) voltages. As the grid has alternating current (AC) voltage, the electricity from the PV cells must be converted to three-phase ac before being connected to the grid. This can be done using inverters.

In a DC-AC converter, several control regimes are usually implemented. Firstly, to control the factors previously mentioned, the DC-AC converter itself comprises control regimes. There exist a large number of algorithms for the schemes, which are not discussed in further detail here. Secondly, for a PV plant, often a maximum power point tracking (MPPT) is employed. [15]

There are several topologies for connecting PV modules to the grid in use today, and the most widely used are described below. The four first topologies are shown in Figure 1.6, and the last is shown in Figure 1.7:

a) Central configuration: PV modules are connected in several series connections, where each series is connected in parallel forming an array which is then connected to one common DC/AC converter. This is used for large PV plants with a large number of panels. Disadvantages of this setup are that DC cables with high voltage must be used between the modules and inverters, mismatches between the modules will have large effects, and the

MPPT and inverter control regimes in the DC/AC converter control the whole plant simultaneously

b) String configuration: Each series connection (string) of PV modules is connected to a separate DC-AC converter. this method decreases the impact of mismatch between modules and each string can be controlled separately

c) Multi-string configuration: A mixture of the two first topologies. Each string is connected to a DC-DC converter, and then a centralized **DC/AC** converter is used to connect to the grid. The control regimes can here be applied separately to each string by the **DC/DC** converters.

d) Individual or paired configuration: Similar to the multi-string configuration, there is a DC-DC converter connected either to each module or to two parallel connected modules. The solution with two modules on each DC-DC converter is used for modules that have high-rated power (either higher than 405 W or higher than 800 W, depending on the converter model). The modules are typically series connected to an inverter [16].

The DC-DC converter inhibits an MPPT tracker. It is also possible to buy PV modules with an integrated DC-DC converter. In Figure 1.6, only the individual setup is shown, but the paired setup is easily achieved by replacing the single PV module with two connected in parallel with the DC-DC converter. Several strings can also be connected to the DC-AC inverter

- **Modular configuration:** Each string is connected with a DC-DC converter to a common dc bus, where after AC-DC inverters connect the bus to the grid

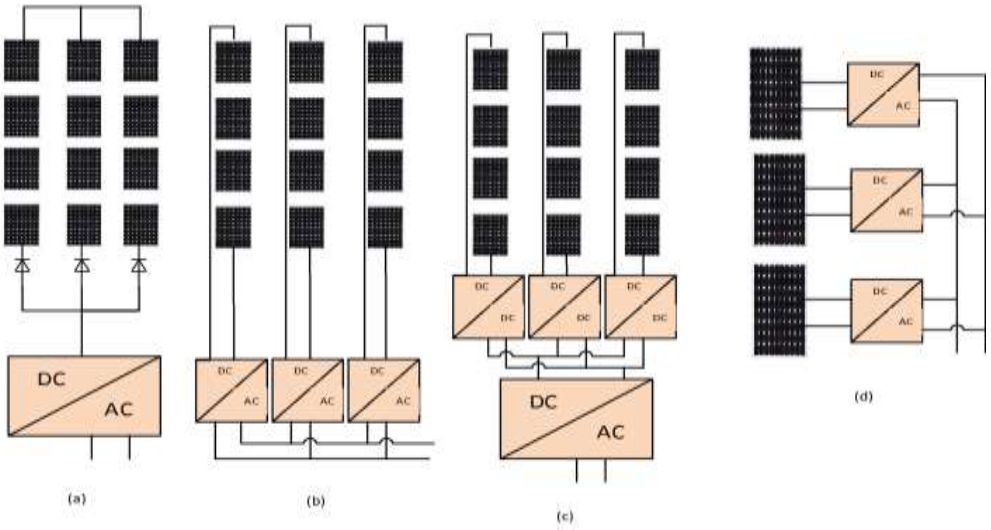


Figure 1.6: Grid-Connected PV System Topologies: (a): Centralized inverter topology. (b): String inverter topology. (c): Multistring inverter topology. (d): AC module inverter topology [17].

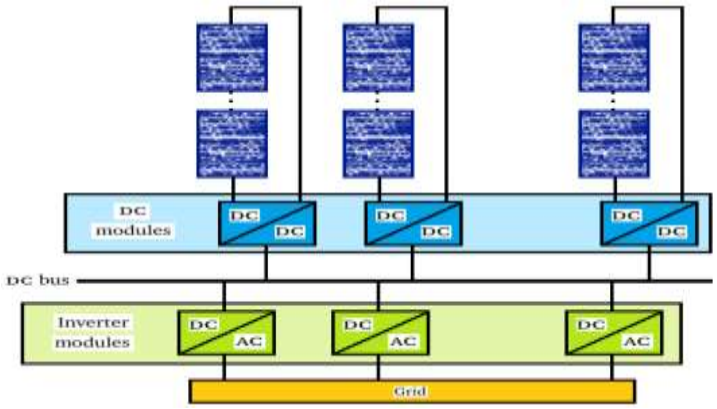


Figure 1.7: Modular topology for connecting PV systems to the grid [18].

I.3.4. Advantages and disadvantages of the photovoltaic system

I.3.4.1. Advantages of the photovoltaic system (VPS)

Photovoltaic technology has several advantages among which we find [19]:

- High reliability: The installation does not have moving parts that make it particularly suitable for isolated regions;
- The module of photovoltaic panels, simple has installed, adaptable, and can be sized for power up to megawatts;
- SPVs have a long lifespan and the cost of maintenance operations is very low; Photovoltaic systems have environmental benefits (non-polluting);
- SPVs operate efficiently in the event of a stand-alone installation by supplying homes and shopping centers.
- No transportation costs or risks compared to other energy sources.

I.3.4.2. Disadvantages of the photovoltaic system

The production of solar energy has some disadvantages [20]:

- The production of the photovoltaic module requires a high investment cost
- The actual conversion efficiency of a module is low, in the order of 5-25% with a Laboratory limit of 40% cell according to Guider Photovoltaic (http://photovoltaique.guidenr.fr).

- Photovoltaic generators are not competitive compared to diesel generators, but they become more profitable, especially in isolated areas where the transportation of fuel costs a fortune;
- Dependent on weather conditions that cause yield decline;
- The energy storage system is more expensive.

I.4. wind turbine generation

I.4.1. Definition of wind turbine

A wind turbine is a device that converts the kinetic energy from the wind into electrical energy. It typically consists of a tall tower with a rotor, which is comprised of two or three blades, that spins in response to the wind. The rotor is connected to a generator that produces electricity when the rotor spins. The electricity is then either used on-site or sent to the electrical grid to power homes and businesses. Wind turbines are a type of renewable energy technology that is used to generate clean, sustainable electricity.

I.4.2. History of Wind Uses

Wind as a source of energy has been in use by humans for many centuries and energy purposes date back five thousand (5000) years ago by sailing ships and boats used by the ancient Egyptians. Its use occurs through the conversion of kinetic energy into translational kinetic energy of rotation, using wind turbines to generate electricity, or windmills for mechanical work to pump water from deep wells [16]. The first windmill machines were also used around 2000 years B.C., in ancient Babylon and China, evolving since then to the modern wind turbines. In the Western world, the first application of windmills was the grinding of grain and pumping of water from deep wells [22].

The first modern wind turbine designed especially for electricity generation, was constructed in Denmark in the early 1890 for supplying electricity to rural areas. In the same period, a 12kW of power windmill was constructed in the United States of America (USA). It was a large wind electric generator with 17 meters' diameter of rotor and 144 wooden propellers [21].

The oil crisis in the 1970s sparked interest in wind energy in response to uncertainty about the price and availability of fossil fuels. The wind turbine technology research and development programs that followed this oil crisis during the last century, introduced significant improvements resulting in modern computer-controlled wind turbines, which brought new and more efficient ways of converting wind energy into useful mechanical or electrical power [23].

I.4.3. Types of wind turbines

wind turbines come in two basic configurations based on the direction of the rotating shaft (axis): horizontal axis and vertical axis. They range in size from very small machines that produce a few tens or hundreds of watts to very large turbines producing as much as 5 megawatts of power.

I.4.3.1. Horizontal axis wind turbines

Most wind machines being used today are the horizontal-axis type. Horizontal-axis wind machines have blades like airplane propellers. Horizontal axis wind turbines (HAWTs) predominantly have 2 or 3 blades or a large number of blades. The latter is described as high-solidity devices and includes the multi-blade wind turbines used for water pumping on farms. In contrast, the swept area of wind turbines with 2 or 3 blades is largely void: only a small fraction of this area appears to be solid. These are referred to as low-solidity devices [24].

We can distinguish between wind turbines whose propeller is upstream about the wind, "propeller upwind" (Fig.1.7a), and those whose propeller is downstream concerning the wind, "propeller downwind". (Fig.1.7. b).

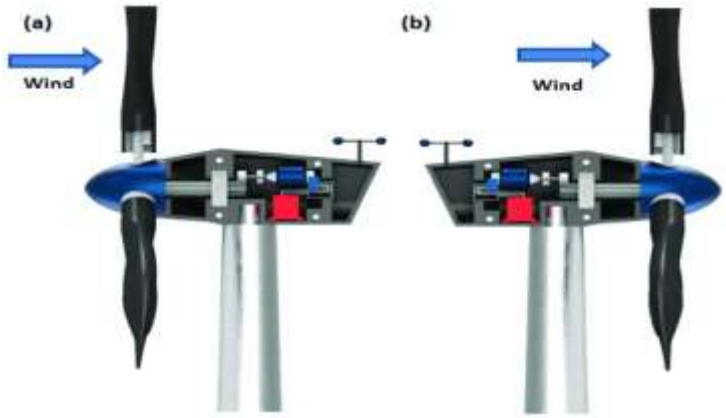


Figure 1.8. (a) Upwind HAWT (b) Downwind HAWT

Upwind turbines, on the other hand, require somewhat complex yaw control systems to keep the blades facing the wind. In exchange for that added complexity, however, upwind machines operate more smoothly and deliver more power. Most modern wind turbines are of the upwind type.

Wind turbines with many blades operate at much lower rotational speeds than those with fewer blades. As the rpm of the turbine increases, the turbulence caused by one blade affects the efficiency of

the blade that follows. With fewer blades, the turbine can spin faster before this interference becomes excessive. And a faster spinning shaft means that generators can be physically smaller in size [25].

I.4.3.2 Vertical axis wind turbines

Vertical axis wind turbines (VAWTs) have blades that go from top to bottom. The most common types of these turbines are Savonius and one of the most popular in the world market, Darrius. These turbines can harness winds from any direction without the need to reposition the rotor when the wind direction changes [26].

The blades of a Darrius VAWT have a curved shape and this likes a shape taken by a spinning rope. This shape is a structurally efficient one, but the unusually shaped blades are difficult to manufacture, transport and install. To overcome these problems, straight-bladed VAWTs have been developed: these include the H-type vertical axis and V-type vertical axis wind turbines [24].



Figures I.9. Darrius-type VAWTs and H-type VAWTs

I.4.4. Main parts of a wind turbine

A wind turbine consists of the following four main parts: the base, tower, nacelle, and blades, as shown in figure.I.10. The blades capture the wind's energy and spin a generator in the nacelle. The tower contains the electrical circuits, supports the nacelle, and provides access to the nacelle for maintenance while the base is made of concrete and steel and supports the whole structure.

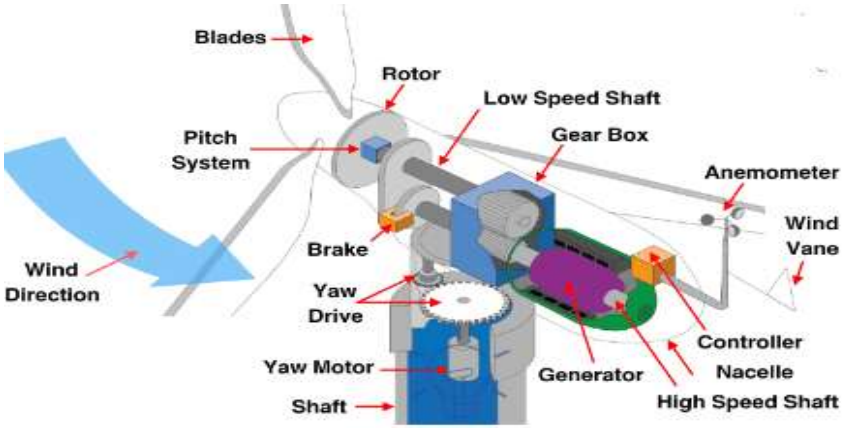


Figure.I.10: Main parts of a wind turbine [26].

I.4.5. Advantages and disadvantages of wind turbines

I.4.5.1. Advantages

- Wind energy is a renewable energy, unlike fossil fuels.
- Wind energy is clean energy. It has no harmful impact on the environment like other energy sources that have caused a drastic change in the climate through the enormous and direct production of CO2.
- Wind energy does not present any risk and does not produce radioactive waste, unlike nuclear energy.
- The mode of operation of wind turbines and the possibility of stopping them at any time gives them the advantage of having a good yield, unlike the continuous modes of operation of most thermal and nuclear power plants.

I.4.5.2. Disadvantages

- The stochastic nature of the wind influences the quality of the electrical power produced, which is a constraint for network managers.
- The cost of wind energy remains higher than other conventional energy sources, especially on less windy sites.
- Noise: It has been significantly reduced due to progress in Multipliers.

I.5. Topologies and development of wind turbine generators

In the 1980s, wind turbine technology started with tens of kW but today it has undergone a significant evolution, and now wind turbines exceed 10 MW. This evolution leads to price variation and multiple choice for different types of generators [27].

In general, the turbines are divided into two types according to their axis of rotation (vertical or horizontal). Those with a vertical axis, do not need orientation following the direction of the wind and turn at a low speed with a high starting torque [28].

Horizontal axis turbines, having two or three blades, generate more power. The orientation of their mechanical system is not necessary.

The change in the direction of the wind causes oscillations that influence their generator. There are several electric generators such as (IG, DFIG, PMSG, and SG) [29].

- **Doubly Fed Induction Generator (DFIG):** the latter has a stator connected directly to the electrical grid via an isolation transformer and converter control. Rotor resistance can influence the voltage stability of the system [30]. Wind variation causes a reduction in energy production. Its rotor is connected to a converter of voltage source type power and has decoupling capability. This converter is controlled by controlling the active and reactive powers to facilitate the flow to the grid [31].
- **Synchronous generator:** this generator has a magnetic field that can be generated by magnets or by an excitation circuit, which imposes a synchronism field. However, the existing types of rotors are wound rotors with smooth poles, salient poles, and permanent magnets. These are the most popular in offshore parks.

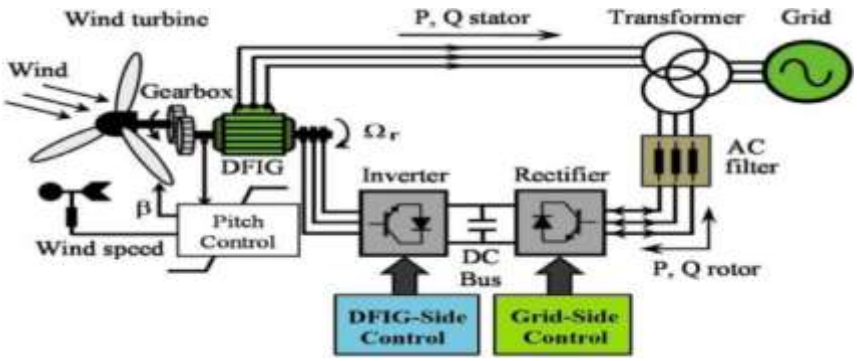


Figure.I.11. DFIG wind turbine connected to the grid

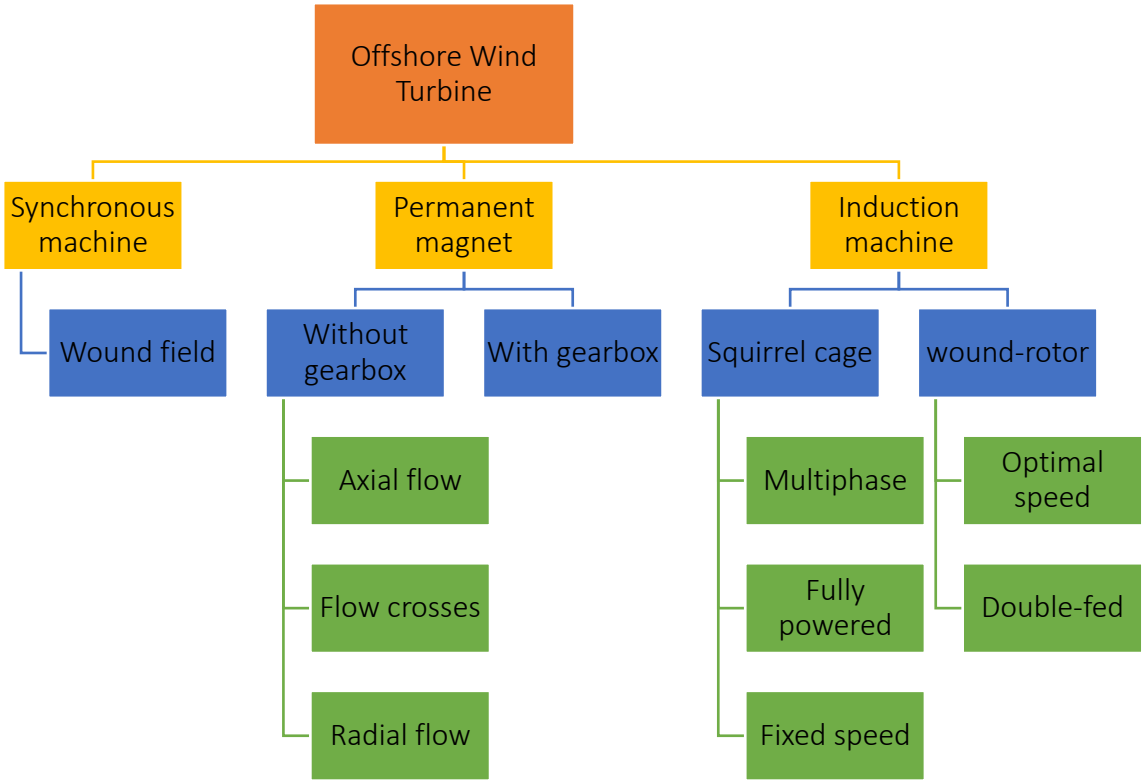


Figure.I.12. Different offshore wind turbine machines [32]

I.5.1. Synchronous machine (SM)

This machine has variable speeds that range from 0 to 100% nominal speed. The machines are listed below:

I.5.1.1. Wound rotor machine (WRSG):

contains high numbers of poles and the rotor rotates at low speeds. It requires installing the excitation circuit and this will reduce efficiency, increase manufacturing and operating costs, and also make modeling and its study very complicated.

Two types of excitation circuits are used:

- The excitation circuit with static converters (addition converters)
- The excitation circuit of the inverted synchronous machine (eliminates rings/brushes).

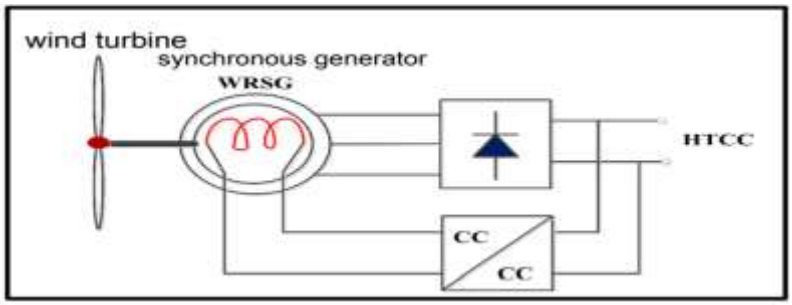


Figure.I.13. Wind turbine diagram and system structure power conversion WRSG

I.5.1.2. The permanent magnet synchronous generator:

This machine has become a very interesting solution in recent years for small and large wind turbine applications. It is important to use a high number of pole pairs to avoid gear boxing to reduce mechanical losses [33]. Moreover, the disadvantage of this machine is the variation of the magnetic characteristics of the rotor and the very high cost of the magnets.

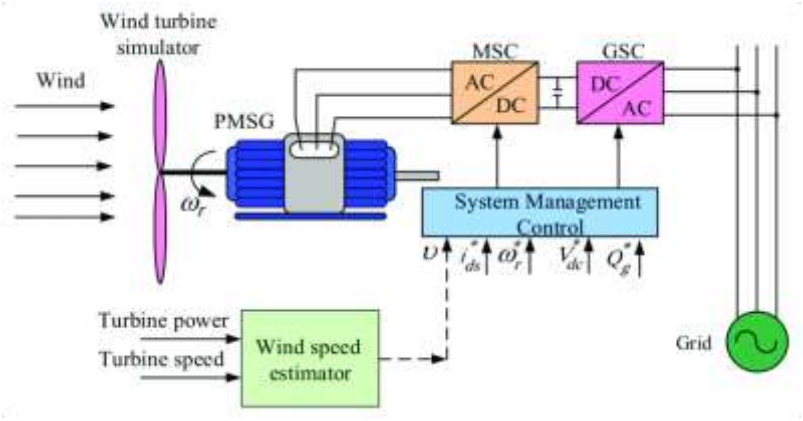


Figure.I.14: Diagram of wind turbine and power conversion system structure of PMSG

I.5.2. Induction Generator

The Induction Generator must be supplied with current to create the magnetic field. It is necessary for the operation of the generator. However, it is possible to operate an Induction Generator in an autonomous system if it has been connected to the capacitors which supply the current necessary for the magnetization. Otherwise, you need a battery and electronics power or a small diesel generator to start the system. The different machines are listed below[32].

I.5.2.1.Squirrel Cage Induction Generator (SCIG)

Figure I.14. shows the generator which operates at a low-speed range and can be accommodated by using a gearbox between the turbine and the generator to provide rated power.

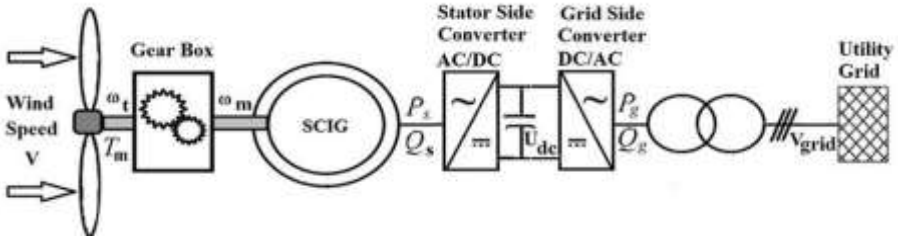


Figure I.15: diagram representation of the squirrel cage induction generator (SCIG)-based wind energy conversion (WEC) system.

I.5.2.2. Doubly Fed Induction Generator (DFIG):

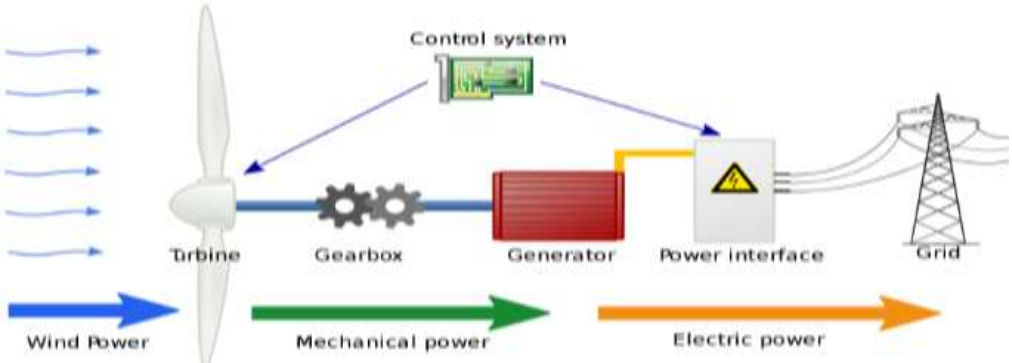
Allows variable-speed operation by adjusting the rotor speed of the generator according to that of the wind. The power factor can reach 30% of the rated power.

I.6. Fixed and Variable Speed Wind Turbine

The wind turbine can operate in two modes: fixed speed or variable speed. Both types of operation can be used onshore and offshore. The paragraphs below summarize the operation, the advantage, and the disadvantage of each mode

I.6.1. Fixed-speed wind turbine directly connected to the offshore station

The generator in Figure I.16 is connected to the converter at the offshore station through a transformer. The wind turbine uses an automatic control system to ensure that it is almost constantly rotating, regardless of the wind speed. In addition, it automatically locks in case of strong wind speed.



Figurer.I.16: Principle diagram of wind turbine connected to the offshore station

I.6.2. Variable speed wind turbine

Variable speed has some attractions but also brings cost and reliability concerns. The turbine was seen as a way of the future, with cost reductions and performance improvements expected in variable speed drive technology. The current trend towards variable speed in new large wind turbines is related to greater operational flexibility and power quality concerns. To optimize the power according to the wind speed, it is possible to adjust the speed of rotation in the wind. The main idea is to choose a generator with a fixed frequency and variable speed.

The variable speed generator allows operation over a wide range of winds, to recover the maximum power. At present, electromagnetic conversion in wind power plants is mainly carried out by synchronous or asynchronous generators.

Recently, wind power stations are closely dependent on wind speed. Considering the instability of the wind, the main advantage of speed variation is to produce power independent of wind speed with MPPT capture by controlling the power delivered with very high efficiency, but the disadvantage of this mode is the need for a power converter.

I.7. Standards for the interconnection of electrical energy sources on the Grid

One of the major challenges that hinder the development of renewable energies is related to the integration of the energy produced within the electrical networks. The interconnection of different energy sources on electrical networks is, therefore, a matter of concern, because the electrical networks were designed beforehand without taking into consideration that there could be the installation of renewable energies.

To maintain the reliability of electrical networks, there is a set of standards governing the interconnection of different energy sources on electrical networks. These standards were drafted by organizations related to the quality of distributed electrical current and the performance of the grid, as well as the safety of people [34].

We will present below the norms and standards to which energy producers must comply to meet the requirements that may allow them to integrate the electrical networks.

Because of the multiplicity of standards on the interconnection of the electricity grid, In this section, we will present those drafted by international organizations, while describing the content that

mainly presents the standards of interconnections to the network, as well as the standards related to the quality of energy in terms of harmonic content.

I.7.1 Interconnection Standards

The IEEE (Institute of Electrical and Electronics Engineers), NFPA (National Fire Protection Association), and UL (Underwriters Laboratories) are three interconnecting organizations [34]

All of the standards drafted by these organizations refer to network performance, security, and the quality of the energy that must circulate in the networks. They can therefore be presented as follows:

- **IEEE 1547 standards**

  This series of standards contains technical requirements that guarantee the performance of electrical networks by setting requirements related to the use, testing, safety, and maintenance of connection points (IEEE 1547, 2003). It is made up of the draft standards presented below:
- **PIEEE 1547.3**:Draft guide for monitoring, information exchange, and control of alternative energy sources interconnected to power grids. It describes the functionalities, the variables as well as the methodologies for the monitoring, the exchange of information as well as the control of the alternative energy sources connected. to the distribution network (IEEE 1547.3).
- **PIEEE 1547.4:** Draft guide for the design, operation, and integration of alternative energy sources. It is mainly used by designers of electrical networks, operators, and equipment manufacturers. This document presents an overview and the problem of integrating decentralized energy sources (IEEE 1547.4)[32].

I.7.2. UL standards (Underwriters Laboratories)

UL has published standards for the use of alternative sources connected to electrical grids. They mainly regulate converters and interconnection equipment.in"Integration of Alternative Sources of Energy, 2006", presents a summary of the UL standard series [34].

I.7.3. Standards related to power quality in terms of harmonic content

There are mainly two international standards that are related to power quality in terms of harmonic content. The IEC 61000-4-7 (IEC, 2002) standard establishes standard techniques for the evaluation of harmonics and inter-harmonics to facilitate interpretation independently of the instruments used to evaluate them[32].

I.8. Conclusion

The chapter provided insights into different types of hybrid systems, including grid-connected hybrids and standalone hybrids. Grid-connected hybrid systems enable the seamless integration of solar and wind energy into existing power grids, leveraging their combined benefits to meet electricity demand and contribute to a greener energy mix. The historical background showcased the evolution of hybrid systems, highlighting significant advancements in technology, increased efficiency, and cost reductions over time. Since their inception, hybrid systems of solar energy and wind energy have demonstrated their potential to contribute to a cleaner and more sustainable energy future.

Chapter II:

Modeling and control of photovoltaic systems

II.1. Introduction

An essential aspect of PV systems is their ability to efficiently convert sunlight into usable electrical energy. Achieving high conversion efficiency requires not only advanced solar panel technologies but also effective system design and control strategies. This is where modeling and analysis play a crucial role in understanding and optimizing the performance of PV systems.

In this chapter, we will focus on the modeling and analysis of a PV system and a specific component known as the boost converter. The PV system model encompasses various elements, including solar panels, inverters, MPPTs, and energy storage, and it is essential to accurately represent their behavior in mathematical equations and simulations

II.2. PV SYSTEM MODELING

The PV system is a set of regularly installed equipment forthe exploitation of solar energy under changes the atmospheric conditions (ambient temperature, sunshine). It consists of a PV generator connected to a load via a DC-DC Boost converter mediator controlled by an MPPT controller, which follows straight the maximum power point (MPP) conformable to the maximum efficiency. Fig II.1 represents thesynoptic structure of a photovoltaic energy production system

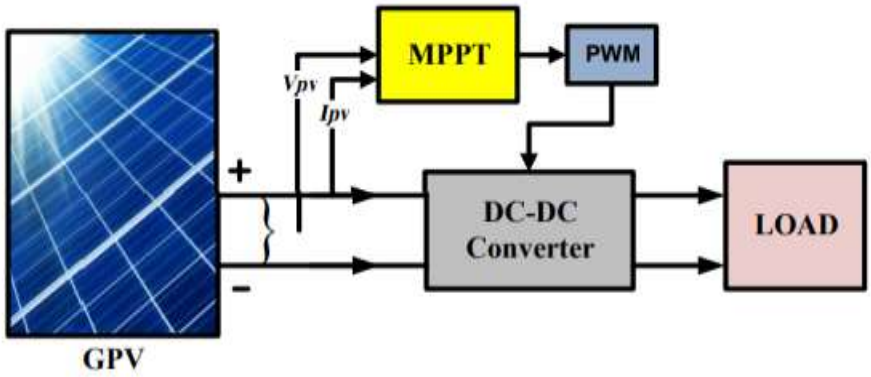


Figure II.1 Synoptic structure of a photovoltaic energy production system.

II.2.1. PV Generator (GPV)

The PV generator is the fundamental element in a photovoltaic system which consists of several PV cells connected in series and parallel format to provide the desired output voltage and current. The PV cell is the basic element of a PV generator which converts solar irradiation into electrical energy. The most widely used model for its simplicity and accuracy is that of a diode, this is illustrated in Figure II.2 [35].

A cell series resistance R_s is attached in series with a parallel combination of cell photocurrent Iph, the exponential diode D, and shunt resistance Rsh. Ipv, and Vpv are the PV cell's current and voltage respectively [36].

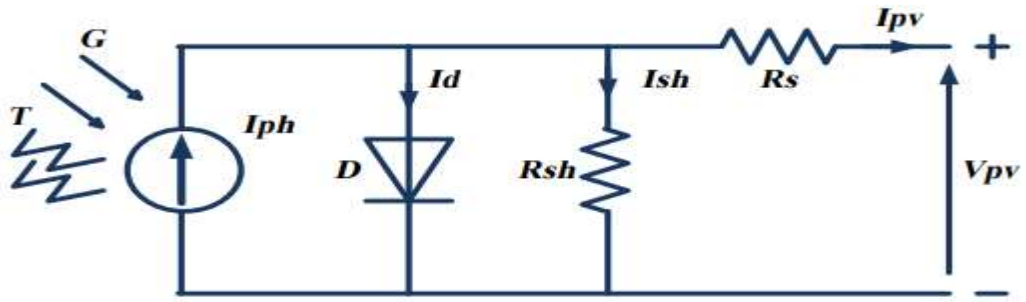


Figure II.2 Equivalent model of the PV cell.

In general, the output current of a photovoltaic cell is put in the following mathematical form:

$$I_{PV} = I_{ph} - I_d - I_{sh} \qquad (II.1$$

With:

- I_{pv}: represents the output current provided by the solar cell.
- I_{ph}: represents the current generated by the solar cell when exposed to the light of the sun.
- I_{sh}: represents the current flowing through resistance R_{sh}.
- I_d: represents the current of the diode,

Module photo-current, I_{ph}

$$I_{ph} = [I_{sc} + K_i(T - 298)] * \frac{I_r}{1000} \qquad (II.2)$$

Where:

I_{ph}: photo-current (A)

I_{sc}: short circuit current (A): a current obtained when array terminals are short-circuited

Ki: short-circuit current temperature coefficient of the cell at 25 °C and $\frac{1000\ W}{m^2}$

T: operating temperature (K)

Ir: solar irradiation (W/m^2)

Module the current of the diode:

$$I_d = I_0 \left[\exp\left(\frac{q(V_{PV} + R_s I_{PV})}{AKT} \right) - 1 \right] \quad (II.3)$$

Module reverse saturation current, I_{rs}:

$$I_{rs} = \frac{I_{sc}}{e^{(qV_{oc}/N_s kAT)} - 1} \quad (II.4)$$

Where:

q: electron charge =1,6.10-19 C

Voc: open circuit voltage (V)

Ns: number of cells connected in series;

A: the ideality factor of the diode =1.6;

K: Boltzmann's constant $= 1.3805 \times 10^{-23}$ J/K

T: is the temperature of the cell (in kelvin).

The module saturation current, I_0

It varies with the cell temperature, which is given by:

$$I_o = I_{rs} \left(\frac{T}{T_r} \right)^3 \left[e^{\frac{qE_{go}}{Ak}\left(\frac{1}{T} - \frac{1}{T_r}\right)} \right] \quad (II.5)$$

Where:

Tr: nominal temperature $= 298$ K

Eg0: band gap energy of the semiconductor $= 1.1$eV

The current of the PV cell can then be written in the form:

$$I_{PV} = I_{ph} - I_0 \left[exp\left(\frac{q(V_{PV} + R_s I_{PV})}{nKT} \right) - 1 \right] - \frac{(V_{PV} + R_s I_{PV})}{R_{sh}} \quad (II.6)$$

In general, a photovoltaic generator is composed of several PV cells connected in series and parallel. Moreover, the "current-voltage" characteristic equation of the equivalent circuit for a photovoltaic panel, arranged in parallel cells Np and series Nss, can be defined using the following two equations

$$I_P = N_P I_{pv} \quad (II.7)$$

$$V_P = N_S V_{pv} \quad (II.8)$$

With I_P and V_P are, respectively, the output current and the output voltage supplied by the solar panel. So the current equation becomes as follows:

$$I_{PV} = N_P I_{ph} - N_p I_0 \left[\exp\left(\frac{q\left(V_{PV} + \frac{N_s}{N_p} R_s I_{PV}\right)}{N_s A K T} \right) - 1 \right] - \frac{\left(\frac{N_s}{N_p} V_{PV} + R_s I_{PV}\right)}{R_{sh}} \quad (II.9)$$

II.2.2. Design the PV array solar

- To produce high power capacity in the PV system, a series and parallel combinations of a PV module will be used [32].
- 1Soltech (1STH-215-P) module will be used in this work. This module has the specifications as presented in Table:

Table II. 2 PV Module Parameters

Parameters	Value
Rated Power (W)	213.15
The voltage at maximum power point Vmp (V)	29V
Current at maximum power point Imp (A)	7.35A
Open circuit voltage Voc (V)	36.3V
Short-circuit current Isc (A)	7.84A
Number of cells	60
Series resistance(Rs)	0.39383Ω
Parallel resistance (Rsh)	313.399Ω

- To produce 100 kW power capacity, 47 series, and 10 parallel modules will be required.
  Rated power (PV array) $= P = 47^{*}10^{*}P_{mp} = 47^{*}10^{*}213.13 = 100.2$ kW.
  Output voltage (PV array) $= V_{mp} *$ Number of parallel module $= 29 * 10 = 290$ V

II.2.3. characteristics of the PV module

Therefore, the I-V and P-V characteristics of this module at a fixed temperature of 25°C and an irradiation of 1000 W/m2 are illustrated in Figure II.7.

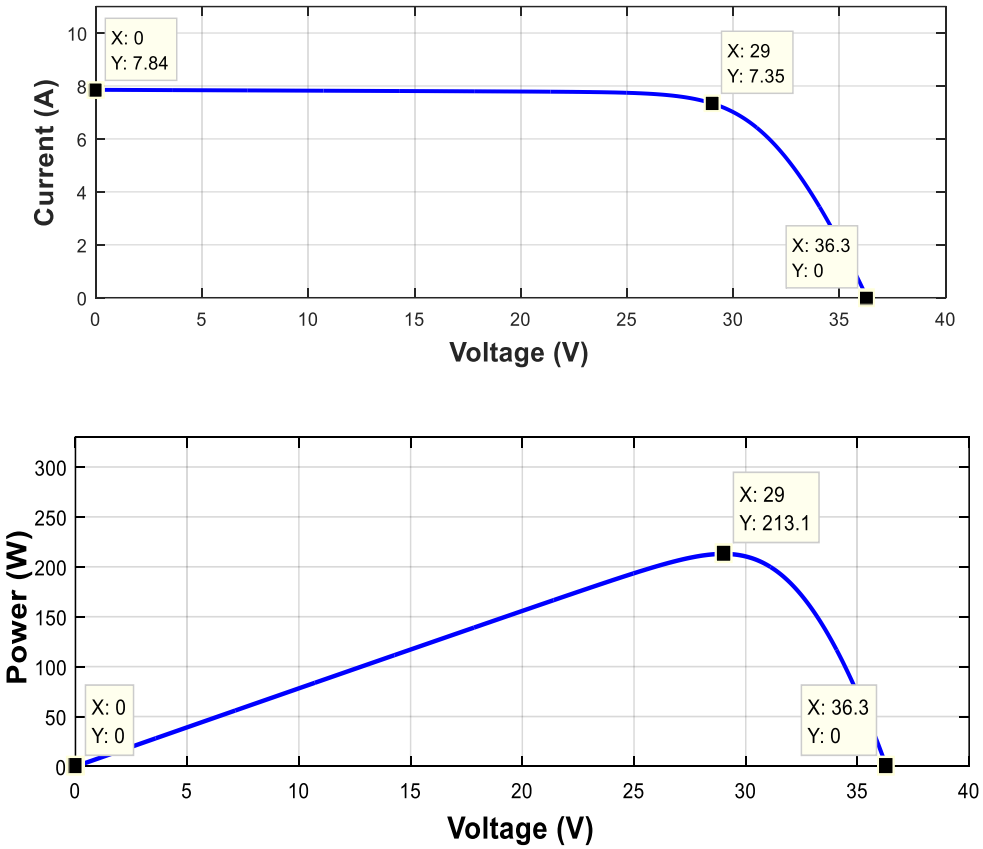


Figure II.3. I_V and P_V characteristics of the PV module offered at 25°C and 1000W/m2

To generate photovoltaic power suitable for injection into the electrical grid, the modules will simply be connected in series and in parallel to form a photovoltaic panel, which will increase the open circuit voltage of the string. So, to obtain a power of 100KW, 47 strings are connected in parallel and each string contains 10 modules connected in series.

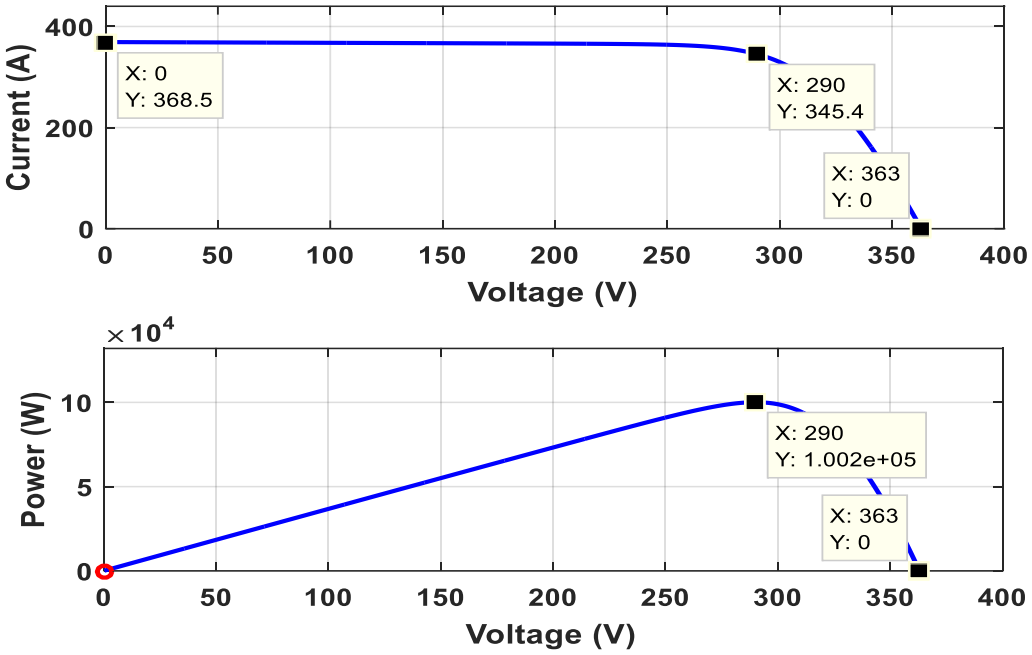


Figure II.4.I-V and P-V characteristics of PV panel at 25°C and 1000W/m2

To study the sensitivity of the panel against the variation of solar irradiation and temperature, the PV panel model is simulated under a constant temperature and different values of irradiation, then, at constant irradiation and different values of temperature.

II.2.4. Influence of irradiation and temperature on the I(V) and P(V) characteristics of (PVG)

II.2.4.1. The effect of irradiation

Figures (II.5) and (II.6) respectively represent the characteristics (I-V) and (P V) of an Array type: 1Soltech 1STH-215-P;10 series modules; 47 parallel strings, for different values of irradiation, at a constant temperature of 25°C**.**

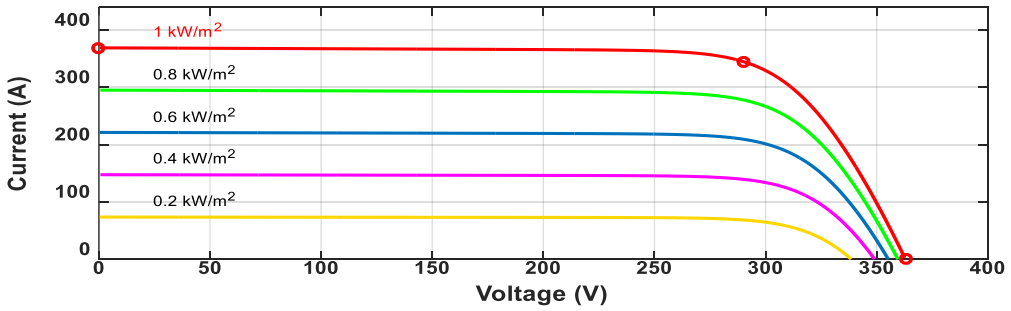


Figure II.5. Influence of irradiation variation on the I-V characteristic at a constant temperature

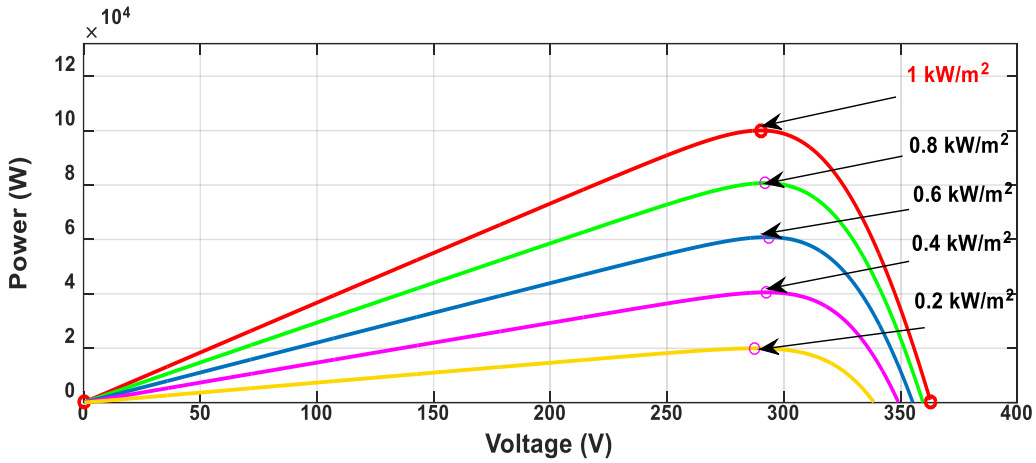


Figure II.6. Influence of irradiance variation on the P-V characteristic at a constant temperature.

The photocurrent created in the PV module is proportional to the incident solar flux, which explains the strong influence of illumination on the current delivered by the PV module. This influence increases the power available in the PV modules. Each time the illumination increases. and to each of the luminous flux values corresponds the maximum electrical power that a PV module could supply.

II.2.4.2 The effect of temperature

Figures (I.15) and (I.16) respectively represent the (I-V) and (P V) characteristics of an Array type: 1Soltech 1STH-215-P;10 series modules; 47 parallel strings, for different temperature values, at a constant illumination equal to 1000KW/m2

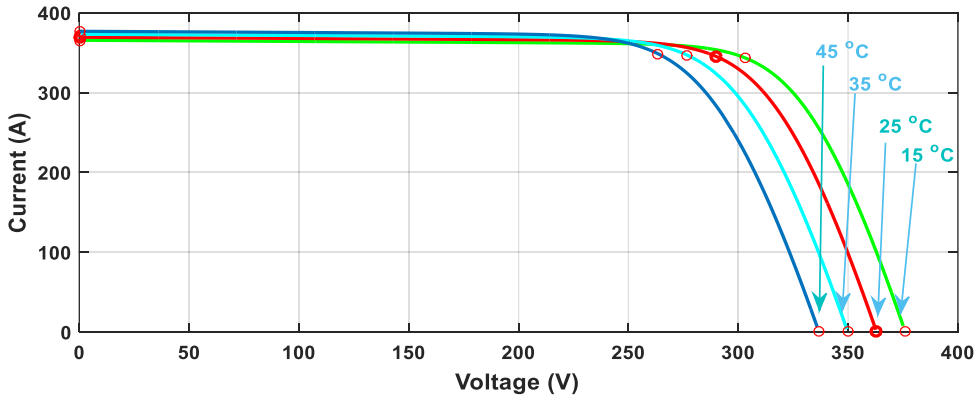


Figure II.7. Influence of temperature on I_V characteristic

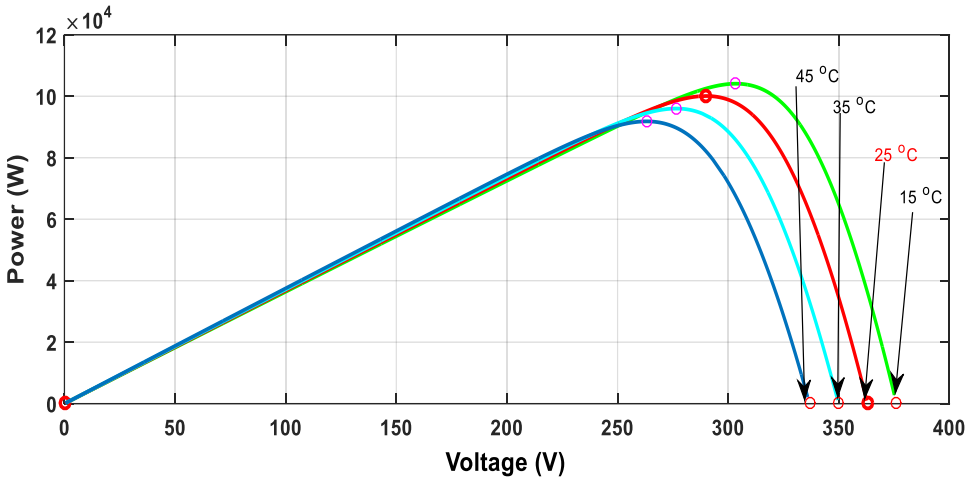


Figure II.8. Influence of temperature on P_V characteristic

An increase in temperature causes a decrease in the open circuit voltage and also results in a decrease in the maximum power available in the PV module.

II.3. "Boost Converter" step-up chopper

A 'Boost' converter, or parallel chopper, is a switching power supply that converts a DC voltage into another DC voltage of a higher value. This type of converter can be used as a source-load adapter when the operating point in direct coupling is to the right of the MPPT

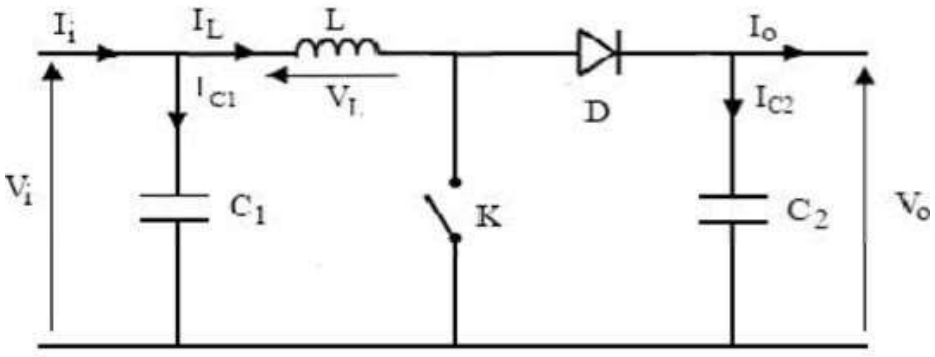


Figure II.9. Circuit diagram of a Boost chopper

Figure (II.9) shows the electrical circuit diagram of a Boost converter. Its typical application is to convert its input voltage to a higher output voltage [38].

II.3.1. Operation Boost converter:

When the switch is closed for the duration, the current in the inductor increases linearly. The voltage across K is zero. During this time, the switch opens and the energy stored in the inductance controls the current flow in the diode-free wheel D. By writing that the voltage across the terminals of the inductor is zero, we arrive at $V_0 (1 - \alpha) = V_i$

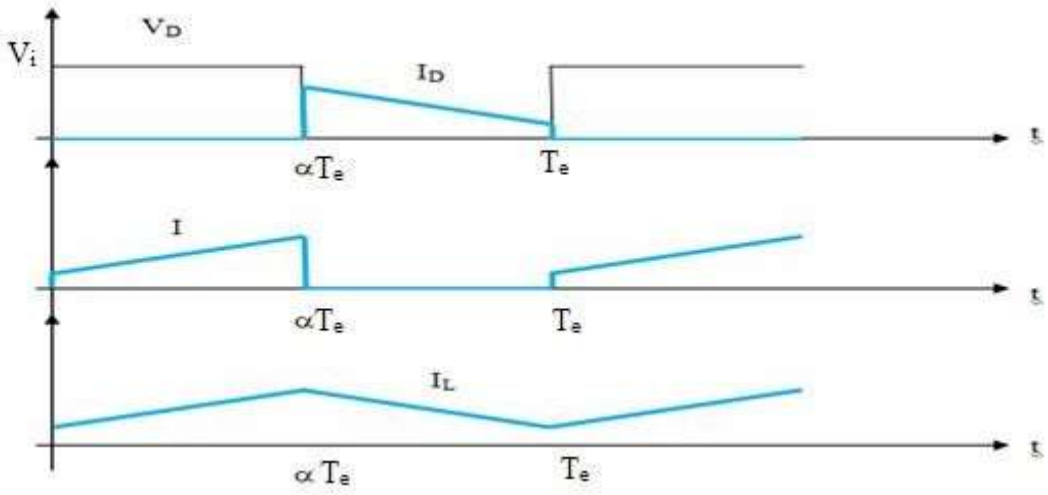


Figure (II.10): Current and voltage timing diagrams of a boost chopper.

II.3.2. Equivalent mathematical model:

To be able to synthesize the functions of the boost chopper in the steady state, it is necessary to present the equivalent diagrams of the circuit at each position of the switch K. of the figure (II.11) presents the equivalent circuit of the boost when K is the operating point in direct coupling is on the right of the closed MPPT i.e. of [0, DTe] [38].

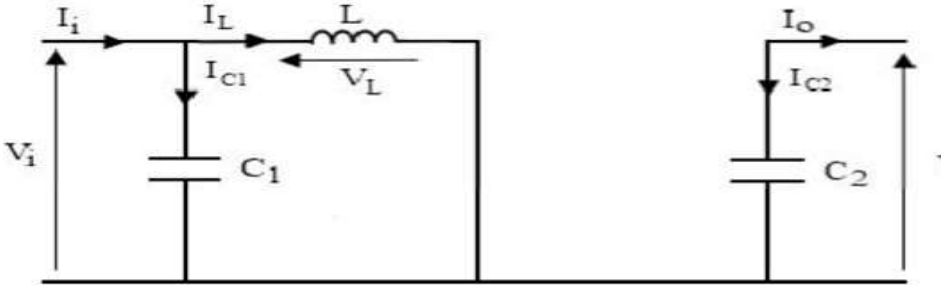


Figure II.11. Circuit diagram of a closed Boost chopper

The application of Kirchhoff's laws on equivalent circuits gives the following calculations:

$$\mathrm{I_{c1}}(t) = C_1 \frac{dvi(t)}{dt} = I_i(t) - I_L(t) \qquad (\mathrm{II.10})$$

$$\mathrm{I_{c2}}(t) = C_2 \frac{dv0(t)}{dt} = -I_0(t) \qquad (II.11)$$

$$\mathrm{V_L}(t) = L \frac{dIL(t)}{dt} = V_i(t) \qquad (II.12)$$

The open state of the switch K, the circuit equivalent to the operation of the Boost is as follows:

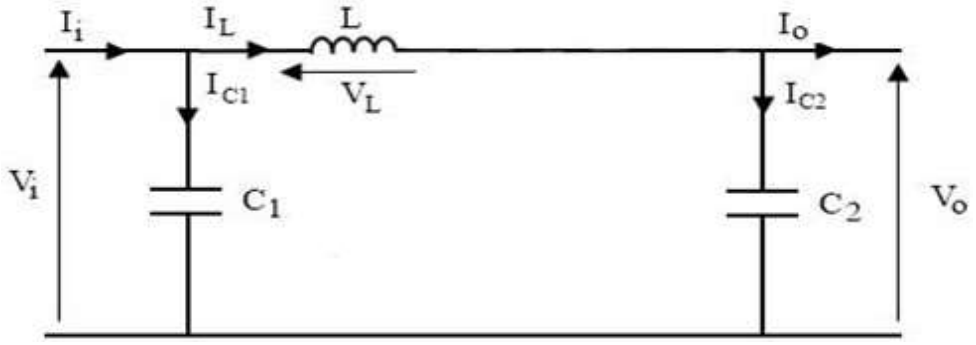


Figure II.12. Circuit diagram of an open Boost chopper

$$\mathrm{I_{c1}}(t) = C_1 \frac{dVi(t)}{dt} = I_i(t) - I_L(t) \qquad (\mathrm{II.13})$$

$$I_{c2}(t) = C_2 \frac{dV0(t)}{dt} = I_i(t) - I_0(t) \qquad (II.14)$$

$$\mathrm{V_L}(t) = L \frac{dIL(t)}{dt} = V_i(t) - V_0(t) \qquad (II.15)$$

The input and output voltages and currents of the boost converter can be written as:

$$\frac{V_{out}}{V_{in}} = \frac{I_{in}}{I_{out}} = \frac{1}{(1-D)} \qquad (II.16)$$

Where:

$Vout$: is the output voltage,

Vin : is the input voltage

D: is the duty cycle which is the ratio between the time within which the IGBT.

II.3.3. Calculation of Boost Converter:

II.3.3.1. Selection of inductor (L):

The value of the inductor is chosen based on the estimated inductor ripple current at the maximum the input voltage, presented by equation (7) [39]:

$$L = \frac{V_{\mathrm{in}}\,(V_{out} - V_{\mathrm{in}})}{\Delta IL * f_s * V_{out}} \qquad (\mathrm{II.17})$$

Where:

Vout: DC-DC converters output

fs: The switching frequency

ΔIL: input current ripple =I_0ripple*Io*(Vout/Vin)

Io=Po/Vout

II.3.3.2. Selection of capacitor (C):

The capacitor value is calculated by the variation in output voltage or ripple given in equation [39]:

$$C = \frac{I_o(V_o - V_{in})}{f_s^* \Delta V_o * V_o} \qquad (II.18)$$

Where:

ΔV: Output voltage ripple=Vout*0.5/100

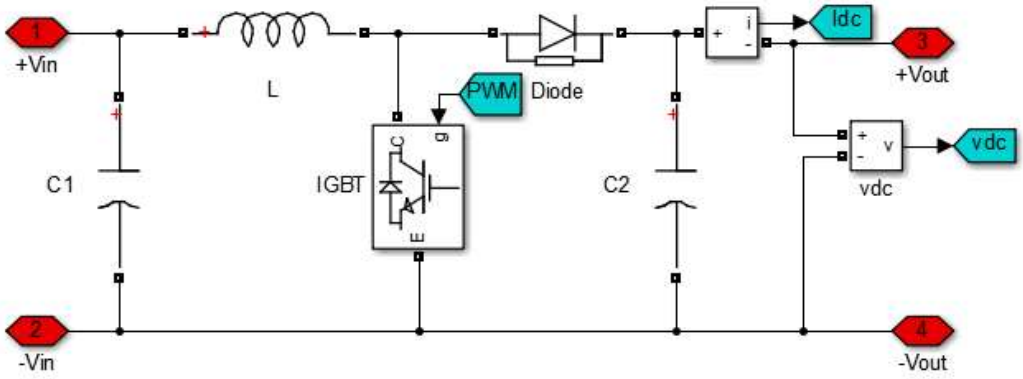


Figure II.13. Boost chopper simulation scheme

II.4. Maximum Power Point Tracking (MPPT)

Photovoltaic systems require control algorithms to extract the maximum power MPPT (Maximum Power Point Tracking) available. This power varies with the irradiation rate and the temperature [32].

The purpose of the MPPT is to constantly maintain the operation of the PV system around the maximum point of instantaneous power even under changing atmospheric conditions.

II.4.1. Principle of MPPT

By definition, an MPPT control, associated with an intermediate adaptation stage, makes it possible to operate a PV generator to permanently produce the maximum of its power. Thus, whatever

the meteorological conditions (temperature and illumination), the control of the converter places the system at the maximum operating point (Vmpp, Impp) [40].

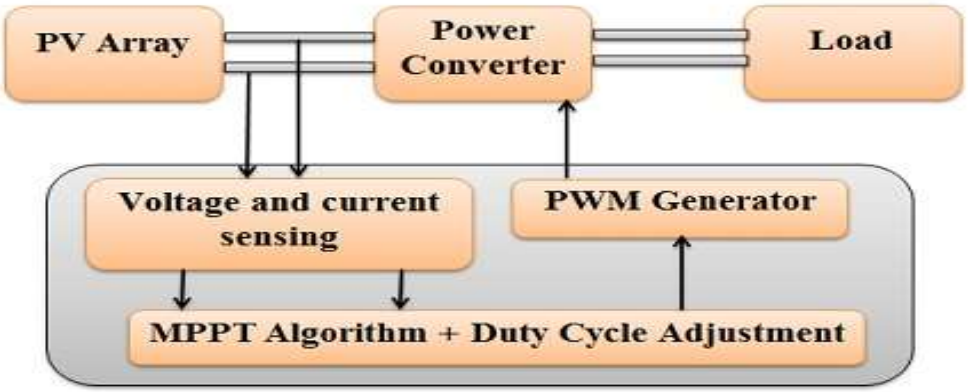


Figure II.14 Solar energy conversion chain including MPPT control

- **Maximum power point (Pmax):** is the point M (Vopt, I opt) of the figure (II.11) where the power dissipated in the load is maximum

$$P_{Max} = I_{opt} \times V_{opt} \qquad (II.19)$$

With:

Vopt: The optimal voltage.

Iopt: The optimal current.

- **Maximum efficiency:** the ratio between the maximum power and the power at the input of the solar cell

$$\mu = \frac{P_{max}}{P_{in}} = \frac{V_{opt} \times I_{opt}}{A_{pv} \times Ir} \qquad (II.20)$$

With:

Ir: irradiation which represents the light power received per unit area (W/m2).

Apv**:** Effective cell area.

The standardized test conditions for solar panels are characterized by instantaneous radiation of 1000W/m2 at an ambient temperature of 25°C and a spectrum AM of 1.5. AM represents the Air

Mass which is the thickness of the atmosphere that the light must penetrate. These conditions are called STC.

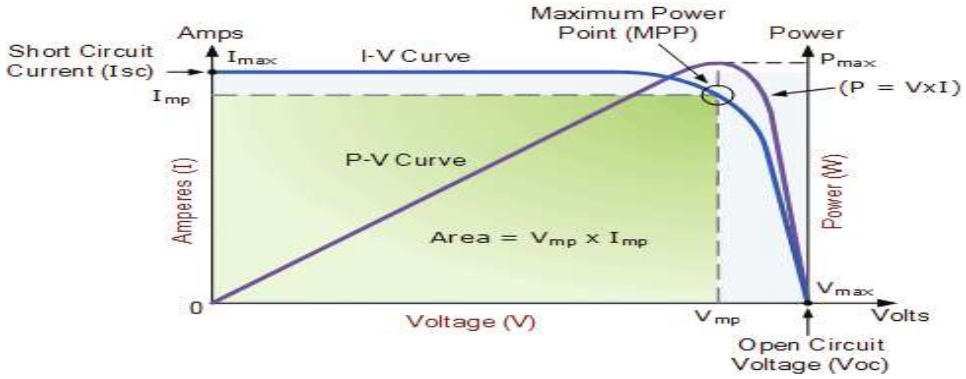


Figure II.15 Principe de la commande MPPT

II.4.2. Classification of commonly used MPPT Technique

There are many algorithms used to find the maximum power point. Ideally, power tracking is done automatically to adapt to varying weather conditions [32].

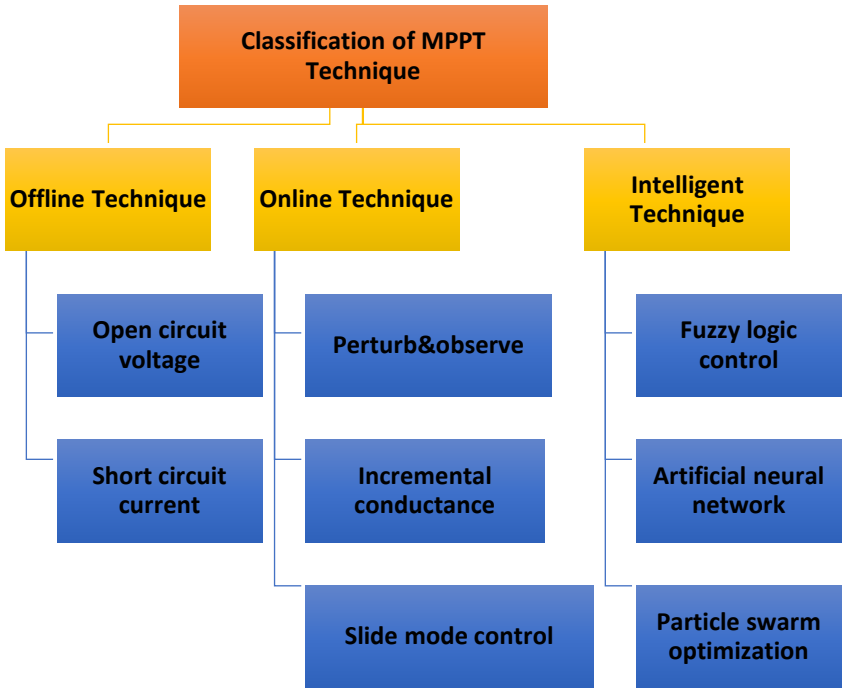


Figure II.16. Classification of commonly used MPPT

II.4.2.1. Perturb & Observe (P&O) algorithm

P&O is the most well-established and widely used method to track the maximum power point of a PV system [40].

This method is based on perturbing the output voltage of the PV system to produce a perturbed power which is further analyzed to calculate the maximum power point. The flowchart shown in (Figure II.17) depicts the P&O MPPT algorithm in detail and the method is briefly explained below:

- The output voltage and current from the PV array are first measured and multiplied to obtain the output power.
- Change in power (ΔP) is then measured. If $\Delta P=0$, then the PV array is operating at the maximum power point.
- If $\Delta P<0$, then it means that the increasing voltage is causing the power reduction. Hence, the voltage must be increased to increase the power
- On the other hand, if the change in power is positive, i.e. $\Delta P>0$, and the algorithm verifies that $\Delta V0$ and $\Delta V>0$, then the algorithm continues to increase the voltage for the power to increase.
- The algorithm repeats the process continuously to ensure that the operating point of the PV array achieves and continues to stay on the maximum power point.

To summarize, if perturbed power perturbation is less than the initial value, then the direction of perturbation of operating voltage is reversed to find the maximum power and if it is more than the initial value then voltage perturbation is continued in the same direction until we reach the maximum power point [40]. (Figure II.18) depicts the P-V characteristics curve of the P&O algorithm, as explained above.

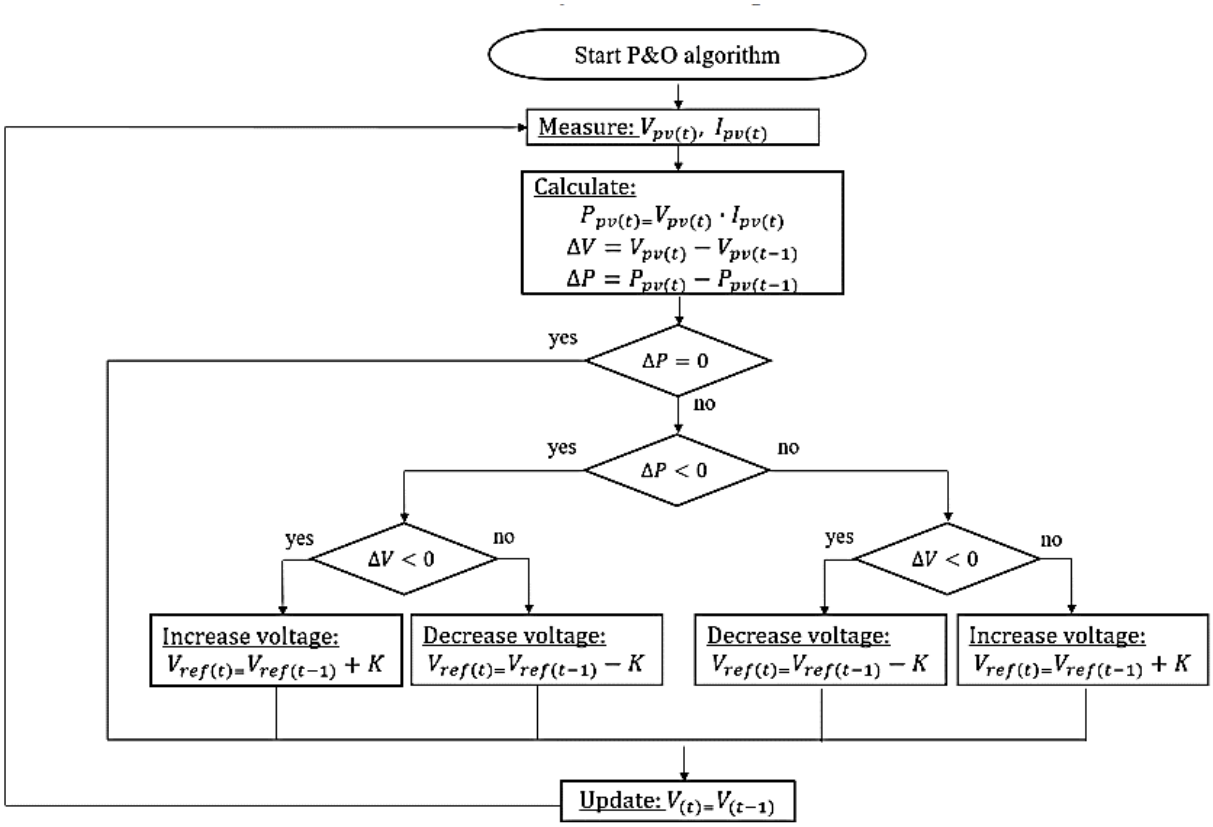


Figure II.17. P&O Algorithm

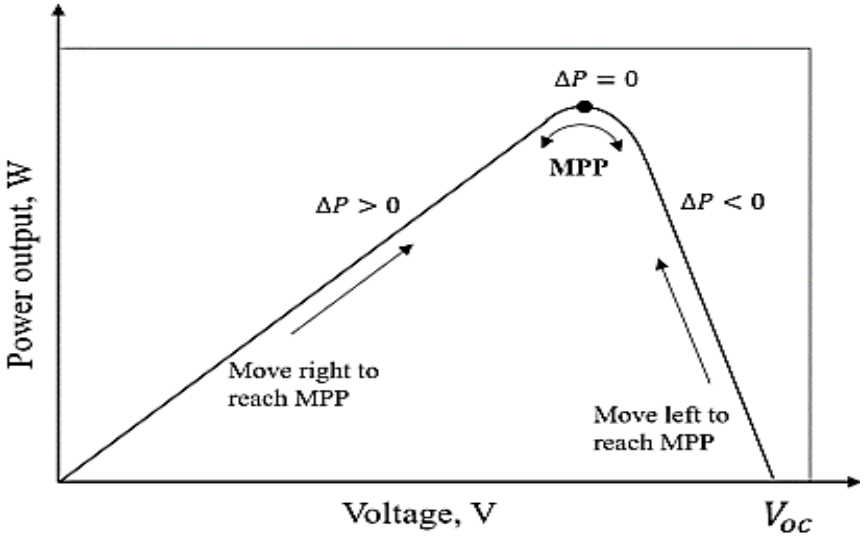


Figure II.18. P-V characteristics of the P&O algorithm

The P&O algorithm was adapted for this model due to its cost-effectiveness, uncomplicated structure, involvement of fewer parameters, and ease of implementation [42].

The P&O algorithm code, based on Figure II.16, was written in Matlab to obtain the maximum power point. The algorithm was embedded into the Simulink model of P&O MPPT as shown in Figure II.19.

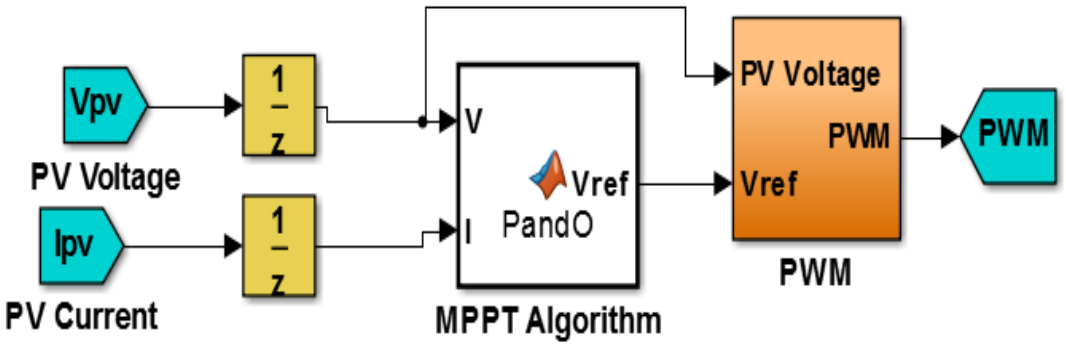


Figure II.19. Simulink Model of P&O MPPT

A PWM signal generator was implemented to generate pulses that were used as an input to the switching- IGBT of the boost converter. PWM generator generates pulses for carrier-based pulse width modulated converters by using two signals - reference signal and carrier signal. For the designed system, the input dc signal was used as reference and a repeating sequence block was used to obtain the triangular carrier signal. As shown in (figure II.20) a PI compensator is commonly implemented within the PWM control with the primary objective of reducing the steady-state error. In addition to the low steady-state error, the PI compensators are widely used because they are easy to configure, easy to implement, and relatively inexpensive [43].

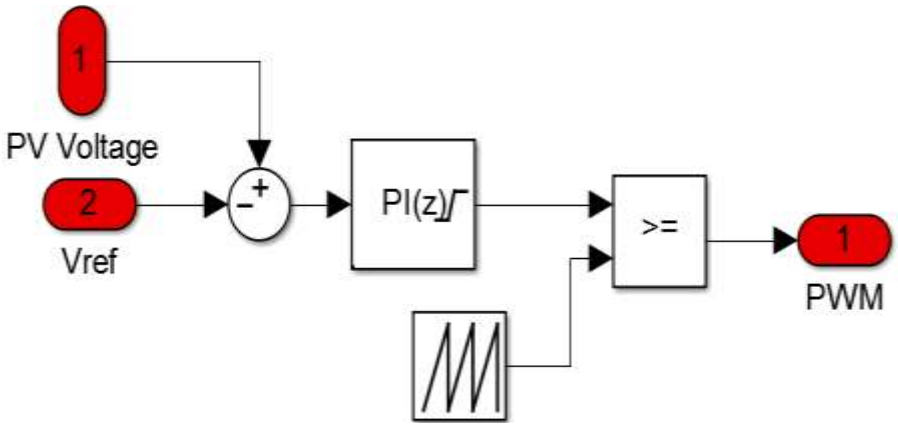


Figure II.20. Simulink Model of PWM signal generator

Ii.5. Simulation Results

The Simulink block of PV and boost converter was illustrated in Figure II.21

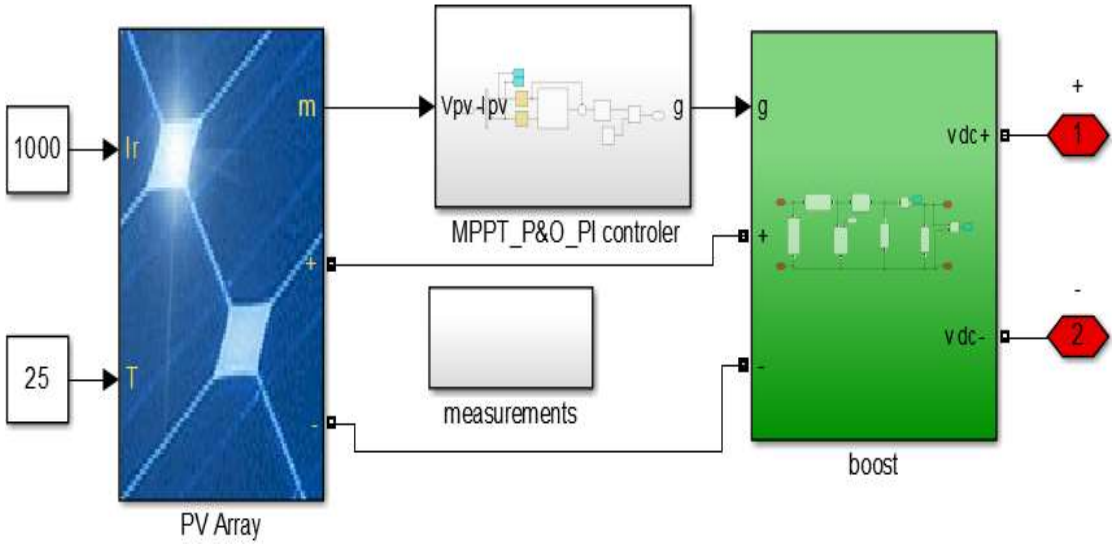


figure II.21. the block diagram in MATLAB SIMULINK PV system

The simulation results of the PV system under standard climatic conditions (1000W/m2, 25C°) were presented below including the out voltage, current, and power, respectively in (Figure II.22, II.23, and II.24)

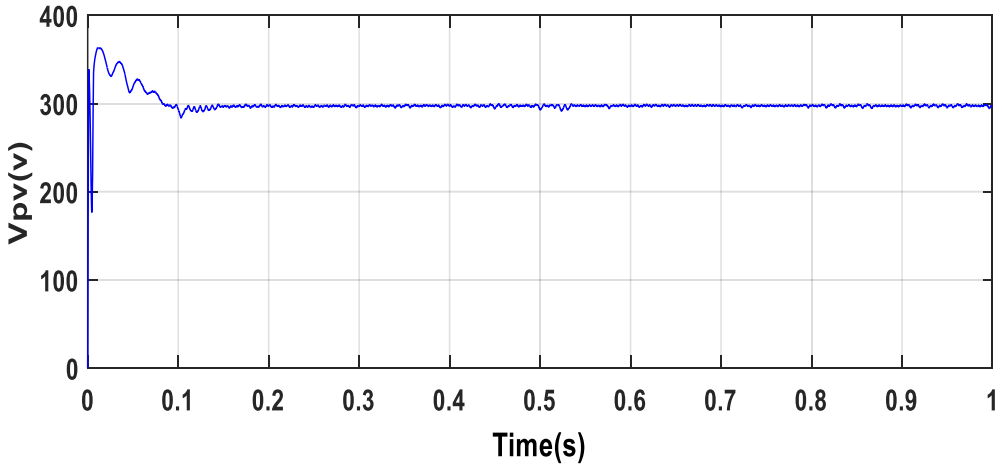


figure II.22. The photovoltaic output voltage

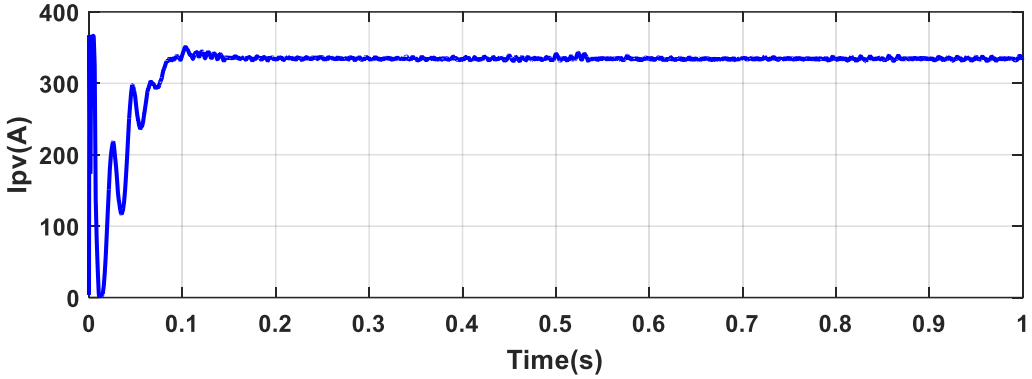


Figure II.23. The photovoltaic output current

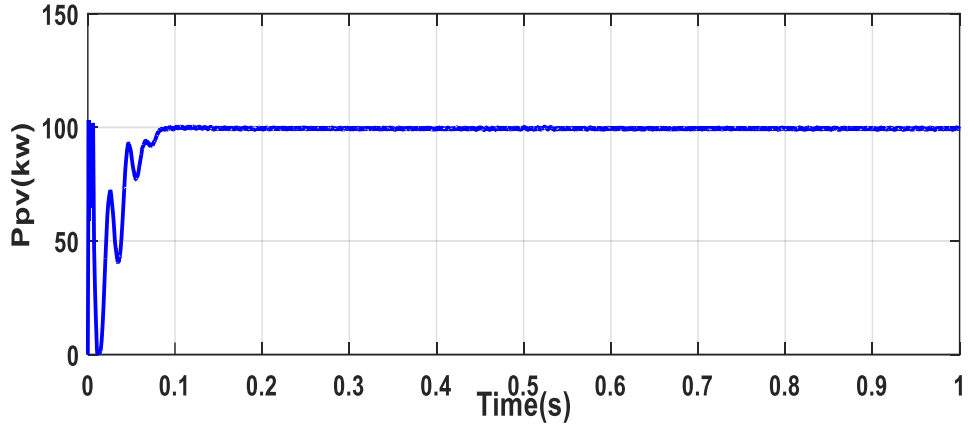


Figure II.24. The photovoltaic output power

The simulation results of the PV system under variation of irradiance (600 W/m2, 800 W/m2, and 1000W/m2, 25C°) were presented below including the out voltage, current, and power, respectively in (Figure II.25, II.26, and II. 27) the result appear the MPPT technique operate successfully.

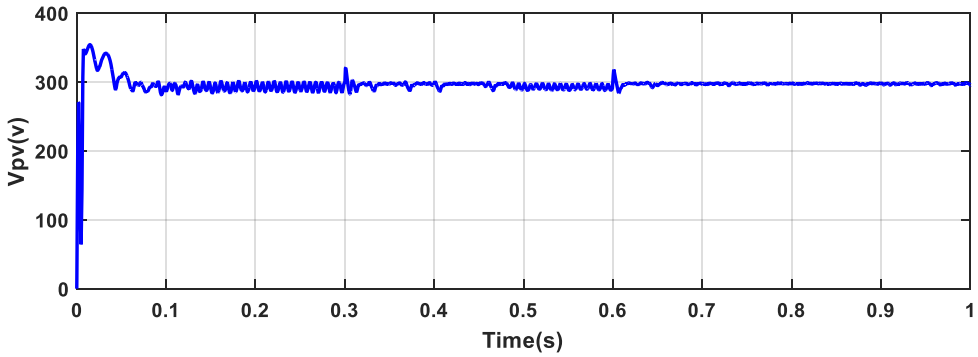


Figure. II.25. The photovoltaic output voltage with the variation of irradiation

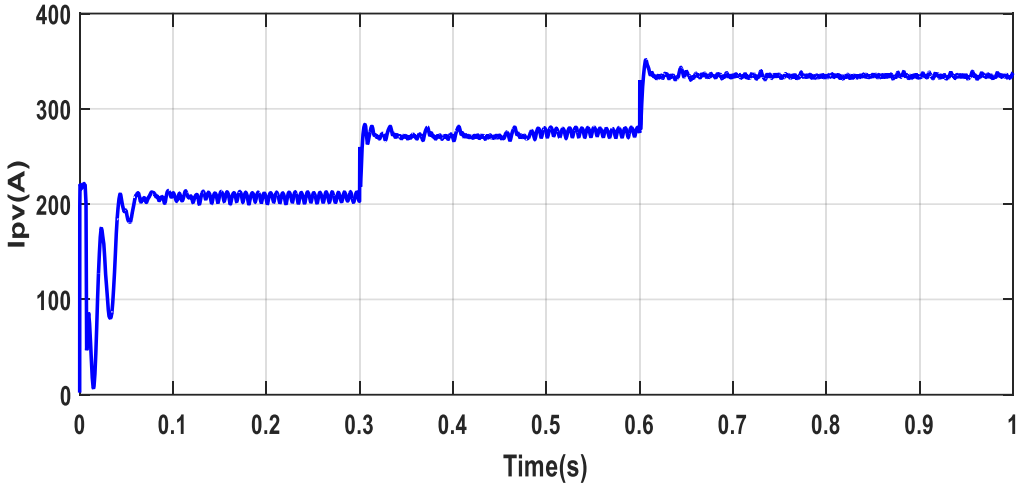


Figure II.26. The photovoltaic current with the variation of irradiation

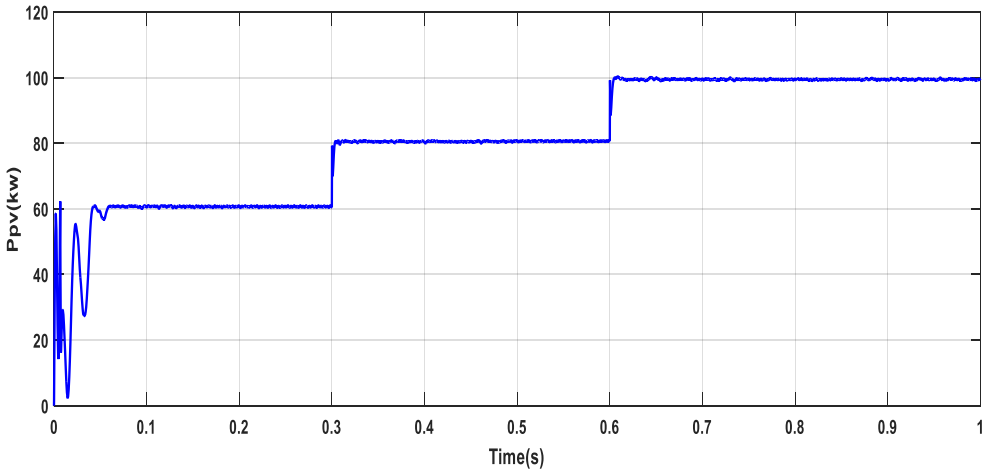


Figure II.27. The photovoltaic power with the variation of irradiation

II.6. Conclusion

This chapter discussed the importance of accurate modeling in understanding the behavior and performance of the PV system. A typical PV system model includes components such as solar panels, Boost, and a maximum power point tracker (MPPT). By developing mathematical equations and using simulation tools, we can simulate the PV system's performance under different conditions and optimize its design. Furthermore, we explored the boost converter, which plays a crucial role in maximizing the power output of the PV system. The boost converter increases the low DC voltage generated by the solar panels to a higher level suitable for the load.

We examined the operating principles of the boost converter and its control strategies, such as pulse-width modulation (PWM), to achieve efficient voltage regulation.

globally, modeling and analyzing a PV system and a boost converter is essential for understanding their behavior, optimizing their performance, and ensuring their efficient and reliable operation.

Chapter III:

Modeling and Control of Wind Turbine System

III.1. Introduction

The utilization of wind energy through turbines has gained significant attention as a sustainable and clean method of electricity generation. The design of an efficient and reliable wind energy system requires careful consideration of various components and control strategies.

In this chapter, our primary focus will be on the turbine, PMSG, and the control system employing Direct Power Control with a rectifier converter.

III.2. Wind turbine modeling

III.2.1. Modeling of a horizontal axis wind turbine

The wind turbine captures the kinetic energy of the wind and converts it into torque that spins the rotor blades. Three factors determine the ratio of wind energy to mechanical energy harvested by the rotor: air density, area swept by the rotor, and wind speed. Air density and wind speed are site-dependent climatological parameters [44]. The turbine model consists of three blades of length R driving a generator through a gain speed multiplier G, as shown in Figure III.1 [45].

We then obtain a global model composed of three subsystems:

- The turbine.
- The multiplier.
- The shaft

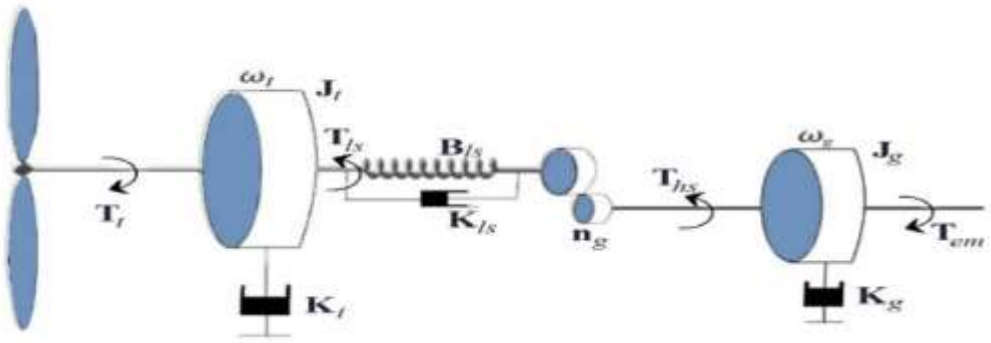


Figure. III.1. Simplified mechanical model of the turbine

III.2.1.1. Modeling of the Wind Turbine

The wind turbine captures the kinetic energy of the wind and converts it into torque that turns the rotor blades. Three factors determine the relationship between wind energy and mechanical energy recovered

by the rotor: air density ρ, the surface swept by the rotor A and wind speed Vw. Air density and wind speed are climatological parameters that depend on the site [46]. Incidental power (theoretical power of the wind), due to the wind exerted on the blades of a wind turbine is expressed as follows:

$$P_t = \frac{1}{2}\rho A V w^3 \qquad (III.1)$$

In a wind system, and because of the different losses, the wind turbine can only recover one part of the wind power:

$$P_t = \frac{1}{2}\rho A C_p(\lambda,\beta) V w^3 \qquad (III.2)$$

Where:

ρ: air density;

$A = \pi R^2$: Area swept by the rotor blades;

R: Radius of the turbine blade;

C_p: Power coefficient of the wind turbine;

β: Blade pitch angle;

V_w: Wind speed

λ: The speed ratio is defined as the ratio between the linear speed of the turbine and the wind speed, its expression is given as follows:

$$\lambda = \frac{R * \omega_m}{V_w} \qquad (III.3)$$

where ω_m: (rad/s) is the mechanical speed of the turbine shaft.

The torque exerted by the wind on the turbine shaft (or mechanical torque at the turbine outlet) is defined by:

$$T_t = \frac{P_t}{\omega_t} = \frac{1}{2}\rho\, \pi R^3 V w^2 C_{torque}(\lambda,\beta) \qquad (III.4)$$

Where T_{orque} represents the torque coefficient:

$$C_{torque} = \frac{C_p}{\lambda} \qquad (III.5)$$

III.2.1.2. Analytical model of the power coefficient

The power coefficient Cp depends on the number of rotor blades and their geometric and aerodynamic shapes (length and profile of sections). These are designed according to the characteristics

of the site, the desired nominal power, the type of regulation (pitch or stall), and the type of operation (fixed or variable speed).

The power coefficient C_p represents the aerodynamic efficiency of the wind turbine. Numerical approximations have been developed in the literature to model the coefficient, the model given above corresponds to the turbine proposed by the manufacturer German ENERCON [47]:

$$C_p(\lambda,\beta) = C_1\left(\frac{C_2}{\lambda_i} - C_3\beta - C_4\right) * e^{-\frac{C_5}{\lambda_i}} + C_6\lambda \qquad (III.6)$$

$$\lambda_i = \left(\frac{1}{\lambda + 0.008\beta} + \frac{0.035}{\beta^3 + 1}\right)^{-1} \qquad (III.7)$$

where:

C1 to C6 represent coefficients of wind turbine characteristics (C1 =0,5176, C2 = 116, C3 = 0.4, C4 = 5, C5 = 21, C6 =0,0068) and β is the blade pitch angle expressed in degrees. Figure III.2. shows the simulation results under MATLAB/SIMULINK of the evolution of the power coefficient Cp as a function of the relative speed λ for some pitch angles β.When the wind turbine is stationary (ω_t= 0), the speed ratio λ vanishes. The power of the turbine must also be zero since Pt = Tt. ω_t (where Ct is the mechanical torque of the turbine). This does not mean that the torque Ct exerted by the wind on the turbine is zero. When the rotational speed increases concerning the wind speed (λ increases), Cp increases to a maximum value. If λ becomes too large, the power coefficient Cp can take a negative value which causes a reversal of the power flow on the turbine shaft (figure III.2). This means that from a certain rotational speed of the turbine, and for a given wind speed, the turbine finds itself in "propulsion" mode and functions as a fan.

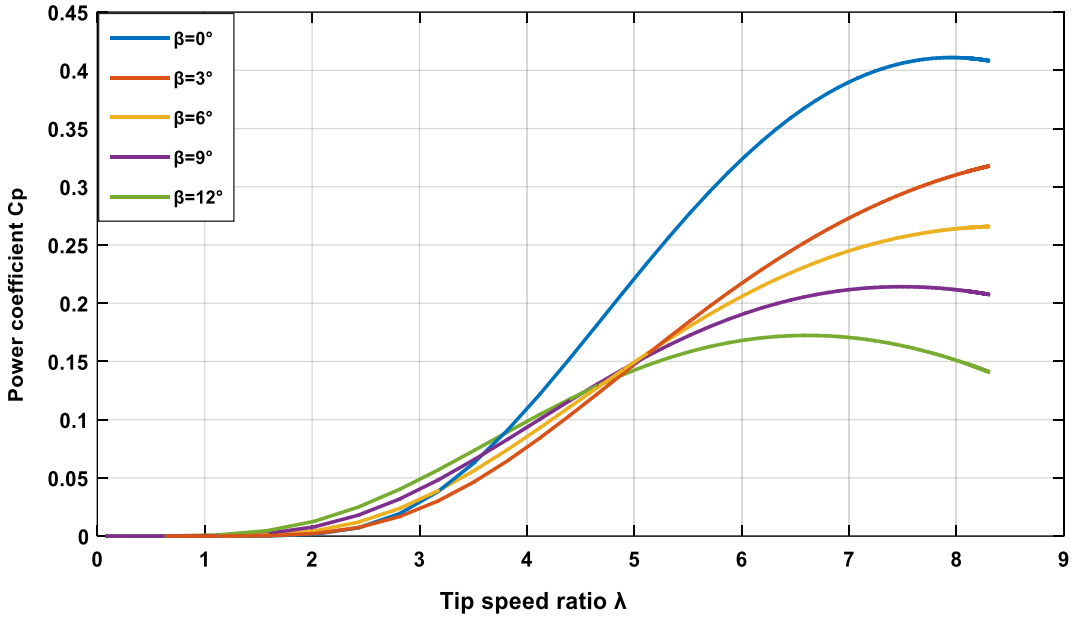


Figure.III.2. Power coefficient curves of and Cp tip speed ratio λ for different pitch blade angles β

From Figure III.2., it can be seen that for each pitch angle β, there is an optimal speed ratio λ which maximizes the coefficient Cp. We can also see in Figure (III.2). that this coefficient Cp passes through a maximum (Cp-max = 0.41) for a pitch angle (β = 0°) and a particular value of the speed ratio which is designated λopt (where λopt = 8.1).

Equation (II.27) shows that to maintain λ at its optimal value, and therefore maximize the power of the wind turbine, the rotational speed ωt must be varied linearly with the wind speed V_w . In this case, the optimum rotation speed ωt^{opt} for the maximum mechanical transmission of the wind turbine is given by:

$$\omega t^{opt} = \frac{\lambda_{opt}}{R} V_w \qquad (III.8)$$

III.2.1.3. Speed Multiplier Model

The speed multiplier is the connection between the turbine and the generator. Aims to adapt the speed of the turbine $\mathbf{w_t}$, the multiplier is assumed to be rigid and defined by a simple gain. Energy losses in the multiplier are considered zero.

This is a very complex device that we modeled very simply using the following two equations [48]:

$$\omega_t = \frac{\omega_m}{G} \qquad (III.9)$$

$$T_m = \frac{T_t}{G} \qquad (III.10)$$

Where:

G: The speed multiplier gains

T_m: The mechanical torque available on the generator shaft

T_t: The torque of the turbine

w_m: The mechanical speed of the generator

w_t: The speed of the turbine

w_m: The rotation speed of the generator shaft

III.2.1.4. Mechanical shaft model

The mass of the wind turbine is transferred to the turbine shaft in the form of inertia J_t and includes the mass of the blades and the mass of the turbine rotor. The proposed mechanical model considers the total inertia J consisting of the inertia of the turbine transferred to the rotor of the generator and the inertia of the generator [49].

$$J = J_t G^2 + J_g \qquad (III.11)$$

It should be noted that the generator rotor inertia is very low compared to the turbine inertia reported by this axis. The fundamental equation of dynamics is used to determine the evolution of mechanical speed from mechanical torque T_m applied to the rotor

$$\Sigma T = T_m = J\frac{d\omega_m}{dt} \qquad (III.12)$$

The mechanical torque is a function of the electromagnetic torque produced by the generator, the torque of viscous friction, and the torque from the multiplier

$$T_m = T_{shaft} - T_{em} - T_{visc} \qquad (III.13)$$

The friction of the blades, of the hub, as well as of the shaft, are grouped in a single coefficient of friction brought back to the shaft of the generator and called B_f.

$$T_{visc} = B_f * \omega_m \qquad (III.14)$$

The dynamic equation of mechanical motion of wind turbine system is given by [50]:

$$T_t + T_{em} = J\frac{\omega_m}{dt} + B_f * \omega_m \qquad (III.15)$$

where:

T_t: The mechanical torque of wind turbine;

T_{em}: The electromagnetic torque of the generator;

J: The total inertia of the system;

B_f: The coefficient of viscous friction.

The block diagram corresponding to the modeling of the wind turbine is easily deduced from the equations above and is represented by Figure III.3

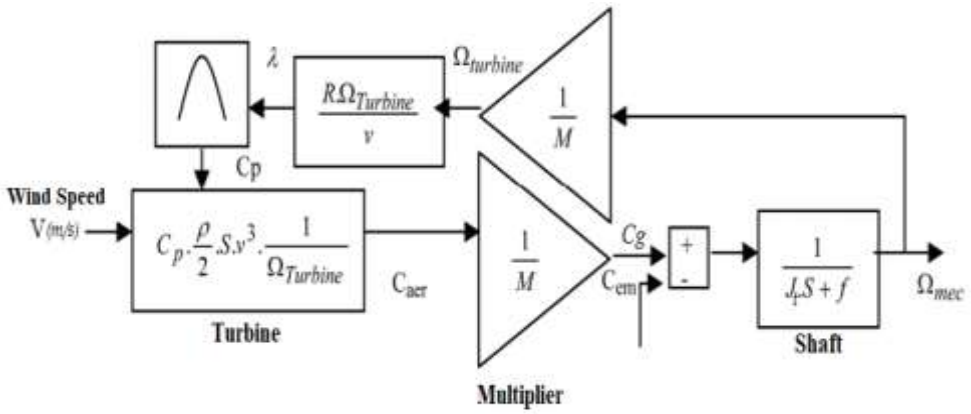


Figure III.3. Schematic diagram of the turbine model [44]

This figure shows that the turbine produces an aerodynamic torque T_w from the kinetic power of wind P_w. The speed multiplier transforms the torque aerodynamic T_w of the turbine in the torque of the multiplier. The mechanical speed of the generator shaft Wm results from the application of the engine torque available at the output of the T_{shaft} multiplier as opposed to the electromagnetic torque T_{em}. The control of the mechanical speed of the generator can therefore be performed through the electromagnetic torque of the generator.

III.3. PMSG Modeling

The PMSG electrical equation is expressed below [51]:

$$u_{abc_s} = \frac{d\psi_{abc_s}}{dt} + R_s i_{abc_s} \qquad (III.16)$$

where, $\boldsymbol{u_{abc_s}}$ are the instantaneous a, b, and c three-phase stator voltages, and i_{abc_s} are the instantaneous three-phase stator currents. R_s being the stator winding resistance per phase. ψ_{abc_s} are the instantaneous flux linkages induced by the three-phase AC currents and the P_M.

Applying Park transform, (II.1) becomes:

$$\begin{bmatrix} u_{d_s} \\ u_{q_s} \end{bmatrix} = [P(\theta_m)][R_s][P(\theta_m)]^{-1} i_{dq_s} + [P(\theta_m)][P(\theta_m)]^{-1} \frac{d}{dt}[\psi_{dq_s}] + [P(\theta_m)]\left(\frac{d}{dt}[P(\theta_m)]^{-1}\right)[\psi_{dq_s}] \qquad (III.17)$$

Where:

$P(\theta_m)$: is park transformation expressed as follows [47]:

$$P(\theta_m) = \frac{2}{3}\begin{bmatrix} cos(\theta_m) & cos\left(\theta_m - \frac{2\pi}{3}\right) & cos\left(\theta_m + \frac{2\pi}{3}\right) \\ -sin(\theta_m) & -sin\left(\theta_m - \frac{2\pi}{3}\right) & -sin\left(\theta_m + \frac{2\pi}{3}\right) \\ \frac{1}{2} & \frac{1}{2} & \frac{1}{2} \end{bmatrix} \qquad (III.18)$$

θ_m: is the angle between the q-axis and the main stator axis with:

$$\begin{bmatrix} \psi_{d_s} \\ \psi_{q_s} \end{bmatrix} = \begin{bmatrix} L_d & 0 \\ 0 & L_q \end{bmatrix} \begin{bmatrix} i_{d_s} \\ i_{q_s} \end{bmatrix} = \begin{bmatrix} \psi_f \\ 0 \end{bmatrix} \qquad (III.19)$$

ψ_f : represents the constant permanent magnet flux linkage.

On the other hand, and as is expressed in (III.20)

$$[P(\theta_m)][P(\theta_m)]^{-1} \frac{d}{dt}[\psi_{dq_s}] = \frac{d}{dt}(\theta_m) * P\left(\frac{\pi}{2}\right) * [\ \psi_{dq_s}] = \omega_s [\ \psi_{dq_s}\ ]' \qquad (III.20)$$

where:

$$[\psi_{dq_s}]' = \begin{bmatrix} -L_q & 0 \\ 0 & L_d \end{bmatrix} \begin{bmatrix} i_{q_s} \\ i_{d_s} \end{bmatrix} + \begin{bmatrix} 0 \\ \psi_f \end{bmatrix} = \begin{bmatrix} -\psi_{q_s} \\ \psi_{d_s} \end{bmatrix} \quad (III.21)$$

In addition:

$$[\, u_{dq_s}] = [\, R_s\,][\, i_{dq_s}] + \frac{d}{dt}[\, \psi_{dq_s}] + \omega_s[\, \psi_{dq_s}]' \quad (III.22)$$

Replacing (III.21) in (III.22), (III.23) is deduced: [48]

$$\begin{cases} u_{d_s} = -\omega_s \cdot \psi_{q_s} + (R_s + pL_d) i_{d_s} \\ u_{q_s} = \omega_s \cdot \psi_{d_s} + (R_s + pL_q) i_{q_s} \end{cases}, \quad (III.23)$$

ω_s : is the basic electrical angular frequency of the PMSG and can be deduced from Ω_m as follow:

$$\omega_s = n_p * \Omega_m \quad (III.24)$$

Where: n_p is the PMSG pole pair.

ψ_{d_s} and ψ_{q_s} are the stator flux linkages corresponding to d-axis and q-axis, respectively.
Substituting (III.19) in (III.23), (III.25) is obtained:

$$\begin{cases} u_{d_s} = -\omega_s . L_{q_s} i_{q_s} - \omega_s \cdot (R_s + pL_d) i_{d_s} \\ u_{q_s} = \omega_s . L_{d_s} i_{d_s} + (R_s + pL_q) i_{q_s} + E_s \end{cases} \quad (III.25)$$

with $E_s = \omega_s \psi_f, L_{d_s}$ and L_{q_s} are the two-phase stator windings self-inductances corresponding to d-axis and q-axis. i_{d_s} and i_{q_s} are the armature currents for the d-axis and q-axis, respectively. (p) is the differential operator symbol. In the d − q axis rotation coordinate system, (III.26) expresses the electromagnetic torque of PMSG [54].

$$T_e = \frac{3}{2} n_p [\psi_d i_{q_s} + (L_d - L_q) i_{d_s} i_{q_s}] \quad (III.26)$$

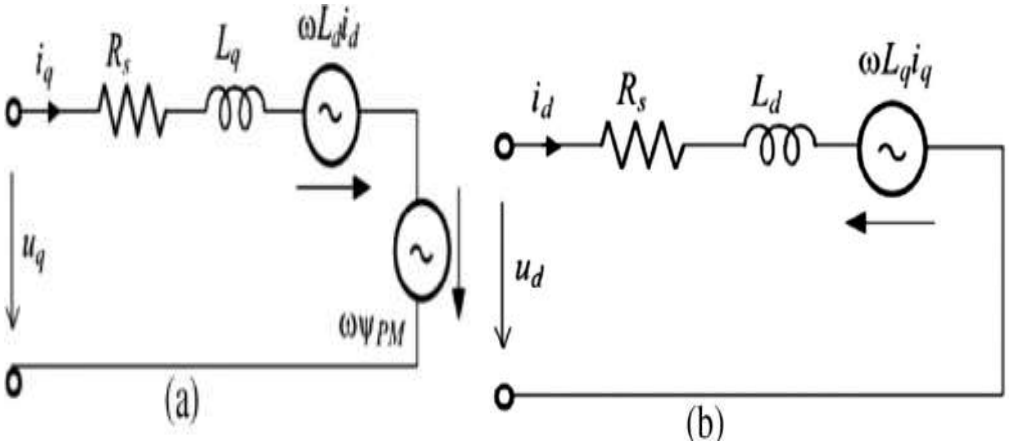


Figure III.4. Equivalent circuit, (a) in q axis and (b) in d axis.

III.4. Three-phase PWM rectifier

III.4.1. Three-Phase PWM rectifier Principle

The voltage rectifier works by keeping the DC bus voltage at a desired reference value, using closed-loop control. To accomplish this task, the DC bus voltage is measured and compared with a reference voltage, the error signal produced from this comparison is used to switch the six rectifier switches on and off. This way power can flow in either direction depending on the conditions on the measured DC bus voltage across capacitor C. When the current output rectifier is positive, capacitor C is discharged, and the error signal requests the control block for more power from the AC source. The control block takes power from the AC source producing an appropriate PWM signal for all six switches. This way, more current flows from the AC source to the DC side, and the capacitor voltage is recovered. Conversely, when the current output rectifier is negative, capacitor C is overcharged, and the error signal instructs the control block to discharge the capacitor, and power returns to the AC source [55].

The PWM control can not only control the active power, but also the reactive power, and therefore this type of rectifier allows the correction of the power factor. In addition, the waveforms of the source currents can be maintained as nearly sinusoidal, which reduces source distortion [56].

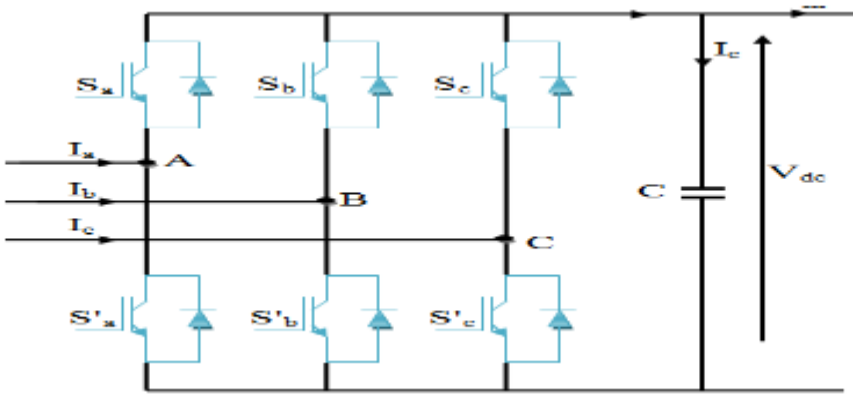


Figure III.5. structure of a three-phase rectifier

III.5. Direct power control (DPC)

III.5.1. Definition

The general definition describes the (DPC) as the control technique which directly uses the instantaneous powers as control variables, without using current loops or modulation blocks because the rectifier switching states are chosen directly by a switching table [57].

III.5.2. Principle of direct power control

The principle of DPC consists in selecting a sequence of switching orders (Sa Sb Sc) of the semiconductors constituting the PWM rectifier, from a switching table. The selection is made based on the digitized errors, Sp and Sq between the active and reactive power references (P* and q*) and the actual values (P and q), provided by two hysteresis comparators at two levels, as well as on the angular position of the network voltage vector; α, β. For the latter, the α-β plane is divided into twelve or six sectors**.** Each of the control sequences (Sa Sb Sc) corresponds to a voltage vector at the input of the rectifier, the whole of which is represented in Fig III.6 [58].

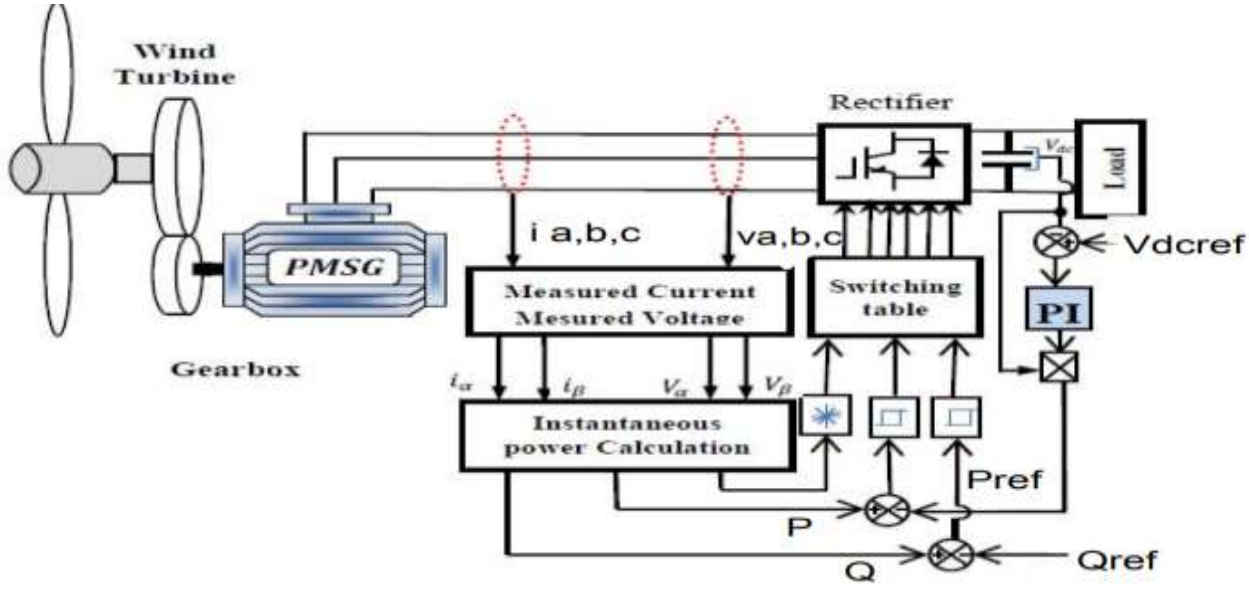


Figure III.6: General configuration of the DPC command.

The overall structure of the DPC, applied to the three-phase PWM bridge rectifier is shown in Figure III.6. It is analogous to that of the direct torque control (DTC) of induction machines. Instead of torque and stator flux, it is the active and reactive instantaneous powers that are the controlled quantities.

III.5.3. The voltage estimator

The working sector of the line voltage is necessary, to determine the switching commands. Moreover, it is important to estimate the line voltage correctly, even with the existence of harmonics, it gives a high power factor. The voltage drop across the inductor can be calculated by differentiating the current. So the voltage can be calculated by adding the reference voltage at the input of the converter with the already calculated voltage drop [59].

The following expression gives the line currents ia, ib, ic in stationary coordinates:

$$\begin{bmatrix} i_\alpha \\ i_\beta \end{bmatrix} = \sqrt{\frac{2}{3}} \begin{bmatrix} 1 & -\frac{1}{2} & -\frac{1}{2} \\ 0 & -\frac{\sqrt{3}}{2} & -\frac{\sqrt{3}}{2} \end{bmatrix} \begin{bmatrix} i_a \\ i_b \\ i_c \end{bmatrix} \qquad (III.27)$$

We can write the expressions of the active and reactive powers as follows:

$$\begin{cases} p = \bar{v}_{s(abc)} \cdot \bar{l}_{(abc)} = V_{s\alpha} \cdot i_\alpha + V_{s\beta} \cdot i_\beta \\ q = \bar{v}_{s(abc)} . \bar{l}_{(abc)} = V_{s\beta \cdot i_\alpha} - V_{s\alpha} \cdot i_\beta \end{cases} \qquad (III.28)$$

The matrix notation of expression active and reactive powers are:

$$\begin{bmatrix} p \\ q \end{bmatrix} = \begin{bmatrix} V_{s\alpha} & V_{s\beta} \\ V_{s\beta} & -V_{s\alpha} \end{bmatrix} \cdot \begin{bmatrix} i_\alpha \\ i_\beta \end{bmatrix} \quad (III.29)$$

The voltage can be estimated by the following equation:

$$\begin{bmatrix} V_{s\alpha} \\ V_{s\beta} \end{bmatrix} = \frac{1}{\left(i_\alpha^2 + i_\beta^2\right)} \begin{bmatrix} i_\alpha & -i_\beta \\ i_\beta & i_\alpha \end{bmatrix} \begin{bmatrix} p \\ q \end{bmatrix} \quad (III.30)$$

The inverse Concordia transform of the line voltage is written:

$$\begin{bmatrix} V_{sa} \\ V_{sb} \\ V_{sc} \end{bmatrix} = \sqrt{\frac{2}{3}} \begin{bmatrix} 1 & 0 \\ -\frac{1}{2} & \frac{\sqrt{3}}{2} \\ -\frac{1}{2} & -\frac{\sqrt{3}}{2} \end{bmatrix} \begin{bmatrix} V_{s\alpha} \\ V_{s\beta} \end{bmatrix} \quad (III.31)$$

III.5.4. Estimated instantaneous power

For a three-phase system, the instantaneous active power is defined by the scalar product of the line currents and voltages. Reactive power is defined by the modulus of their vector product. These powers are expressed respectively by the relation [60]:

$$S = V \cdot I = p + jq \quad (III.32)$$

$$S = v_a i_a + v_b i_b + v_c i_c + j\frac{1}{\sqrt{3}}[(v_b - v_c)i_a + (v_c - v_a)i_b + (v_a - v_b)i_c] \quad (III.33)$$

However, expressions (III-53) and (III-54) require information on the line voltage, which must be eliminated for sensorless control. So that the instantaneous active and reactive powers can be estimated without measuring the line voltage. The expressions allowing this estimation are based on the measurement of the line currents of the DC bus voltage and the states of the switches, which are given as follows [57]:

$$P = L\left(\frac{di_a}{dt} i_a + \frac{di_b}{dt} i_b + \frac{di_c}{dt} i_c\right) + V_{dc}(S_a i_a + S_b i_b + S_c i_c) \quad (III.34)$$

$$q = \frac{1}{\sqrt{3}}\left[3L\left(\frac{di_a}{dt} i_c - \frac{di_c}{dt} i_a\right) - V_{dc}\big(S_a(i_a - i_c) + S_b(i_c - i_b) + S_c(i_a - i_b)\big)\right] \quad (III.35)$$

The first parts of the two expressions (III-34) and (III-35) represent the power in the line inductors. The active power dissipated in the internal resistances of the inductors is negligible compared to the power involved. This implies that the value of the resistance is much lower, the other parts represent the power of the converter [61]. According to expressions III.34 and III.35, the power changes instantaneously according to the switching commands of the converter.

III.5.5. Switching table

The switching table can be considered the heart of direct power control. It selects an appropriate rectifier voltage vector to allow the instantaneous active and reactive power to move in the direction desired, also based on the position of the vector of the source voltage and the errors of the active and reactive powers [57]. Digitized error signals and angular position are entered into a commutation table in which all switching states S$\boldsymbol{p}$ and S$\boldsymbol{q}$ are stored in the converter which takes state "1" for an increase of the controlled variable (P or q) and the state "0" for a decrease. Using this switching table; the optimum switching states of the converter can be uniquely selected at each specific instant depending on the combination of digitized input signals, as shown in Table.III.1 [63].

Table III. 3 Switching table twelve Sector of the DPC command

Sp	Sq	S1	S2	S3	S4	S5	S6	S7	S8	S9	S10	S11	S12
1	0	V_6 (101)	V_7 (111)	V_1 (100)	V_0 (000)	V_2 (110)	V_7 (111)	V_3 (010)	V_0 (000)	V_4 (011)	V7 (111)	V5 (001)	V0 (000)
	1	V_2 (110)	V_7 (111)	V_3 (010)	V_0 (000)	V_4 (011)	V_7 (111)	V_5 (001)	V_0 (000)	V_6 (101)	V7 (111)	V1 (100)	V0 (000)
0	0	V_6 (101)	V_1 (100)	V_1 (100)	V_2 (110)	V_2 (110)	V_3 (010)	V_3 (010)	V_4 (011)	V_4 (100)	V5 (001)	V5 (001)	V6 (101)
	1	V_1 (100)	V_2 (110)	V_2 (110)	V_3 (010)	V_3 (010)	V_4 (011)	V_4 0110	V_5 (001)	V_5 (001)	V6 (101)	V6 (101)	V1 (100)

III.5.6. Sector determination

Knowledge of the estimated voltage sector is necessary to determine the optimal switching states. For that, the work plan (α, β) is divided into twelve or six sectors. the latter can be determined by the following relation [64]:

$$(2n-3)\frac{\pi}{6} < \hat{t}_n < (2n-1)\frac{\pi}{6} \qquad n = 1,2 \dots \dots 6 \qquad \text{(III. 36)}$$

$$(n-2)\frac{\pi}{6} < \hat{t}_n < (n-1)\frac{\pi}{6} \qquad n = 1, \dots 12 \qquad \text{(III. 37)}$$

Depending on the angle of the source voltage vector referenced on the (α) axis, the sector where the vector is located will be selected. The angle is calculated using the inverse trigonometric function, based on the vector components of the voltage in the frame (α, β), indicated by equation (III.38) [62].

$$\hat{t}_n = \tan^{-1}\left(\frac{V_{s\beta}}{V_{s\alpha}}\right) \qquad \text{(III. 38)}$$

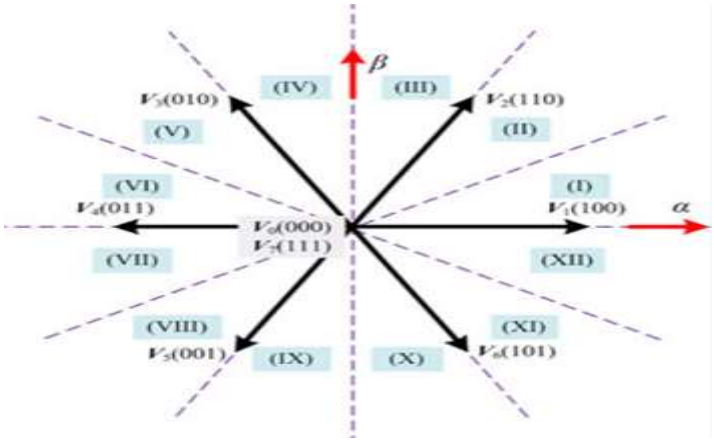


Figure.III.7. Sectors in (α, β) plan

The sectors are used to optimize the switching of the converters, and this is by the choice of the adjacent vectors. We divide the plane into 12 sectors for more precision and also to avoid the problems encountered at the borders of each control vector [61].

III.5.7. DC bus voltage control using the conventional PI regulator:

The role of the DC bus voltage regulation loop is to maintain this voltage at a constant reference value as shown in (Figure III.8) by controlling the charging and discharging process of the capacitor.

To ensure a good quality of compensation for voltage disturbances in cases of extreme operation of the PMSG, conventional PI-type regulators were used.

Thus, the multiplication of the maximum amplitude of the source currents (Imax) with the voltage of the capacitor (Vdc) gives the reference active power (P^*) which was used as a control variable in classical DPC control [65].

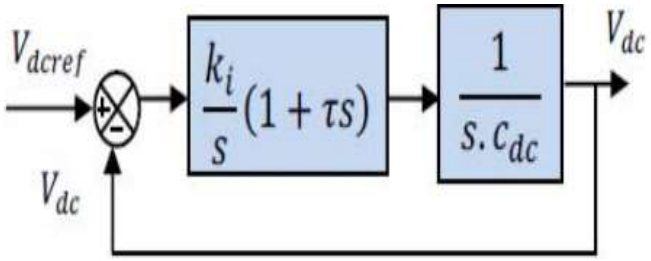


Figure.III.8. DC-link control system structure

$$\begin{cases} k_i = C_{dc} * \omega o^2 \\ k_p = 2 * C_{dc} * \omega o^2 * \xi \end{cases} \quad (III.39)$$

With:

k_i: Integrator gain

k_p: Proportional gain

ξ: Damping factor

ω_0: Angular frequency

III.5.8. Hysteresis controller:

The main idea of direct power control is to maintain the instantaneous active and reactive powers within a desired band.

This control is based on two hysteresis comparators which use as input the error signals between the reference and measured values of the active and reactive powers [66].

The outputs of the hysteresis controllers given by the Boolean variables Sp and Sq indicate the overshoots or undershoots of the errors of the powers according to the logic below [61].

$$S_p \begin{cases} 1 & P < P_{ref} - H_p \\ 0 & P > P_{ref} + H_p \end{cases} \qquad S_q \begin{cases} 1 & q < q_{ref} - H_p \\ 0 & q > q_{ref} + H_p \end{cases} \quad (III.40)$$

where Hp and Hq are the hysteresis bands.

III.6. Simulation Results

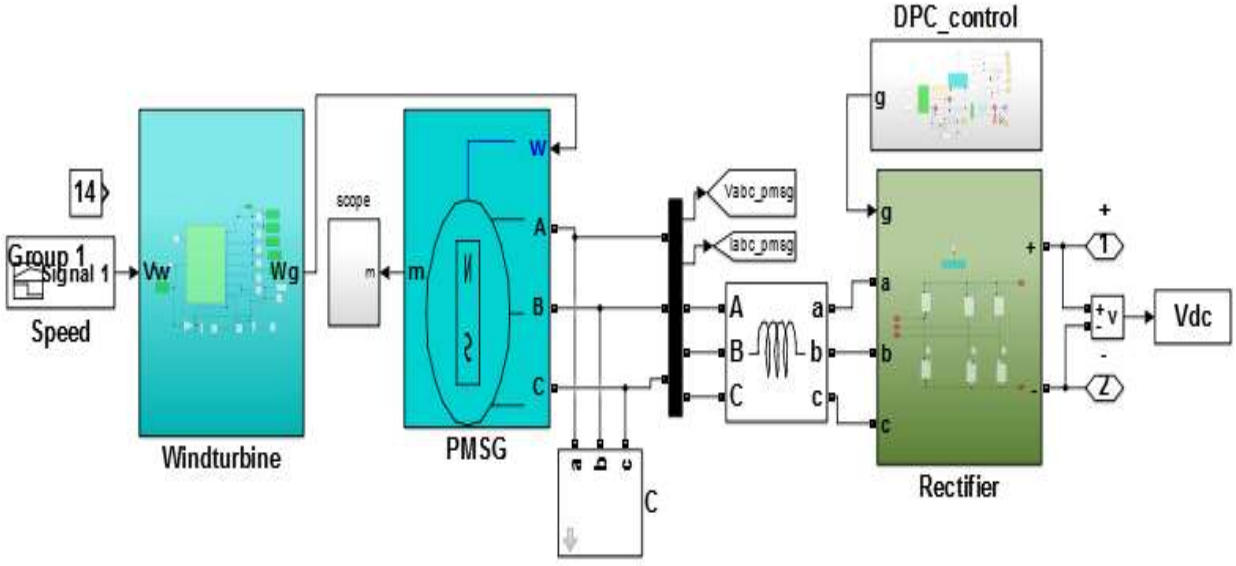


Figure.III.9. The blok windturbin matlab simlink

To verify the performance of the proposed control strategy of PMSG driven by WECS, Simulation tests have been carried out under these conditions:

- The wind turbine is driven with variable speeds.
- The DC bus voltage maintains constant at 600V whole simulation time.

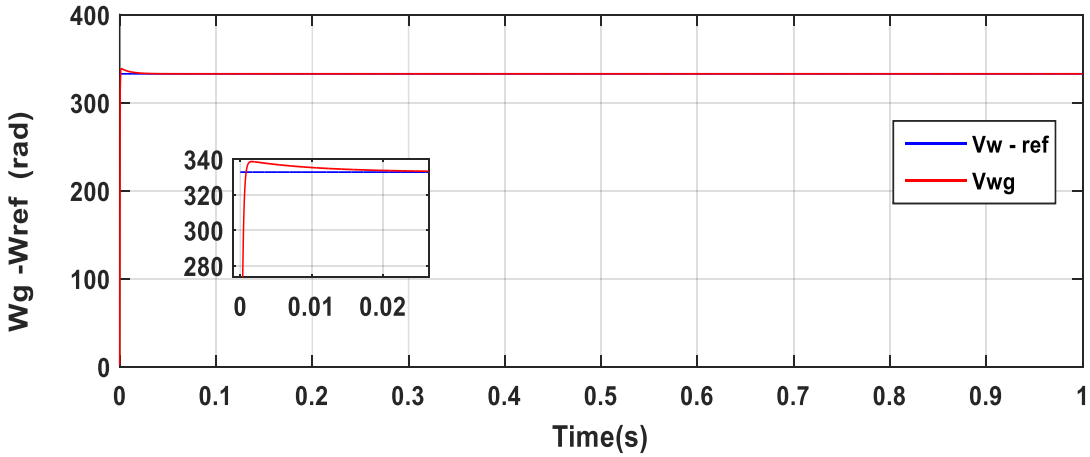


Figure.III.10. Mechanecal Speed and reference

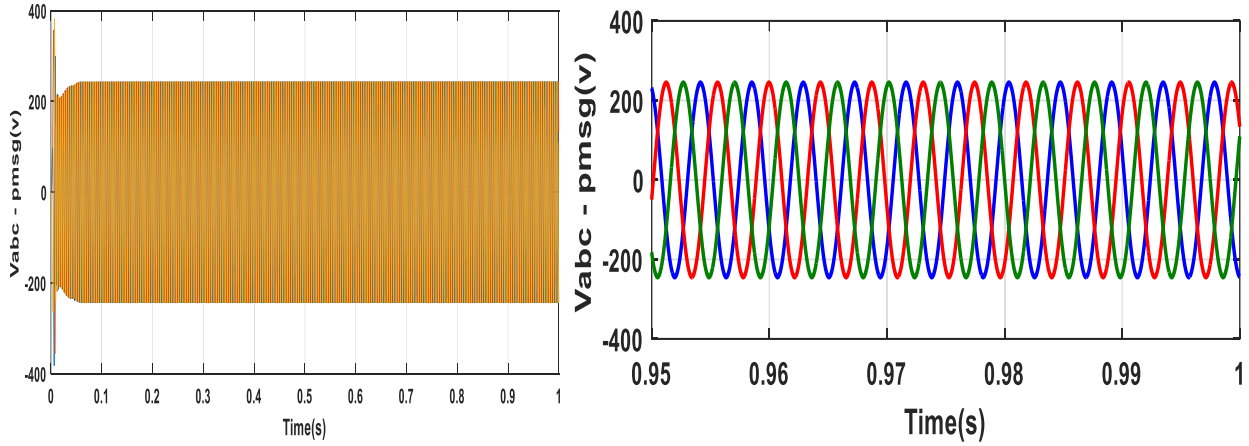


Figure.III.11. PSMG output voltages

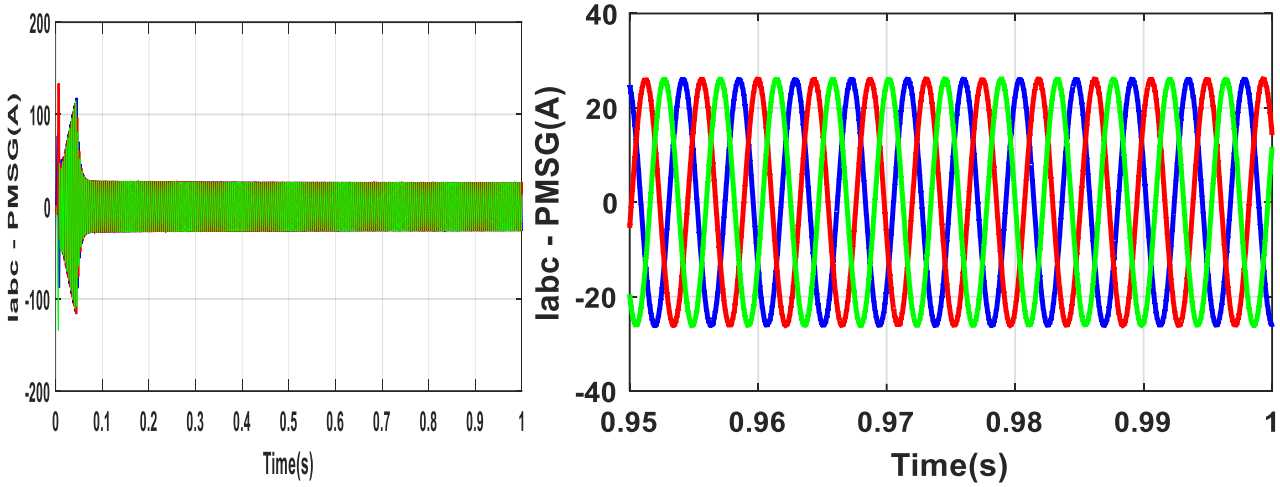


Figure.III. 12. PSMG output currents

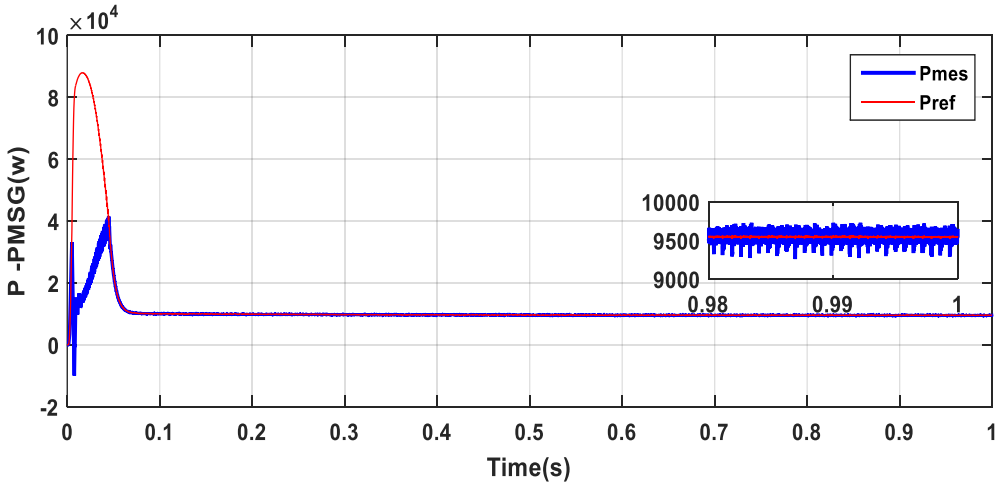


Figure.III.13. Active power PMSG.

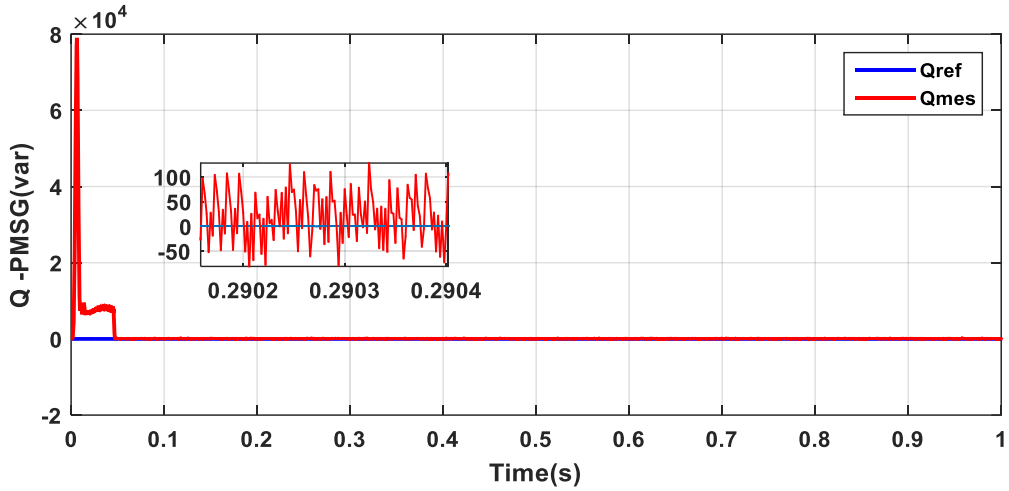


Figure.III.14. Reactive power PMSG.

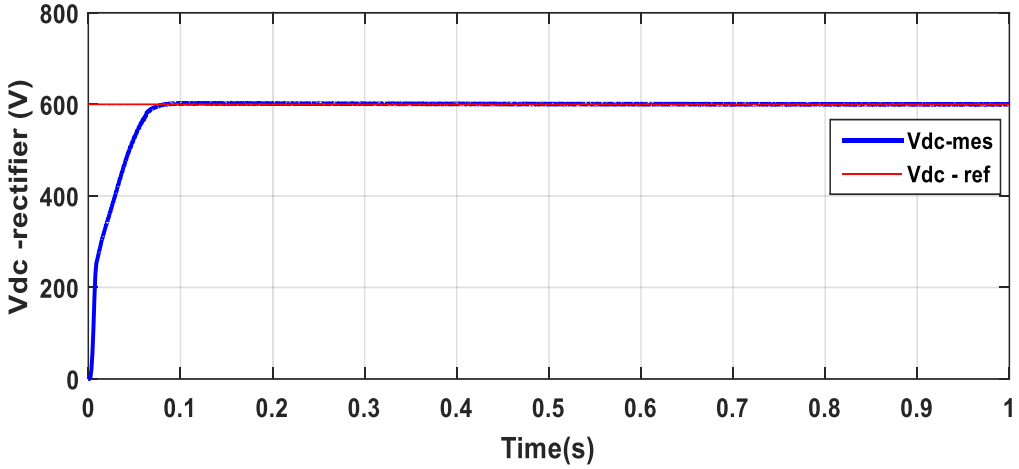


Figure.III.15. DC bus voltage.

III.7. Discussion Results

Figure.III.10. while the value of the aerodynamic speed equal 332 (rad/s)

Figure.III.11-12. shows the output voltage and currents of the generator according to the wind profile used in this simulation.

Figure.III.13-14. show simulation results for the control of active and reactive powers from the curves. It can be noticed that, with the change of active power reference, the active power always follows the reference signal. Reactive power is maintained at zero.

The result of the DC link voltage control is represented in Figure.III.15, where the curve indicates the robust PI controller in the follow-up of reference with a short response time and an acceptable overrun (near zero).

III.8. Conclusion

This chapter has provided insights into the modeling, analysis, and design considerations for a wind turbine system incorporating a PMSG and a control system utilizing DPC with a rectifier converter. The PMSG was highlighted as a key component in converting the mechanical energy from the turbine into electrical energy. We examined its modeling and development, considering its construction, electromagnetic characteristics, and power generation capabilities. The inherent features of PMSG such as the absence of rotor windings and excitation systems, contribute to their efficiency and compactness. Additionally, we discussed the implementation of Direct Power Control (DPC) with a rectifier converter as the control system for the wind turbine-PMSG system. DPC enables precise control of power flow and rapid dynamic response in the PMSG, ensuring efficient and reliable operation of the system.

Chapter IV:

Hybrid System Solar and Wind Energies Connected to the Grid Via Inverter Controlled by SRF Strategy

IV.1 Introduction

Wind and solar energy are the most promising and abundant sources of renewable energy.

WECS using PMSG has attractive features of high efficiency and minimal maintenance requirements, Maximum energy extraction from renewable energy sources, and DC bus voltage regulation further improving the overall efficiency, profitability, and reliability of the system [67].

In this chapter, a simple and robust control strategy is presented to improve the quality of grid-connected renewable energy. This strategy is based on the maximum power delivered to the grid from wind and solar PV sources. The considered system is composed of a photovoltaic array and a wind energy conversion system (WECS) based on a permanent magnet synchronous generator (PMSG).

The developed SRF control algorithm is modified by applying it to the grid-connected VSC inverter. It does improve the desired power quality and minimizes total harmonic distortion (THD) and fast DC bus voltage regulation. The efficiency and robustness of the proposed system is demonstrated by the nature of the performance of the simulated results. The proposed controller ensures a regulation action of the desired value, fast and without any adjustment in climatic conditions and load variations.

IV.2. hybrid PV-PMSG wind turbine system connected to the grid

The system studied and presented in (Figure IV.1) includes a PMSG wind turbine, a photovoltaic system, linear and non-linear loads, and an electrical grid.

PMSG is most used for small, medium, and large variable-speed wind turbines to produce high efficiency and high reliability, with lower production costs. The wind turbine in this part is connected to a photovoltaic installation at the DC bus level avoiding a storage system. The energy supplied by the hybrid system is consumed by the linear and non-linear load, and the rest is transferred to the electrical grid.

As we explained in Chapter II and Chapter III about how to control wind turbines and PV by using control, we used MPPT control for PV, and we used DPC control for PMSG.

The diagram in Figure IV.1. illustrates the topology of a wind turbine and photovoltaic hybrid system, which is connected to the grid via two power electronics converters, AC/DC and DC/DC, which will have the role of controlling the generator to extract the maximum power.

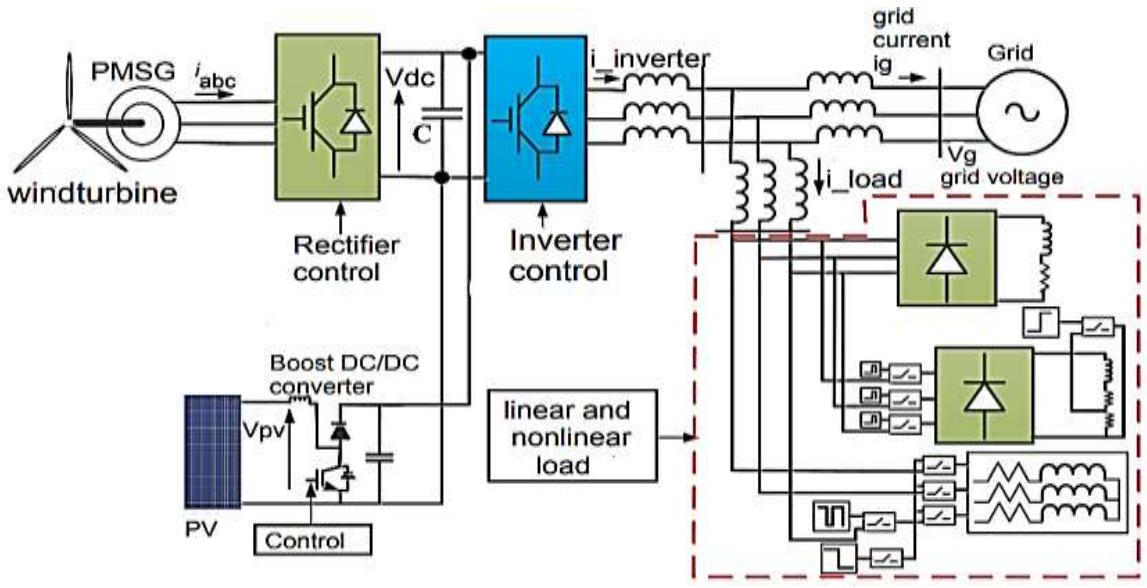


Figure IV.1. Grid Connected Hybrid (Photovoltaic-PMSG) System Diagram

IV.3. Invertre control on the electrical grid side

The SRF control strategy based on the PI-anti-windup controller is used to control the grid-side inverter as shown in Figure IV.3 by estimating the AC grid reference currents [32].

The hybrid system is connected to the grid via a DC/AC inverter. The inverter assists power flow to the load and the utility grid and keeps the DC bus voltage stable, the latter remains constant and stable in the different operating states.

IV.3 .1. SRF algorithm

PI Anti-windup-based SRF based on the estimation of AC reference currents by controlling VSC is considered one of the most attractive techniques. based on current regulations. This control system is shown in Figure IV.3. Load currents (iLa, iLb, iLc), grid voltages (Vga, Vgb, Vgc) and DC link voltage (Vdc) of VSC are the main measured signals. The transformation (dq0) can be used to convert the load currents in the plane (ABC) is given as [32]:

$$\begin{bmatrix} i_{Ld} \\ i_{Lq} \\ i_{LO} \end{bmatrix} = \frac{2}{3} \begin{bmatrix} cos(\theta) & cos\left(\theta - \frac{2\pi}{3}\right) & cos\left(\theta + \frac{2\pi}{3}\right) \\ -sin(\theta) & -sin\left(\theta - \frac{2\pi}{3}\right) & -sin\left(\theta + \frac{2\pi}{3}\right) \\ \frac{1}{2} & \frac{1}{2} & \frac{1}{2} \end{bmatrix} \begin{bmatrix} i_{La} \\ i_{Lb} \\ i_{LC} \end{bmatrix} \qquad (IV.1)$$

Where the elements (sin(θ) and cos(θ)) of the equation are obtained from the PLL (Phase Locked Loop) circuit at the PCC measuring point of the voltage (Vga, Vgb, Vgc). Harmonics are eliminated by the low pass filter (LPF). The reference current in the dq axis which contains the fundamental and the harmonic current can be written as follows:

The d-axis and q-axis currents consist of fundamental and harmonic currents.

$$i_{Ld} = i_{ddc} + i_{dac} \qquad (IV.2)$$

$$i_{Lq} = i_{qdc} + i_{qac} \qquad (IV.3)$$

The DC and non-DC (harmonics) quantities are separated by the SRF controller using LPF. Now only DC quantities are in the reference signals.

IV.3 .2. Unity power factor

For unity power factor using reactive power compensation, the control algorithm considers that AC mains must deliver a direct axis component of load currents along with an active power component of the current for regulating common DC bus voltage constant and for feeding the VSC losses (iw). The DC bus PI controller provides the active power transfer required to regulate DC link voltage and for compensation of VSC losses. The current component to meet losses is given as [68].

$$i_w(k) = i_w(k-1) + K_{pd}\left(v_{de^{(k)}} - v_{de^{(k-1)}}\right) + K_{id}\left(v_{de^{(k)}}\right) \qquad (IV.4)$$

where Vde (k) is, Vde (k) =V* (k)-V(k) is a voltage error between a reference voltage (Vdc*) and sensed voltage (Vdc) of a common DC bus at Kth sampling instant. Kpd and Kid are the gains for the DC bus voltage PI controller.

The amplitude of the reference AC mains current is given as

$$i_d^* = i_{ddc} + i_w \qquad (IV.5)$$

The active power component of reference AC main currents must be in the phase of PCC voltages. It is obtained by reversing Park's transformation:

$$\begin{bmatrix} i*_a \\ i*_b \\ i*_0 \end{bmatrix} = \begin{bmatrix} \cos(\theta) & \sin(\theta) & 1 \\ \cos\left(\theta - \frac{2\pi}{3}\right) & \sin\left(\theta - \frac{2\pi}{3}\right) & 1 \\ \cos\left(\theta + \frac{2\pi}{3}\right) & \sin\left(\theta + \frac{2\pi}{3}\right) & 1 \end{bmatrix} \begin{bmatrix} i_d^* \\ i_q^* \\ i_0^* \end{bmatrix} \qquad (IV.6)$$

From reverse Park's transformation with id* as in (IV.5) and iq* and i0* as zero from (IV.6) reference AC mains currents (i*a, i*b, i*c) are estimated for control of VSC.

IV.3 .3. AC voltage regulation

The voltage regulation (VR) at PCC of the proposed system considers that AC mains must deliver the same direct axis component id* along with the same quadrature-axis current (iqdc) and PI voltage controller output (iqr) to regulate the voltage at PCC. The voltage error from the amplitude of AC terminal voltage (Vg) and its reference (Vg*) is regulated using a PI voltage controller. The output of the PI PCC voltage controller is a reactive power component of AC mains current.

The amplitude of the terminal voltage is calculated as [32].

$$V_g = \sqrt{\frac{2}{3}\left(v_{ga}^2 + v_{gb}^2 + v_{gc}^2\right)} \qquad (IV.7)$$

The voltage is regulated by the voltage error between Vg and Vg* by using a PI voltage controller and the reactive power component current is given as

$$i_{qref}(k) = i_{qref}(k-1) + K_{pq}\left(v_{te^{(k)}} - v_{te^{(k-1)}}\right) + K_{iq}\left(v_{te^{(k)}}\right) \qquad (IV.8)$$

where:

Vte(k) is, Vte(k) = V g*(k)-Vg(k) is a voltage error between reference (Vg*) and sensed (Vg) PCC voltage at a kth sampling instant. Kpq and Kiq are the gains of the PCC voltage PI controller.

The amplitude of the reference quadrature current is given as:

$$i_q^* = i_{qref} - i_{Lq_dc} \qquad (IV.9)$$

The reference AC mains currents (i*ga, i*gb, i*gc) are estimated by reverse Park's transformation using (IV.6) with i*d from (IV.5), i*q from (IV.9) and i0 =0.

IV.3 .4. DC voltage control by PI anti-windup

Figure IV.2 shows that the circuit voltage is regulated using the anti-windup PI regulator.

It is a smart controller with a better response. The objective of using this controller is to set the Vdc value to its V*dc reference value and not to exceed the current limit using the saturation block in the event of system disturbances.

The error (Vdcer = ε) is the difference between the reference (V*dc) and the measured voltage (Vdc) of VSC is given as:

$$\mathcal{E}(\mathrm{k}) = \mathrm{v_{dcer}}(\mathrm{k}) = \mathrm{v_{dc}^{*}}(\mathrm{k}) - \mathrm{v_{dc}}(\mathrm{k}) \qquad (\mathrm{IV}.10)$$

$$\begin{cases} \dfrac{dy}{dt} = k_i\big(\varepsilon - k_l(i - i_{max})\big) \\ i = y + \varepsilon k_p \end{cases} \qquad (IV.11)$$

In consequence.

$$\frac{dy}{dt} + k_i k_l^{*} y = k_i \varepsilon\big(1 - k_p k_l\big) + k_i k_l i_{max} \qquad (IV.12)$$

The answer to this differential equation is provided below.

$$y(t) = \frac{\varepsilon\big(1 - k_p k_l\big) + k_l i_{max}}{k_l} + \frac{k_l y_0 - \varepsilon\big(1 - k_p k_l\big) - k_l i_{max}}{k_l} e^{-k_i k_l t} \qquad (IV.13)$$

$$\mathrm{y(t)} = \frac{\varepsilon\big(1 - k_p \mathrm{k_l}\big) + \mathrm{k_l} i_{max}}{\mathrm{k_l}} + \frac{\mathrm{k_l} y_0 - \varepsilon\big(1 - k_p \mathrm{k_l}\big) - \mathrm{k_l} i_{max}}{\mathrm{k_l}} e^{-k_i \mathrm{k_l} t} \qquad (IV.14)$$

Where y0 is y's initial value.

We can infer the subsequent information based on relationships (5) and (32).

$$i(\mathrm{t}) = \left(\frac{\varepsilon}{\mathrm{k_l}} + i_{max}\right) + \frac{\mathrm{k} l y_0 - \varepsilon\big(1 - k_p \mathrm{k_l}\big) - \mathrm{k_l} i_{max}}{\mathrm{k_l}} e^{-k_l \mathrm{k_l} t} \qquad (IV.15)$$

In a steady state, the second term of the equation tends to zero.

$$i = \frac{\varepsilon}{\mathrm{k_l}} + i_{max} \qquad (IV.16)$$

We can schematize the previous equations by the following block:

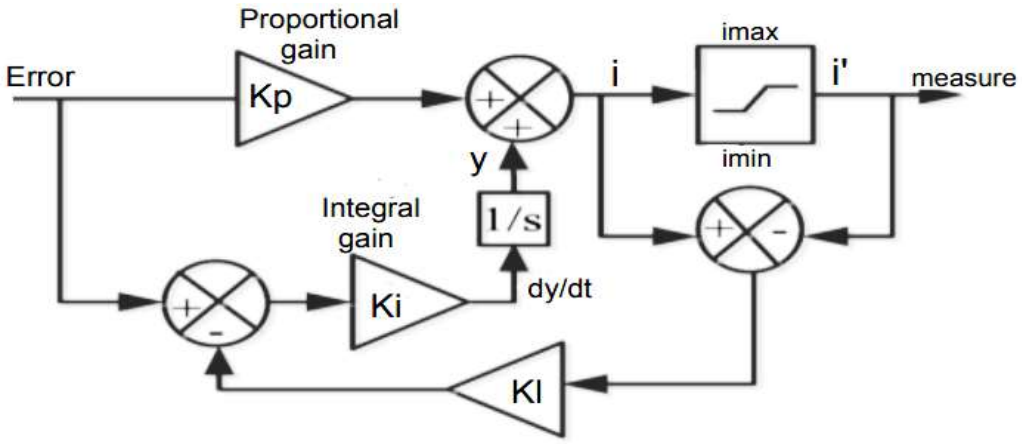


Figure IV.2. Structure of a PI anti-windup controller [32]

Finally, the control system (SRF) is represented by the following figure.

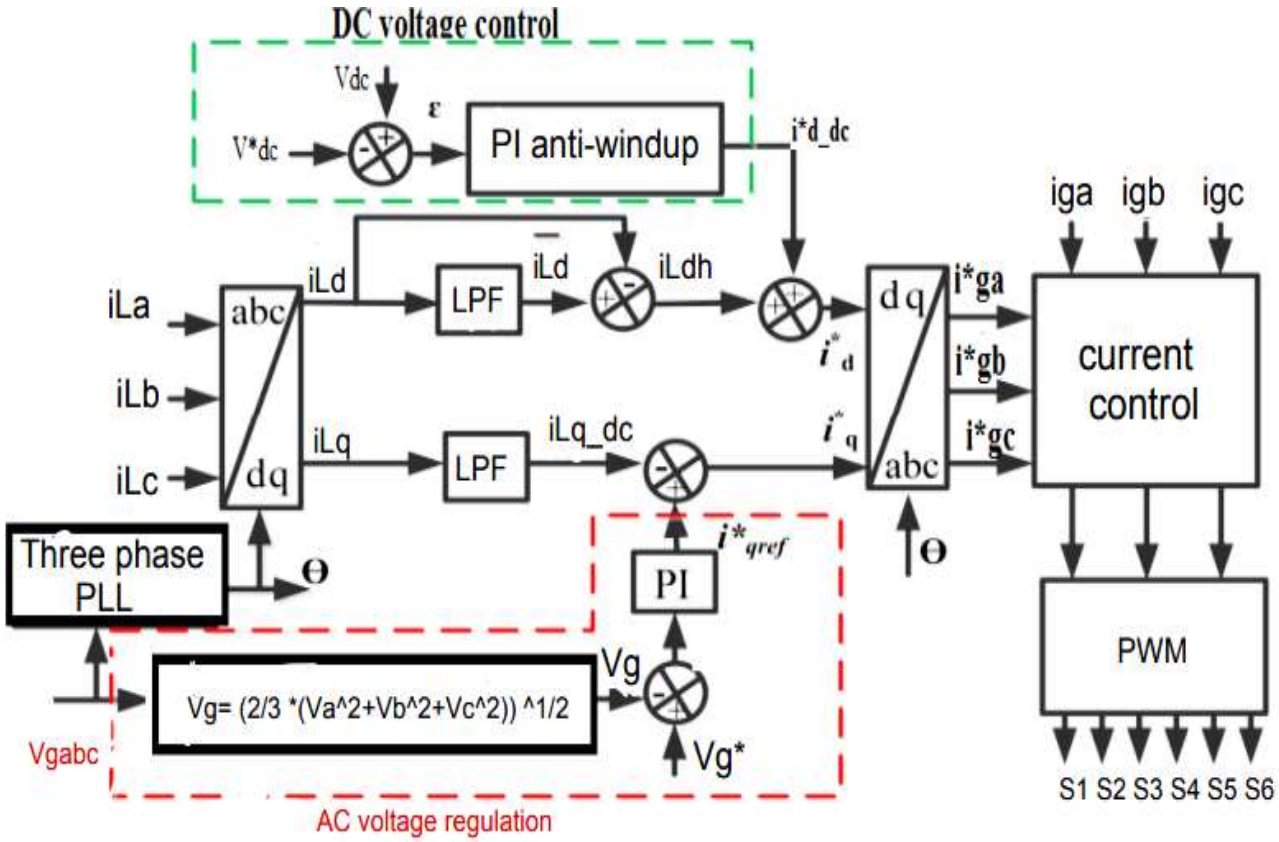


Figure IV.3. Structure SRF-controlled inverter of a hybrid system

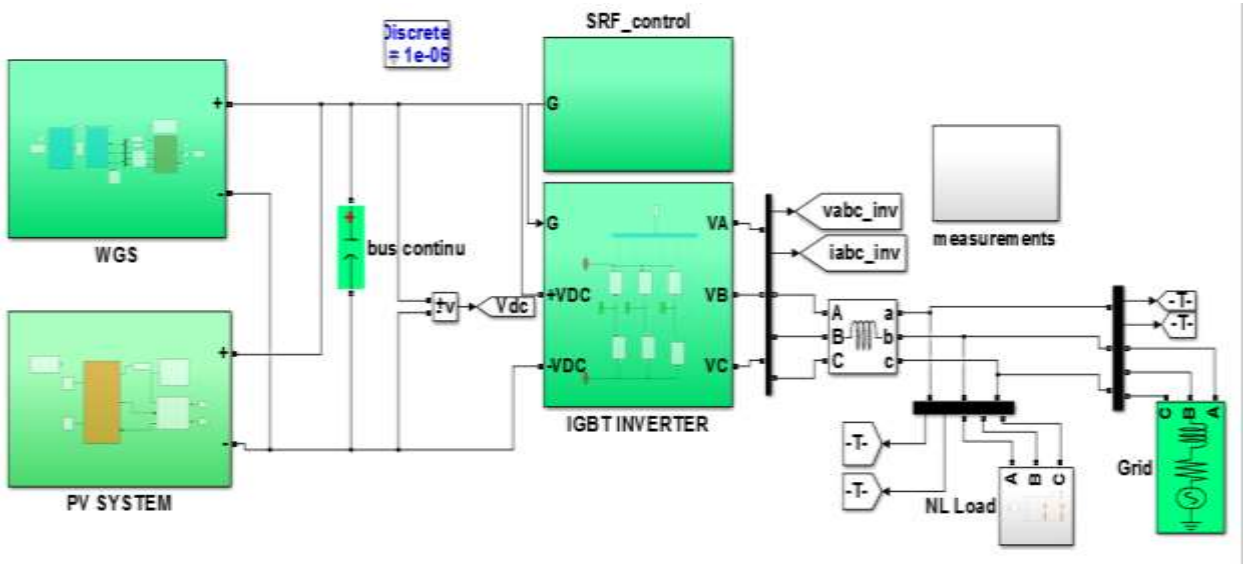


Figure IV.4: General model simulink of the Matlab hybrid system.

IV.4. Simulation Results

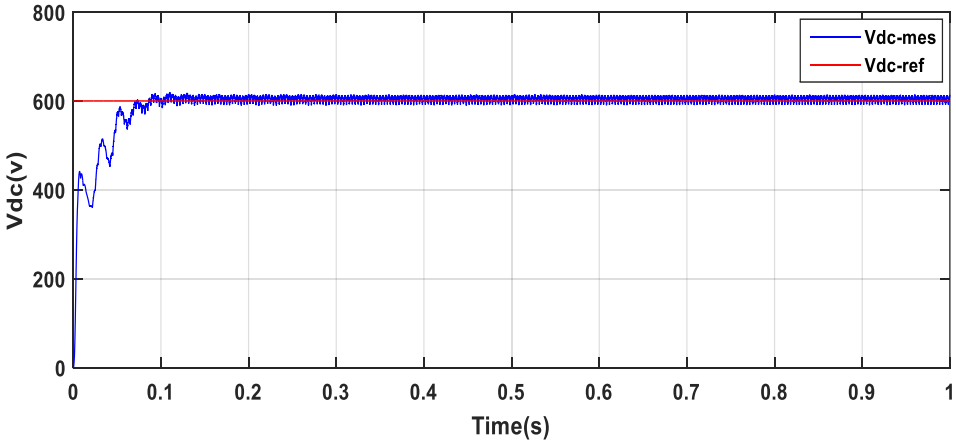


Figure IV.5. DC bus voltage and reference

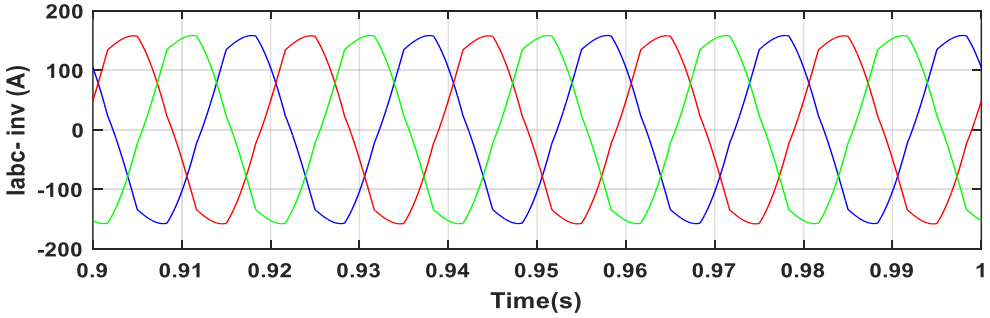


Figure. IV.6. The output current of the inverter

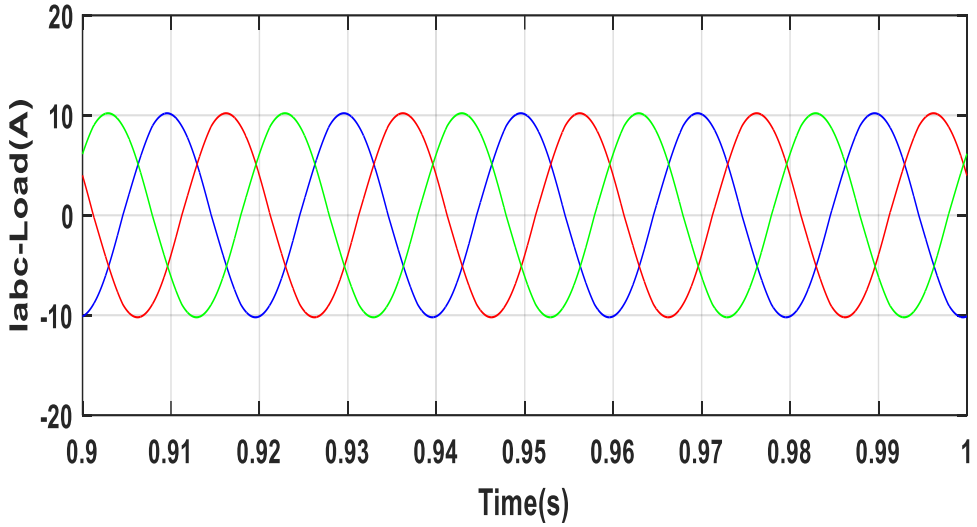


Figure. IV.7. The current of the Nonlinear Load

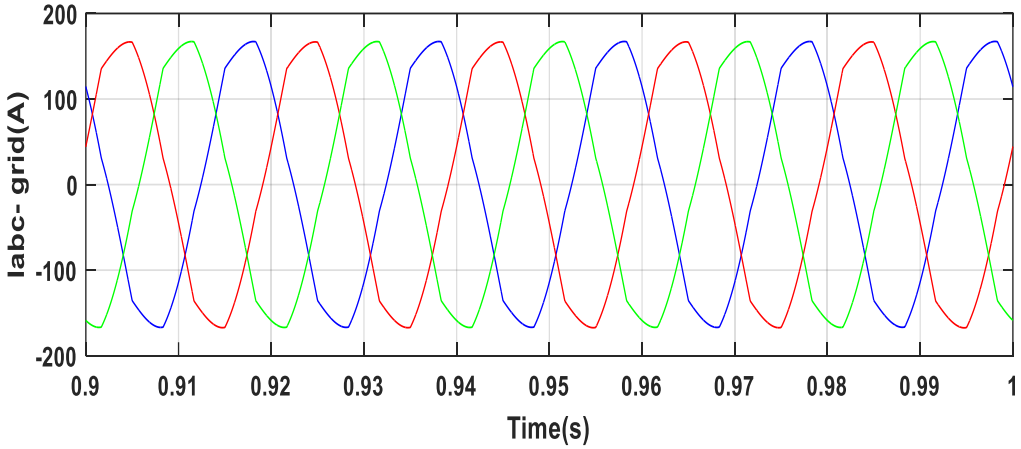


Figure. IV.8. The current of the grid

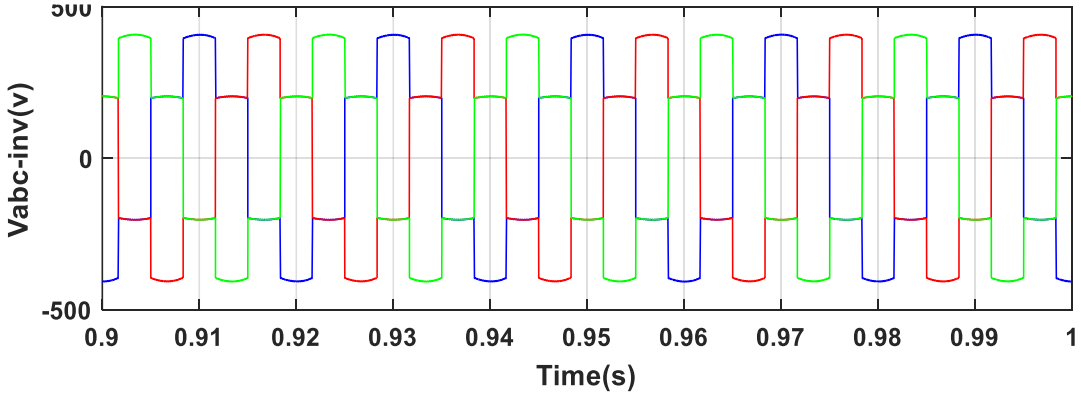


Figure IV.9. The output voltage of the inverter

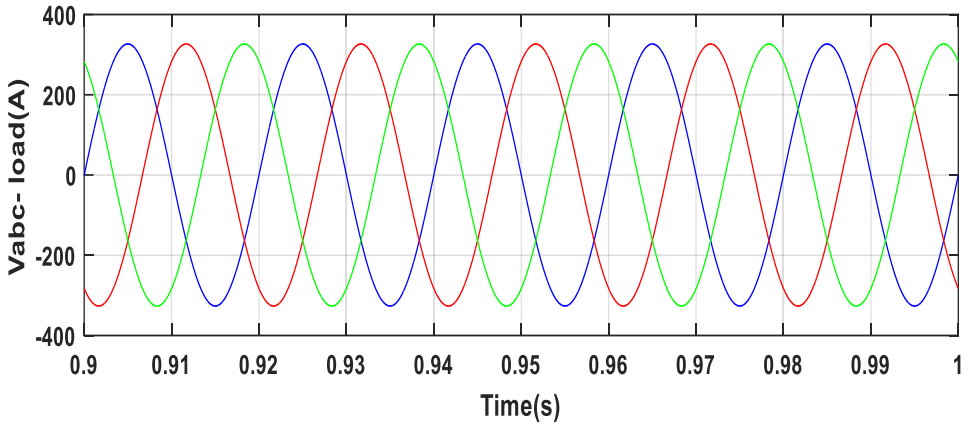


Figure IV.10. The voltage of the Nonlinear Load

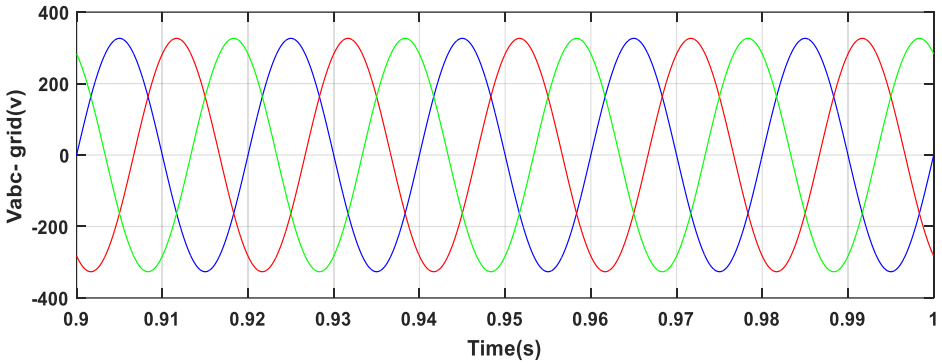


Figure IV.11. The voltage of the grid

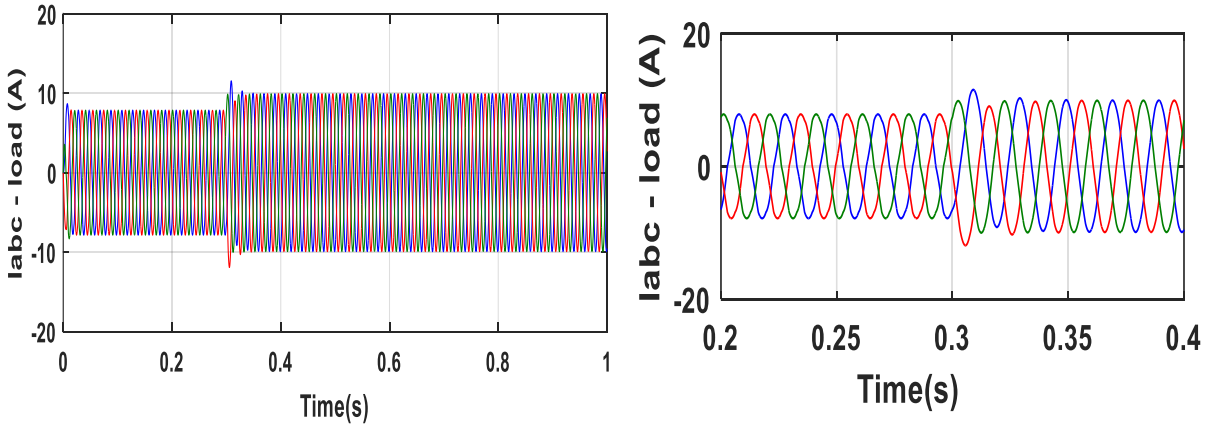


Figure. IV.12. The current of the load

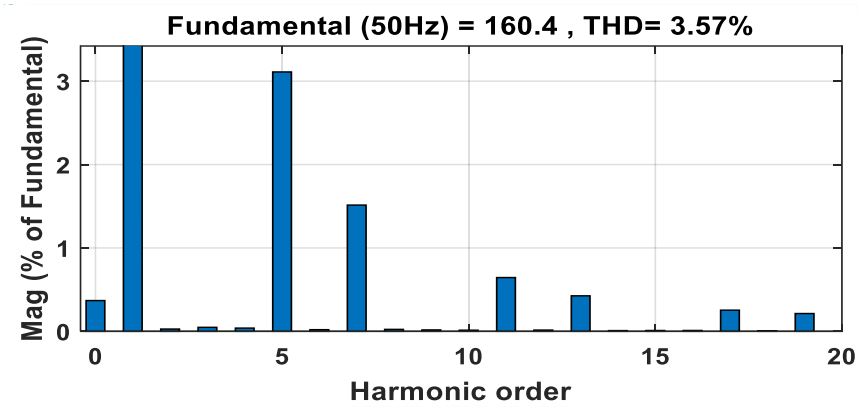


Figure. IV.13. THD output Current of the inverter

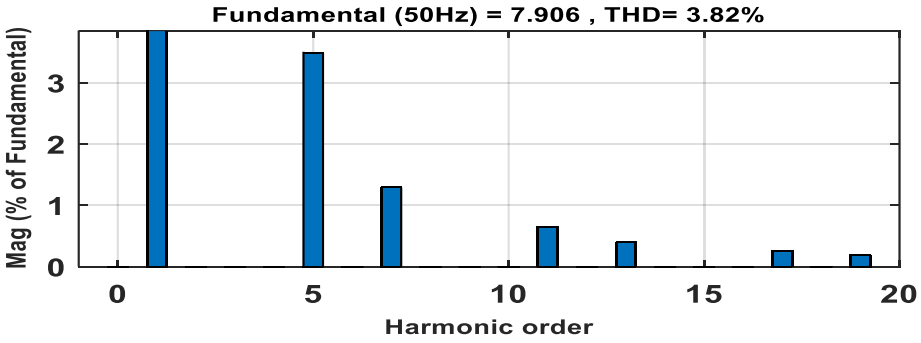


Figure. IV.14. THD Current of the nonlinear load R1

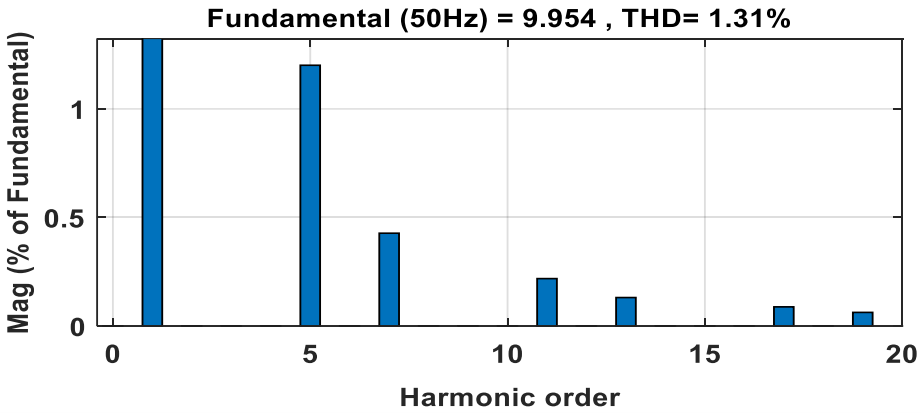


Figure. IV.15. THD Current of the nonlinear load R2

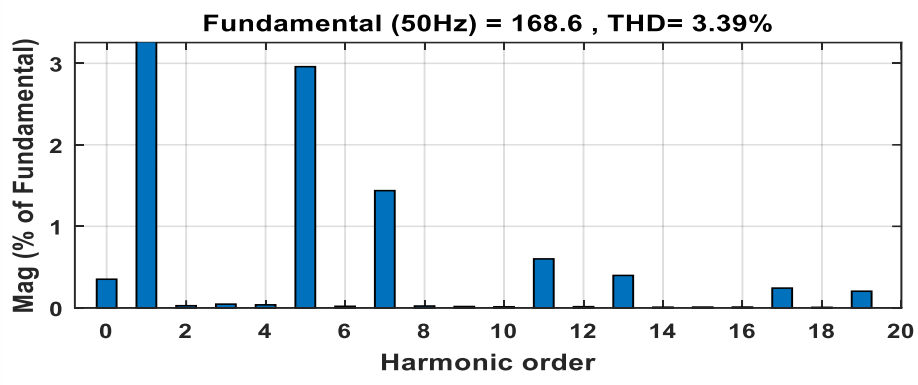


Figure. IV. 16. THD Current of the grid

IV.5. Discussion results

Figure IV.5: Show the DC bus voltage and its reference it is clear that the DC bus voltage follows its reference rapidly with a short time response of less than 0.1s and is more stable in a steady state.

Figure IV.6, Figure IV.7, and Figure IV.8 show the waveforms of the inverter, load, and grid currents, respectively its clear, that the three-phase currents have a sinusoidal form with THDs=3.57%, 1.31%, and 3.82% as shown in figure IV.13, figure IV.15 and figure IV.16 respectively.

while Figure IV (9,10 and 11) is the waveform's voltage of the inverter, load, and grid, respectively.

In terms of the robustness of the SRF strategy, a variable load has been added in t=0.3s we note the fast response and adapted performance with the variable added load in t=0.3s as shown in figure IV.12, as a result of the inductive load the THD is also changed from THD=3.82 % to THD =1.31% that confirm that the load has a filtered be have could perform the quality of waveforms to be of ripple

IV.6. Conclusion

The simulation and detailed analysis of the performance of a new controller for a hybrid system based on wind turbine and photovoltaic power generation have been presented for a three-phase grid. The performance of the system is obtained under different operating conditions, such as the disturbance and the variation of the load. The controller (SRF) of the VSC converter is used to correct harmonics. The results obtained demonstrate a THD of less than 5% (within the limits of IEEE standards) with sinusoidal waveforms of the currents at the PCC. The controller results show fast and efficient reference tracking, which validates the concept of the proposed hybrid system and the effectiveness of the SRF technique based on the anti-windup PI controller.

General Conclusion

A hybrid renewable energy system is a combination of two or more different power sources, in this study renewable energy sources with wind and solar power have been employed. The importance of hybrid systems lies in their ability to provide more reliable and sustainable energy solutions. Renewable energy sources have been a significant topic and have had great attention throughout the last decades due to the major drawbacks related to non-renewable energy sources and fuel sources to realize sufficient sources of the word consummation of energy. To compensate for the decrease in PV or wind generation, the hybrid system has been achieved.

This work is organized as follows: In the 1st chapter is interested in the general overview of both renewable energy sources wind and PV systems to present the importance of renewable energy sources and their significant role in the industrial and literature fields. And the different elements constituting them and their choice is presented. The different topologies and configurations of the hybrid system connected the VSC to the grid.

The 2nd chapter presented a detailed study of the modeling of the PV system to know the different parameters of the solar system that distinguish the performance during atmospheric conditions such as temperature and irradiance.in addition, it shew the final simulation results of the boost converter that allows extracting the maximum of power that product from the solar panel via the MPPT strategy based on the perturbation and observation method.

The 3rd chapter is concerned with the modeling and control of the wind turbine system. therefore, the MPPT technique is presented to maximize the power generated by wind turbines. Also, Direct power control has been used to control the active and reactive power.

The 4th chapter represents the major attention of our study because gathers and concludes the previous PV and wind generation. A three-phase inverter is controlled via the synchronous reference frame strategy.

After the simulation results, the results findings proved the effectiveness and robustness of the embedded control method SRF, this technique of control is a powerful tool for controlling the power flow and output voltage of DC-AC converters in power electronics applications.

We can note after the obtained results that the SRF technique improved the sign waves of the grid's current and decreased the broadband oscillations and mitigated the ripples that could be generated via the external perturbations of internal turbulences. Furthermore, the SRF technique was adapted and robust in the different scenarios of the system

LIST OF BIBLIOGRAPHIC REFERENCES

[1] A. Bouraiou *et al.*, "Status of renewable energy potential and utilization in Algeria," *J. Clean. Prod.*, vol. 246, p. 119011, Feb. 2020, doi: 10.1016/j.jclepro.2019.119011.

[2] https://www.iea.org/reports/global-energy-review-2021/renewables

[3] H. Azoug, H. Belmili, and F. Bouazza, "Grid-connected control of PV-Wind hybrid energy system," *Int. J. Power Electron. Drive Syst. IJPEDS*, vol. 12, no. 2, p. 1228, Jun. 2021, doi: 10.11591/ijpeds. v12.i2. pp1228-1238.

[4] E. Chavero-Navarrete, M. Trejo-Perea, J. C. Jáuregui-Correa, R. V. Carrillo-Serrano, and J. G. Ríos-Moreno, "Expert Control Systems for Maximum Power Point Tracking in a Wind Turbine with PMSG: State of the Art," *Appl. Sci.*, vol. 9, no. 12, p. 2469, Jun. 2019, doi: 10.3390/app9122469.

[5] Seghir Benhalima. Modélisation et Contrôle des Systèmes Éoliens-Solaire Intégrés au Réseau VSC-HVDC. University doctoral thesis. École de technologie supérieure université du québec, 2019.

[6] AHMED BOUBENIA. Analysis of hybrid renewable energy systems integrating Power-To-Gas Concept: Performances optimization based on artificial intelligence techniques University doctoral thesis. Boumerdes: University M'Hamed Bougara –Boumerdes,2019.

[7] "Renewable Energy" Godfrey Boyle second edition (2008).

[8] Berino, F; a Nelso, a. Feasibility Study of Solar-Wind Hybrid Power System for Rural Electrification at the Estatuene Locality in Mozambique. Master of Science Thesis. Mozambique: KTH School of Industrial Engineering and Management Energy Technology

[9] Wortman, A. J. 1983. Introduction to Wind Turbine Engineering. Woburn, MA 01801 Boston, U.S.A: Butterworth Publishers, 1983. pp. (Chp1) 1-5, (Chp2) 7-12, (Chp3) 3-5.

[10] Bhavin K Madhu. Dynamic Analysis of Grid Connected Hybrid System of PV Panel and Wind Turbines for a Light Commercial Building. University Master's thesis. Tennessee: University of Tennessee at Chattanooga,2010,109p.

[11] Baoshan Zhu, Xuhe Wang, Lei Tan, Dongyue Zhou, Yue Zhao, and Shuliang Cao, Optimization design of a reversible pump–turbine runner with high efficiency and stability. Renewable Energy, 2015, vol. 81, pp. 366-376.

[12] FERRAH BILLEL. Etude d'un système Hybride (photovoltaïque –éolien). La thèse de master. ANNABA : universite badji mokhtar annaba, 2015,102p.

[13] Akikur R.K., Saidur R., Ullah K.R., Hajimolana S.A., Ping H.W., Hussain M.A., Economic feasibility analysis of a solar energy and solid oxide fuel cell-based cogeneration system in Malaysia. Clean Technologies and Environmental Policy, 2016, vol. 18, no. 3, pp. 669-687.

[14] Autor Klaus Jäger, Olind Isabella, Arno H.M. Smets, René A.C.M.M. Solar Energy. Delft, the Netherlands: Copyright Delft University of Technology, 2014,

[15] Karoline Ingebrigtsen. Case Study of a Large-Scale Solar, Wind, and Hydro Power Hybrid System in Skibotndalen. Master's thesis in Energy. Troms: UNIVERSITY OF NORWAY,2017,24-26p.

[16] Hassaine, L., OLias, E., Quintero, J., and Salas, V. (2014). Overview of power inverter topologies and control structures for grid-connected photovoltaic systems. Renewable and Sustainable Energy Reviews, 30:796–807.

[17] A. M. Noman, A. A. Al-Shamma'a, K. E. Addoweesh, A. A. Alabduljabbar, and A. I. Alolah, "Simulation and comparison of three-phase CHB MLI and three phases cascaded voltage source MLI topologies for grid-connected PV applications," in *IECON 2017 - 43rd Annual Conference of the IEEE Industrial Electronics Society*, Beijing: IEEE, Oct. 2017, pp. 2681–2688.

[18] Romero-Cadaval, E., Spagnuolo, G., Franquelo, L. G., Ramos-Paja, C.-A., Suntio, T., and Xiao, W.-M. (2013). Grid-connected photovoltaic generation plants: Components and operation. IEEE Industrial Electronics Magazine, 7(3) :6–20

[19] Nakoul, Z. (2010). "Optimisation d'une centrale solaire à base d'un générateur PV [Application Aux Sites Tlemcen Et Bouzaréah]."

[20] Nichiporuk, O. (2005). Simulation, fabrication et analyse de cellules photovoltaïques à contacts arrières interdigités, Lyon, INSA.

[21] Burton, T, et al. 2011. Wind Energy Hand Book. Chichester, UK: John Wiley & Sons, Ltd, 2011.

[22] IOWA. 2013. IOWA Energy Center. IOWA Energy Center. [Online] September 10, 2013. [Cited: September 10, 2013.] http://www.energy.iastate.edu/renewable/wind/wem-index.html.

[23] Ahmed, S. 2011. Wind Energy. Theory and Practice. New Delhi-110001: Asoke K. Ghosh, PHI Learning Private Limited M-97, 2011.

[24] Mahmoud, S, I, A. Simulation of a Hybrid Power System Consisting of Wind Turbine, PV, Storage Battery and Diesel Generator with Compensation Network: Design, Optimization and Economical Evaluation. University doctoral thesis. Nablus, Palestine: An-Najah National University, 2008,16p.

[25] Gilbert M. Masters. Renewable and Efficient Electric Power Systems. Stanford University,2004, 311p.

[26] Wind and Hydro Power Technologies Program. Available at: http:// www. eere .energy.gov/windandhydro/wind_how.html [access date 3 December 2007]

[27] Goudarzi, N. and W. Zhu (2013). "A review on the development of wind turbine generators across the world." International Journal of Dynamics and Control 1(2): 192-202.

[28] Sharma, M., B. Rieger, C. Jou and B. Butka (2012). Development of helical vertical axis wind turbine. Southeast, 2012 Proceedings of IEEE.

[29] Wenzhuan, C., Y. Feng, L. Xiongwei and J. Whitty (2009). Analysis of the passive yaw mechanism of small horizontal-axis wind turbines. World Non-Grid-Connected Wind Power and Energy Conference, 2009. WNWEC 2009.

[30] Zhang, S., K. J. Tseng and T. D. Nguyen (2008). WRIG-based wind conversion system excited by matrix converter with a current control strategy. Sustainable Energy Technologies, 2008. ICSET 2008. IEEE International Conference on.

[31] Feltes, C., H. Wrede, F. W. Koch and I. Erlich (2009). "Enhanced Fault Ride-Through Method for Wind Farms Connected to the Grid Through VSC-Based HVDC Transmission." Power Systems, IEEE Transactions on 24(3).

[32] Seghir Benhalima. Modélisation et Contrôle des Systèmes Éoliens-Solaire Intégrés au Réseau VSC-HVDC. University doctoral thesis. École de technologie supérieure université du québec, 2019.

[33] Merzoug, M., H. Benalla and L. Louze (2011). "Nonlinear control of permanent magnet synchronous generators (PMSG) using feedback linearization." Revue des Energies Renouvelables 14(2) : 357-367.

[34] Farret, F. A. and M. G. Simoes (2006). Integration of alternative sources of energy, John Wiley & Sons.

[35] Analysis of Effects of Sun`s Position in the Sky on Solar Radiation and Solar Panel Output Power authored by Moein Jazeera, Sener Uysal, Member, IEEE, and Kian Jazayeri published in IEEE 978-1-4673- 5943-6/13/$31.00 ©2013 IEEE.

[36] T. H. Assefa, « Modeling and Simulating of Renewable Energy Resources », Innovative Systems Design and Engineering www.iiste.org ISSN 2222-1727 (Paper) ISSN 2222-2871 (Online) Vol.9, No.7, 2018.

[37] W. A. Wan Abdullah and A. Z. Ahmad, "Voltage and Active Power Management Control of PV Source Distributed Generations under Unbalanced Voltage of Non-Islanded Microgrid," *J. Phys. Conf. Ser.* vol.2319, no.1, p.012003, Aug.2022, doi:10.1088/1742-6596/2319/1/012003

[38] M. Mchalikh et CH. Hmada, « Modélisation et simulation d'un système photovoltaïque en fonctionnement autonome et connecté au réseau », Mémoire de Master, Université Kasdi Merbah–Ouargla 2013

[39] R. Noureddine and M. Leila, "Perturb and Observation MPPT algorithm for the performance of Solar Photovoltaic System". Electrotechnical Engineering Department,

[40] M. Fannakh, M.L. Elhafyani, and S. Zouggar, "Hardware implementation of the fuzzy logic MPPT in an Arduino card using a Simulink support package for PV application," IET Renew. Power Gener., vol. 13, no. 3, pp. 510- 518, 2019, doi: 10.1049/it-rpg.2018.5667

[41] R. Alik, and A. Jusoh, "An enhanced P&O checking algorithm MPPT for high tracking efficiency of partially shaded PV module," Solar Energy, vol. 163, pp. 570-580, 2018, doi: https://doi.org/10.1016/j.solener.2017.12.050.

[42] S. A. Mohamed, and M.A.E. Sattar, "A comparative study of P&O and INC maximum power point tracking techniques for grid-connected PV systems," SN Applied Sciences, vol. 2019, pp. 1-174, 2019.doi: https://doi.org/10.1007/s42452-018-0134-4.

[43] A. Azwin, and S. Ahmed, "Induction Motor Speed Control Using Varied Duty Cycle Terminal Voltage via PI Controller," IOP Conference Series - Materials Science and Engineering, vol. 341, no. 1, pp. 1–10, 2018

[44] Fairouz Kendouli "Centrale éolienne et qualité de l'énergie électrique" Thèse de doctorat en Sciences en Electrotechnique de Université Mentouri de Constantine, 2012.

[45] S. El Aimani "Modélisation de différentes technologies d'éoliennes intégrées dans un réseau de moyenne tension" Thèse de Doctorat, Ecole Centrale de Lille, Université des Sciences et Technologies de Lille, 06/12/2004.

[46] Kendal F. Hocine Benalla. and Khoudir Abed. "Modélisation, simulation et contrôle d'une turbine éolienne à vitesse variable basée sur la génératrice asynchrone à double alimentation." Revue des Energies Renouvelables 14.1 (2011) : 109-120.

[47] A. Bechouche, « Utilisation des techniques avancées pour l'observation et la commande d'une machine asynchrone : application à une éolienne » ; Thèse de Doctorat en Electrotechnique, Université de Tizi–Ouzou, Algérie, Avril 2013

[48] T. Ghennam, « Supervision d'une ferme éolienne pour son intégration dans la gestion d'un réseau électrique, Apports des convertisseurs multi niveaux au réglage des éoliennes à base de machine asynchrone à double alimentation » ; Thèse de Doctorat de l'Ecole Militaire Polytechnique d'Alger, Algérie, Septembre 2011.

[49] S. Heier, « Grid Integration of Wind Energy Conversion Systems »; Publications John Wiley & Sons, ISBN 0-471-97143-X, 1998.

[50] S. El Aimani, « Modélisation de différentes technologies d'éoliennes intégrées dans un réseau de moyenne tension » Thèse de Doctorat, Ecole centrale de Lille, France, Décembre 2004.

[51] Ayehunie NA. (2011). MultiPhase Permanent Magnet Synchronous Generators for Offshore Wind Energy System. Norwegian University of Science and Technology Department of Electric Power Engineering.

[52] Ali Z, Christofides N, Hadjidemetriou L, Kyriakides E, Yang Y, Blaabjerg F. Three-phase phase-locked loop synchronization algorithms for grid-connected renewable energy systems: a review. Renew Sust Energ Rev. 2018; 90:434-452.

[53] Xiong L, Li P, Ma M, Wang Z, Wang J. Output power quality enhancement of PMSG with fractional order sliding mode control. Int J Electr Power Energy Syst. 2020; 115:105402.

[54] Elbeji O, Hamed MB, Sbita L. PMSG wind energy conversion system: modeling and control. Int J Mod Nonlinear Theory Appl. 2014 ;3(3) : 88-97

[55] A. Boulahia, 'Etude des Convertisseurs Statiques destinés à la Qualité de l'Energie Electrique. Thèse de Magister. University de Constantine. 2009.

[56] M.P. Kazmierkowski, R. Krishnan, F. Blaabjerg, Control in Power Electronics: Selected Problems. Academic Press, London, UK, 2002

[57] Fekik, Arezki. Commande directe de puissance d'un redresseur à MLI par DSP, Thèse de doctorat, Université Mouloud Mammeri, 2018

[58] Bouafia, Abdelouahab. Techniques de commande prédictive et floue pour les systèmes d'électronique de puissance : application aux redresseurs à MLI, Thèse de doctorat, Université Sétif, 2014.

[59] Bouchakour, S. Commande directe de puissance d'un convertisseur AC/DC triphasé sans capteur de tension. Memory of Magister, Ecole Militaire Polytechnique Algeria (2005).

[60] AFGHOUL, Hamza. Approche avancée du filtrage actif et du contrôle de puissances dans les installations photovoltaïques interconnectées au réseau, Thèse de doctorat, Université de M'sila, 2016.

[61] Kot Yahia. Modélisation et simulation d'un convertisseur Statique AC/DC commandée, Thèse de master, Universitaire d'el-oued, 2014.

[62] Chaoui, Abdelmadjid. Filtrage actif triphasé pour charges non linéaires, Thèse de doctorat, Université Sétif 2018.

[63] Ouchen, Sabir. Contribution a la commande directe de puissance dediee au filtrage actif, associe a une source photovoltaïque, Thèse de doctorate, Université Mohamed Khider-Biskra, 2017.

[64] Chebabhi, A., et al. "Commande d'un filtre actif shunt par la technique de control directe de puissance basée sur le flux virtuel." 7émes Conférence sur le Génie Electrique CGE. Vol. 7. 2011.

[65] A. M. Abdullah, B. Ouahid, and S. Youcef, "Control of a Stand-Alone Variable Speed Wind Turbine with a Permanent Magnet Synchronous Generator," in 2021 18th International Multi-Conference on Systems, Signals & Devices (SSD), Monastir, Tunisia: IEEE, Mar. 2021, pp. 546–550.

[66] GHADBANE, ISMAIL. Etude Et Réalisation D'un Filtre Actif Parallèle En Utilisant Différentes Stratégies De Contrôle, Thèse de doctorat, Université Mohamed Khider-Biskra, 2016.

[67] Wei, C., Z. Zhang, W. Qiao, and L. "An Adaptive Network-Based Reinforcement Learning Method for MPPT Control of PMSG Wind Energy Conversion Systems." IEEE Transactions on Power Electronics 31(11), (2016).

[68] Verma, A. K., B. Singh, and D. T. Shahani. Grid-interfaced solar photovoltaic power generating system with power quality improvement at AC mains. IEEE Third International Conference on Sustainable Energy Technologies (ICSET), (2012.

.

ANNEX

Table 4: PV Module Parameters

Parameters	Value
Rated Power (W)	213.15
The voltage at maximum power point Vmp (V)	29V
Current at maximum power point Imp (A)	7.35A
Open circuit voltage Voc (V)	36.3V
Short-circuit current Isc (A)	7.84A
Number of cells	60
Series resistance(Rs)	0.39383Ω
Parallel resistance (Rsh)	313.399Ω

Table 5: Parameters of the boost converter

Capacitance C1	1000µF
Inductance (H):	1.45mH
Switching frequency	5kHz
Capacitance C2	3227 µF

Table 6: parameters of the wind turbine

Parameters	Value
Blade radius	R=3m
Number of blades	3
Nominal wind speed	Vw=14m/s
Gearbox ratio	G=7.7
Moment of inertia	J= 0.3126 $Kg.m^2$
Viscous friction coefficient	fr= 0.00681 $N.m.s^{-1}$

Table 7: Parameters of the PMSG

Parameters	Value
Direct stator inductances	Ld =3.95mH
Quadrature stator inductances	Lq =3.95mH
Stator phase resistance	Rs =0.425Ω
Inertia	J = 0.00072 $Kg.m^2$
Number of pole pairs	N=5
Rated power	2.5kw

Table 8: Parameters of the load

Parameters	Value
Non-linear load	L_1=20mH, R_1=10Ω L_2= 20mH, R_2=40Ω
Linear load	L=2mH, R=40Ω

Table 9: Parameters of the inverter

Parameters	Value
Voltage dc (V)	600V
Integral gain Ki	300
Proportional gain Kp	0.25

Table 10 Parameters of the Grid

Parameters	Value
Phase-to-phase voltage (V)	400V
Frequency (Hz)	50Hz